

The innate sensor ZBP1-IRF3 axis regulates cell proliferation in multiple myeloma

by Kanagaraju Ponnusamy, Maria Myrsini Tzioni, Murshida Begum, Mark E. Robinson, Valentina S. Caputo, Alexia Katsarou, Nikolaos Trasanidis, Xiaolin Xiao, Ioannis V. Kostopoulos, Deena Iskander, Irene Roberts, Pritesh Trivedi, Holger W. Auner, Kikkeri Naresh, Aristeidis Chaidos, and Anastasios Karadimitris

Haematologica 2021 [Epub ahead of print]

Citation: Kanagaraju Ponnusamy, Maria Myrsini Tzioni, Murshida Begum, Mark E. Robinson, Valentina S. Caputo, Alexia Katsarou, Nikolaos Trasanidis, Xiaolin Xiao, Ioannis V. Kostopoulos, Deena Iskander, Irene Roberts, Pritesh Trivedi, Holger W. Auner, Kikkeri Naresh, Aristeidis Chaidos, and Anastasios Karadimitris. The innate sensor ZBP1-IRF3 axis regulates cell proliferation in multiple myeloma.

Haematologica. 2021; 106:xxx

doi:10.3324/haematol.2020.274480

Publisher's Disclaimer.

E-publishing ahead of print is increasingly important for the rapid dissemination of science. Haematologica is, therefore, E-publishing PDF files of an early version of manuscripts that have completed a regular peer review and have been accepted for publication. E-publishing of this PDF file has been approved by the authors. After having E-published Ahead of Print, manuscripts will then undergo technical and English editing, typesetting, proof correction and be presented for the authors' final approval; the final version of the manuscript will then appear in print on a regular issue of the journal. All legal disclaimers that apply to the journal also pertain to this production process.

The innate sensor ZBP1-IRF3 axis regulates cell proliferation in multiple myeloma

Kanagaraju Ponnusamy¹, Maria Myrsini Tzioni¹, Murshida Begum¹, Mark E Robinson¹, Valentina S Caputo¹, Alexia Katsarou^{1,2}, Nikolaos Trasanidis¹, Xiaolin Xiao¹, Ioannis V Kostopoulos^{1,3}, Deena Iskander^{1,2}, Irene Roberts⁴, Pritesh Trivedi⁵, Holger W Auner^{1,2}, Kikkeri Naresh⁵, Aristeidis Chaidos^{1,2} and Anastasios Karadimitris*^{1,2}

¹Hugh & Josseline Langmuir Centre for Myeloma Research, Centre for Haematology, Department of Immunology & Inflammation, Imperial College London, London, United Kingdom;

²Department of Haematology, Hammersmith Hospital, Imperial College Healthcare NHS Foundation Trust, London, United Kingdom;

³Section of Animal and Human Physiology, National and Kapodestrian University of Athens, Department of Biology, School of Science, Athens, Greece;

⁴Department of Paediatrics and MRC Molecular Haematology Unit, Weatherall Institute of Molecular Medicine, University of Oxford and BRC Blood Theme, NIHR Oxford Biomedical Centre, Oxford, United Kingdom;

⁵Department of Cellular & Molecular Pathology, Northwest London Pathology, Imperial College Healthcare NHS Trust, London, United Kingdom.

***Correspondence**

Anastasios Karadimitris

Hugh & Josseline Langmuir Centre for Myeloma Research

Centre for Haematology

Department of Immunology & Inflammation

Imperial College London

London, United Kingdom, W12 0NN

e-mail: a.karadimitris@imperial.ac.uk

Acknowledgments

We acknowledge funding from Blood Cancer UK (KP, NT, XX, VC) and KKLf (AK), and the Imperial NIHR Biomedical Research Centre, LMS/NIHR Imperial Biomedical Research Centre Flow Cytometry Facility, Imperial BRC Genomics Facility and the MRC/LMS Sequencing Facility for support.

Declaration of Interests

All authors declare no competing interest.

Contributions

K.P and A.K conceived and designed the study. K.P and M.M.T performed ColP and dox-inducible study in vitro. K.P and M.B performed shTBK1 study. P.T and K.N performed immunohistochemistry. A.C processed RNA-seq data for ZBP1. M.E.R processed RNA-seq and ChIP-seq data for ZBP1 and IRF3. K.P performed all other experiments in vitro, in vivo and integrated all the chip-seq and RNA-seq data and performed all other bioinformatics analysis and created all the figures. D.I provided erythroblast cells, V.S.C, A.K, N.T, X.X, I.V.K, I.R, H.W.A provided reagents. A.K supervised the study. K.P and A.K wrote the manuscript.

Abstract

Multiple myeloma is a malignancy of plasma cells (PC) initiated and driven by primary and secondary genetic events. Nevertheless, myeloma PC survival and proliferation might be sustained by non-genetic drivers. Z-DNA-binding protein 1 (ZBP1; also known as DAI) is an interferon-inducible, Z-nucleic acid sensor that triggers RIPK3-MLKL-mediated necroptosis in mice. ZBP1 also interacts with TBK1 and the transcription factor IRF3 but the function of this interaction is unclear, and the role of ZBP1-IRF3 axis in cancer is not known. Here we show that ZBP1 is selectively expressed in late B cell development in both human and mouse cells and it is required for optimal T-cell-dependent humoral immune responses. In myeloma PC, interaction of constitutively expressed ZBP1 with TBK1 and IRF3 results in IRF3 phosphorylation. IRF3 directly binds and activates cell cycle genes, in part through co-operation with the PC lineage-defining transcription factor IRF4, and thereby promoting myeloma cell proliferation. This generates a novel, potentially therapeutically targetable and relatively selective myeloma cell addiction to the ZBP1-IRF3 axis. Our data also show a non-canonical function of constitutive ZBP1 in human cells and expand our knowledge of the role of cellular immune sensors in cancer biology.

Keywords

ZBP1; multiple myeloma; IRF3; IRF4; TBK1; cell cycle

Running title

ZBP1 regulates myeloma cell proliferation via IRF3/IRF4

Introduction

Multiple myeloma (MM) is a common incurable blood cancer of the bone marrow (BM) plasma cells (PC), the immunoglobulin-secreting terminally differentiated B lineage cells.¹⁻³ Primary and secondary somatic genetic events comprising copy

number and single nucleotide variants shape a genomic landscape of extensive, in time and space, genetic heterogeneity and diversification rendering targeted-therapies for MM a challenging task.¹⁻³ In this regard, there is a need for identification of biological pathways that are involved in myelomagenesis independent of the genetic status.

Previous studies of murine late B lineage development identified ZBP1 as one of the genes that define the transcriptional signature of follicular B cell transition to plasmablasts and mature PC.⁴ ZBP1 is an inducible cellular DNA/RNA sensor with two Z α domains that bind pathogen-derived or cellular Z-DNA^{5,6} or Z-RNA.^{7,8} Z α -dependent nucleic acid (NA) sensing induces a RHIM-RHIM domain interaction of ZBP1 with receptor-interacting protein kinase 3 (RIPK3) which ultimately triggers mixed lineage kinase domain like pseudokinase (MLKL)-mediated necroptosis.⁷⁻¹⁰ This process is counteracted by RIPK1, preventing for example ZBP1-dependent cell death and inflammation in the developing skin.¹¹⁻¹³

In addition, like other NA sensors e.g., cGas/STING, ZBP1 has been shown to associate with serine/threonine kinase TBK1 with subsequent phosphorylation of the transcription factor IRF3 (pIRF3). Activation of STING and other NA sensors triggers translocation of pIRF3 to the nucleus where it directly activates transcription of interferon (IFN) type I response genes;¹⁴⁻¹⁶ however this has been disputed in the case of ZBP1.^{17,18} Therefore, the role ZBP1-TBK1-IRF3 in innate sensing or in the context of cancer remains unclear. Nevertheless, it is clear that ZBP1 itself is an IFN-inducible gene as its expression is induced by type I and II IFN that leads to RIPK3-dependent necroptosis^{7,13,19} and IFNAR1^{-/-} cells fail to upregulate virus-induced ZBP1 expression.²⁰ Since recent work demonstrated an active type I IFN vs proliferative

transcriptional signature prevailing in early diagnosis vs relapsed patient myeloma PC or myeloma cell lines respectively,²¹ we hypothesized that ZBP1 might regulate myeloma PC biology.

Methods

Cell culture, primary samples

U266 and NCI-H929 (DSMZ, Germany), MM.1R and MM.1S (ATCC, Manassas, VA, USA), and HeLa, HEK293T, DU145, MCF7, HCC95, SF295, LNCAP, K562, Jurkat and C1R cells were cultured in either 10% FBS, RPMI-1640 or DMEM. Primary myeloma cells were collected under ethical committee approval (REC no. 11/H0308/9) and cultured with IL-6 (10ng/ml).

Cell cycle, proliferation and apoptosis

Cell cycle status was assessed using flow cytometry after staining cells with 10 μ M Hoechst-33342 in RPMI-1640 medium for 1 hour. Cytostatic effect of constitutive or inducible shRNAs-transduced cells were measured as shown in supplementary figure S3C. Annexin V (BioLegend) staining was performed according to manufacturer's instructions.

Subcutaneous tumor model, Immunization

Subcutaneous tumor study was performed in NOD/SCIDgamma mice (licence PPL70/8586), by subcutaneously injecting 10⁷ doxycycline-inducible shRNA-

transduced cells with Matrigel (Corning). Tumor volume was calculated by the formula $(1/2(\text{length} \times \text{width}^2))$. Animals were administered with 100 $\mu\text{g}/\text{ml}$ doxycycline in drinking water and 0.2mg/kg intraperitoneally.

Zbp1^{-/-} animals¹⁸ obtained from Manolis Pasparakis, Institute of Genetics, Cologne, Germany. Ten-twelve weeks-old littermates were immunized by intraperitoneal injection of 4mg/kg NP-KLH (Santacruz Biotech) with Alum Adjuvant (Thermoscientific) at 3:1 ratio followed by NP-KLH-booster dose on day 4. Serum NP-KLH-specific antibodies were measured.

qPCR, RNA-sequencing

Total RNA was isolated using Nucleospin RNA kit (Macherey-Nagel) followed by cDNA synthesis using RevertAid cDNA synthesis kit (Thermoscientific). Indicated cDNAs were quantified using the primers shown in supplementary methods. Poly (A)-tail mRNA was isolated, from total RNA of FACS-purified GFP+ cells with either scramble or shRNA targeting *ZBP1* or *IRF3* on day 4 post-transduction when >80% knock-down achieved, using NEBNext poly(A) mRNA Magnetic Isolation Module, and prepared library using NEBNext Ultra II RNA library prep kits (New Engand Biolabs). 2nM DNA library (350-400bp) was sequenced using Illumina HiSeq 2500 (for shZBP1) or NextSeq500 (for shIRF3) for paired-end 150bp reads.

ChIP-seq, ChIP-re-ChIP

MM.1S cells were cross-linked with 1% formaldehyde and lysed with hypotonic lysis buffer followed by nuclear lysis buffer. The lysate was sonicated to shear the chromatin up to 500bp followed by pre-clear with protein A/G magnetic beads and

immunoprecipitation with IRF3 antibody or equivalent isotype control. CHIP DNA was collected with AMPure XP-beads after reverse cross-linking. CHIP DNA (1ng) used for library preparation using NEBNext kit. 2nM DNA library (400-500bp) was sequenced using Illumina NextSeq500. For CHIP-re-CHIP, pulled chromatin was eluted in 1% SDS and diluted 10 times with elution buffer and repeated re-CHIP with the appropriate antibody. The detailed protocols are provided in supplementary methods.

Co-immunoprecipitation, Immunoblotting

Co-immunoprecipitation was performed as described¹² with 5% anti-strep-tagII-magnetic bead slurry (IBA) or 2µg anti-ZBP1 or anti-V5-Tag or anti-IRF3 or their equivalent isotype control antibodies conjugated with protein A/G magnetic beads. For immunoblot, total cell proteins denatured in 1x LDS Sample Buffer (ThermoFisher Scientific) and resolved in 10% SDS-PAGE and transferred to PVDF membrane followed by probing with appropriate antibodies shown in supplementary methods.

Data analysis

The detailed data analysis provided in supplementary methods. In brief, RNA-seq and CHIP-seq reads were aligned using STAR or Salmon and BWA MEM^{22,23} to GRCh38 genome respectively. Differential expression analysis was performed using DESeq2 or limma-voom.^{22,24,25} CHIP-seq-peaks were called with MACS2²⁶ and tracks with Deeptools²⁷ and visualized in IGV.²⁸ Homer used for Motif analysis²⁹ and BETA-

plus package³⁰ to integrate RNA-seq and ChIP-seq data. GSEA³¹ and Enrichr web tool³² used for pathway analysis.

Data availability

All next-generation sequencing data for RNA-seq and ChIP-seq experiments can be accessed via GEO (GSE163497).

The details of shRNA sequences, cloning strategies, reagents, antibodies and additional methodologies are provided in supplementary methods.

Results

Restricted and constitutive expression of ZBP1 in normal and myeloma plasma cells

By searching for genes selectively expressed in MM we identified *ZBP1* as highly and selectively expressed in MM cell lines (MMCL) but not in other cancer cells (CCLE dataset; **Online Supplementary Figure S1A, B**). While there is no difference in *ZBP1* expression between normal and the whole cohort of myeloma PC, its expression is significantly higher in the hyperdiploid subgroup of myeloma PC (Arkansas GSE4581 microarray dataset; **Online Supplementary Figure S1C**). *ZBP1* is universally expressed in primary myeloma PC (MMRF CoMMpass dataset; n=767 patients; **Online Supplementary Figure S1D**) at similar levels as the PC-defining transcription factor *PRDM1* (BLIMP1). In human B-cell lineage, *ZBP1* expressed at very low level in germinal center B cells (GCB) and moderately detected in naive and memory B cells

but PC show by far the highest expression (Blueprint DCC Portal data; **Online Supplementary Figure S1E**). We confirmed expression of ZBP1 mRNA and protein in MMCL (**Figure 1A, B**) and also in primary myeloma PC (**Figure 1C, D**) but not in other hematopoietic or epithelial cancer cells (**Online Supplementary Figure S1F, G**), normal blood lineage cells (**Online Supplementary Figure S1H, I**) or healthy non-hematopoietic tissues (**Online Supplementary Figure S1J**).

Immunohistochemistry of human tonsils and lymph nodes showed expression of ZBP1 primarily in a group of PAX5⁺IRF4⁺ GCB cells i.e., those committed to PC differentiation^{33,34} and in interfollicular and subepithelial IRF4⁺ PC, with low level expression in mantle zone B-cells (**Figure 1E and Online Supplementary Figure S1K, L**). In BM, expression of ZBP1 is mostly restricted in myeloma and normal PC but no other blood lineage cells (**Figure 1F, and Online Supplementary Figure S1K, M**). These results show constitutive and restricted expression of ZBP1 in myeloma PC as well as in late GCB cells and normal PC.

ZBP1 is required for optimal T-cell-dependent humoral immune responses in mice

Consistent with a conserved expression pattern, a previous transcriptome analysis of murine B-cell development identified *Zbp1* as one of the signature genes that define transition from follicular B-cells to plasmablasts and mature PC⁴ (**Online Supplementary Figure S2**). To determine the role of ZBP1 in GCB and PC development, we assessed the humoral immune responses against the T-cell-dependent antigen NP-KLH using alum as adjuvant. We found that while *Zbp1* mRNA is undetectable in fluorescence-activated cell sorting (FACS)-purified GCB cells and PC from *Zbp1*^{-/-} mice in response to either NP-KLH-alum or alum-only control, it

increased from GCB cells to PC in wild type (WT) littermates and this increase was more pronounced upon immunization with NP-KLH-alum (**Figure 2A**).

Splenic frequency of B220⁺CD19⁺GL7⁺CD95⁺ GCB cells (**Figure 2B, C**) and B220^{lo}CD138⁺ PC (**Figure 2D, E**) showed no baseline differences between *Zbp1*^{-/-} and their WT littermates. Similarly GCB cell frequency was not significantly different in WT and *Zbp1*^{-/-} animals after NP-KLH-alum immunization; however, the increase in PC frequency and NP-KLH-specific IgG (but not IgM) serum levels in immunised *Zbp1*^{-/-} animals was significantly lower as compared to immunised WT littermates (**Figure 2D-G**). These findings suggest that although *Zbp1* is not required for GCB cell and PC development under steady-state, it is required for optimal T-cell-dependent humoral immune responses. Whether cellular NA in complex with *Zbp1* play a role in this process remains to be addressed.

ZBP1 is required for myeloma cell proliferation and survival

To investigate the functional role of ZBP1 in MM, we depleted ZBP1 expression in MMCL by targeting both of its main isoforms, i.e., isoform 1 comprising Z α 1 and Z α 2 domains and isoform 2 which lacks Z α 1. Depletion of either isoform 1 or both isoforms 1 and 2 by shRNA1- or shRNA2-mediated knockdown respectively was toxic to H929 and U266 cells while shRNA3 did not deplete ZBP1 and behaved like scramble control without affecting cell viability (**Figure 3A and Online Supplementary Figure S3A-C**). Depletion of ZBP1 by shRNA1/2 was also toxic to MMCL MM.1S and its dexamethasone-resistant derivative MM.1R cells (**Figure 3B and Online Supplementary Figure S3D**). These findings suggest that the observed

effect is mediated by depletion of isoform 1 and cannot be rescued by isoform 2. This effect was specific because the anti-proliferative function was not observed in the shRNA-transduced erythromyeloid K562 or epithelial HeLa cells (**Figure 3C**) which lack ZBP1 expression (**Online Supplementary Figure S1F, 3E**). Further, depletion of shRNA1-transduced myeloma cells was at least in part rescued by overexpression of *ZBP1* cDNA with appropriate silent mutations (**Online Supplementary Figure S3F**). Mutating the seed region of shRNA1, aimed at eliminating off-target effects,³⁵ neither altered the expression of ZBP1 nor cytotoxic effects in MM.1S cells (**Online Supplementary Figure S3G, H**). Using a doxycycline-inducible shRNA,³⁶ we found that ZBP1 depletion inhibited myeloma cell growth *in vitro* (**Online Supplementary Figure S3I, J**) and also subcutaneous myeloma tumor growth *in vivo* (**Figure 3D, E and Online Supplementary Figure S3K, L**). Together, these findings suggest an important role of ZBP1 in myeloma cell biology.

In line with these observations, transcriptome analysis of two ZBP1-depleted MMCL, in which oncogenic transcriptomes are driven by MAF (MM.1S) or MMSET (H929) oncogenes, revealed that 270 genes that are significantly downregulated in both cells and by both shRNAs (**Figure 3F, G and Online Supplementary Table S1**). These genes were highly enriched for cell cycle control pathways (**Figure 3H and Online Supplementary Table S2**).

Further, we validated reduction of the mRNA expression levels of the cell cycle regulators Ki-67, FOXM1 and E2F1 upon ZBP1-depletion by qPCR (**Online Supplementary Figure S4A, B**) and also confirmed at the protein level by

immunoblotting (FOXM1 and E2F1) and flow-cytometry (Ki-67) (**Online Supplementary Figure S4C-E**). Flow-cytometric analysis of cell cycle in ZBP1-depleted cells revealed arrest at G0/G1 phase (**Figure 3I**) in conjunction with increased apoptosis as assessed by Annexin V staining in MM.1S and H929 cells (**Online Supplementary Figure S4F**). Notably, we also confirmed that both anti-ZBP1 shRNAs induce cell cycle arrest in MM patient-derived, BM myeloma CD138⁺ PC (**Figure 3J and Online Supplementary Figure S4G**) and thus confirming the role of ZBP1 in cell cycle regulation in primary myeloma PC as well as MMCL.

In addition to downregulation of the cell cycle pathways, Gene set enrichment analysis (GSEA) also showed significant enrichment for IFN type I pathway in upregulated genes induced by both shRNA1 and shRNA2 in MM.1S cells but in downregulated genes by only shRNA1 in H929 cells (**Online Supplementary Figure S4H**). This disparate effect of ZBP1 depletion on IFN type I response genes might reflect the distinct transcriptomes of MM.1S and H929 MMCL imposed by their primary driver oncogenes.

Previous work demonstrated that a transcriptional proliferative signature identifies a minority of MM patients with adverse prognosis.^{37,38} Accordingly, GSEA of myeloma PC transcriptomes with top 5% highest vs 90% lowest ZBP1 expression revealed significant enrichment in the former for cell cycle regulation pathways amongst over-expressed genes (**Online Supplementary Figure S4I, J and Online Supplementary Table S3**). Interestingly, amongst these over-expressed genes in ZBP1^{hi} patient subgroup, we also observed significant enrichment for IFN type I

signalling consistent with the role of ZBP1 as an IFN-response gene (**Online Supplementary Figure S4I, J and Online Supplementary Table S3**).

ZBP1 interaction with IRF3 and TBK1

We next investigated the downstream processes that might link constitutive ZBP1 expression in myeloma cells with regulation of cell cycle. Unlike in non-malignant cells in which IRF3 phosphorylation/activation requires activation of sensors such as cGAS-STING,^{14,16} we found that IRF3 was constitutively phosphorylated (pIRF3) in myeloma cell lines (**Figure 4A**). In line with previous reports,³⁹ pIRF3 was also detected in other non-myeloma cancer cells (**Figure 4A**). Importantly, pIRF3 was also detected in primary BM myeloma CD138⁺ PC (**Figure 4B**) and thus establishing that IRF3 is constitutively phosphorylated in MM.

Although the functional relationship of ZBP1-IRF3 interaction in the context of cellular innate immune responses is a matter of debate, ZBP1-IRF3 physical interaction was previously shown by their ectopic expression.^{17,40,40} Using protein co-immunoprecipitation assays we found that endogenous ZBP1 interacts with endogenous IRF3 (**Figure 4C, D**) and TBK1 (**Figure 4E**) in MM.1S cells. By co-transfection of *IRF3* cDNA with a full length or C-terminus deletion mutant of *ZBP1* (**Online Supplementary Figure S5A**), we found that ZBP1-IRF3 interaction requires the RHIM domain-containing C-terminus of ZBP1 (**Online Supplementary Figure S5B, C**). Further, while total IRF3 and TBK1 levels were not appreciably altered in ZBP1-depleted cells, pIRF3 and pTBK1 levels markedly decreased in both constitutive shRNA-transduced (**Figure 4F**) and dox-induced shRNAs targeting *ZBP1* (**Online**

Supplementary Figure S5D) in MM.1S cells. These findings suggest a post-translational dependency of IRF3 and TBK1 constitutive phosphorylation on ZBP1. Finally, shRNA-mediated depletion of TBK1 resulted in decrease of IRF3 phosphorylation (**Figure 4G**). Together these data support a model whereby ZBP1 serves as a scaffold for TBK1-dependent constitutive phosphorylation of IRF3 in MMCL.

IRF3 regulates cell cycle in myeloma cells

As observed for ZBP1, IRF3 depletion also induces cell cycle arrest and apoptosis and thereby inhibits myeloma cell growth (**Figure 4H, I and Online Supplementary Figure S6A-C**). Of note, similar effect was observed after depletion of TBK1 (**Online Supplementary Figure S6D-G**). In addition, transcriptome analysis of IRF3-depleted MM.1S cells revealed that amongst 185 genes downregulated by both anti-*IRF3* shRNA1 and shRNA2, 109 genes were also commonly downregulated upon ZBP1 depletion (**Figure 5A, B and Online Supplementary Table S4**) and these are also enriched for cell cycle regulation (**Figure 5C and Online Supplementary Table S5**). However, only 23 genes were shared amongst those upregulated upon depletion of ZBP1 or IRF3.

To identify candidate transcriptional targets of IRF3 in myeloma cells we generated and mapped its genome-wide binding by IRF3 ChIP-seq in MM.1S cells. IRF3-bound regions (promoter, intergenic and intronic; **Online Supplementary Figure S7A**) were highly enriched for IRF3 binding motifs (**Figure 5D**). In the same cells, we correlated genome-wide IRF3 binding with chromatin accessibility as assessed by ATAC-seq,

RNA Polymerase II binding, activating (H3K27ac and H3K4me1/2/3) and repressive (H3K27me3) histone marks (**Figure 5E**). This showed that IRF3 binding occurs in nearly 28000 highly accessible chromatin regions with activating transcriptional potential as revealed by Pol II binding and presence of activating histone marks. Thus, constitutively phosphorylated IRF3 in myeloma cells is highly transcriptionally active in the nucleus.

Next, to obtain the compendium of genes directly regulated by IRF3 in MM.1S cells, we integrated the IRF3-depleted transcriptome for each anti-IRF3 shRNA with the IRF3 cistrome using BETA-plus software (**Figure 5F and Online Supplementary Figure S7D**). After intersection of anti-IRF3 shRNA1 and shRNA2 data, we found that the 770 genes predicted to be directly activated by IRF3, included the key cell cycle regulators *E2F1*, *E2F2*, *AURKB*, *CCNE1*, *MKI67* and MCM2–7 complex (**Figure 5G and Online Supplementary Figure S7E, F and Online Supplementary Table S6**), and were significantly enriched for cell cycle regulation pathways (**Online Supplementary Figure S7B and Online Supplementary Table S7**). Notably, the 339 genes predicted to be repressed by IRF3 were not enriched for IFN type I response genes (**Figure 5F and Online Supplementary Figure S7C and Online Supplementary Table S6, 7**). Consistent with this, while IRF3 binds in the regulatory regions of *IFNA1* (but not of *IFNB1*) and *ISG15*, that are hallmark type I IFN response genes, expression of these genes was not altered upon IRF3 depletion (**Online Supplementary Figure S7G, H**).

IRF3 regulates transcription of and co-operates with IRF4 to regulate cell cycle in myeloma cells

IRF4 is a transcription factor critical for normal PC development³⁴ while in myeloma PC it co-operates with MYC to establish a transcriptional circuitry to which myeloma cells are highly addicted.⁴¹ Since the IRF4 motif was amongst the top-most enriched regions bound by IRF3 (**Figure 5D**), we explored potential synergy between IRF3 and IRF4 by overlaying our in-house-generated genome-wide binding profile of IRF3 with that of previously published IRF4 ChIP-seq in MM.1S cells.⁴² First, we observed co-binding of the two transcription factors at the promoter and the previously established super-enhancer of IRF4⁴³ (**Figure 6A**). This observation and the fact that *IRF4* expression is significantly downregulated following IRF3 as well as ZBP1 depletion (**Figure 6B**) suggested that *IRF4* transcriptional regulation is, at least in part, under control of the ZBP1-IRF3 axis.

At a genome-wide level, 21614 IRF3-bound chromatin regions were co-bound by IRF4 (**Figure 6C, D**). Correlating these with transcriptome changes following IRF3 depletion, we identified 612 and 267 genes predicted to be co-activated or co-repressed respectively by both IRF3 and IRF4 (**Figure 6D, E**) with the former highly enriched in cell cycle regulators (**Figure 6F and Online Supplementary Table S8, 9**). To validate this on-chromatin association of IRF3 with IRF4, we performed ChIP-re-ChIP assays at IRF3-IRF4 co-binding regions using a region upstream of *IRF4* where no binding of either transcription factor was observed as a negative control. In all tested regions we found specific co-occupancy of IRF3 and IRF4 including at the *IRF4* promoter and super-enhancer regions (**Figure 6G, H**) and also at genes regulating cell cycle including *E2F1*, *E2F2*, *MCM2* and *AURKB* (**Online Supplementary Figure S8A, B**).

Discussion

Here we demonstrate that the Z-nucleic acid sensor ZBP1 is an important and novel determinant of MM biology. We link the myeloma-selective constitutive expression of ZBP1 to constitutive IRF3 activation and regulation of IRF3-dependent IRF4 expression and myeloma cell proliferation.

While other NA sensors e.g., cGAS-STING are expressed constitutively and are activated upon NA binding,^{14,16} ZBP1 differs in that as its expression is only detected in response to NA, viral pathogens or inflammatory stimuli including IFNs.^{17,8,20,44} Our extensive analysis confirmed that ZBP1 expression is low or not detected in all human normal and cancer cells tested with the striking exception of cells in the late B-cell development trajectory and in particular PC. Reflecting their cell of origin, we found constitutive ZBP1 expression also in MMCL and primary myeloma PC.

While our data does not address the molecular role of Zbp1 in late B-cell development, at cellular level it identifies suboptimal humoral immune response to a T-cell-dependent antigen in *Zbp1*^{-/-} mice. Of note, in contrast to our results, Ab levels in *Zbp1*^{-/-} mice were previously found to be intact in response to DNA vaccination;¹⁸ the different routes and process of immunisation might account for these differences.

We found that ZBP1 depletion had a profound and selective effect on MMCL proliferation and survival *in vitro* and *in vivo*. Similarly, in primary myeloma PC which

are less proliferative than MMCL, depletion of ZBP1 also induced cell cycle arrest. Based on appropriate design of *ZBP1*-targeting shRNA we could determine that myeloma cell proliferation is sustained by the isoform 1 that retains both Z α 1 and Z α 2 domains but not isoform 2 that retains only Z α 2 domain. Future research will explore the nature and origin of NA that are bound by the Z α domain and their impact on the pro-proliferative function of ZBP1 in myeloma cells.

Transcriptomes of ZBP1-depleted myeloma cells, that are driven by distinct primary oncogenes i.e., MAF (MM.1S cells) and MMSET (H929 cells), highlighted cell cycle regulation as one of the main pathways regulated by ZBP1. This novel pro-proliferative function of ZBP1 contrasts with the anti-proliferative potential of IFN β which can induce and sustain expression of ZBP1.^{45,20} However, although GSEA suggested that ZBP1 mediates repression of IFN type I response in ZBP1-depleted MM.1S cells, study of a large number of primary myeloma PC transcriptomes revealed a strong IFN type I response transcriptional signature as well as enrichment for cell cycle pathways amongst upregulated genes in ZBP1^{hi} myeloma PC. Together, these findings are consistent with a model whereby an active IFN type I response restrains myeloma PC proliferation in the low proliferative early phase myeloma PC but sustains ZBP1 expression which exerts a limited pro-proliferative function. In contrast, while the IFN type I transcriptional programme is attenuated or even repressed in the highly proliferative MMCL such as MM.1S cells, that are representative of advanced MM,^{21,46} persistent ZBP1 expression regulates proliferation that is not constrained by IFN type I response. In line with this model, a recent comparison of primary myeloma PC and MMCL transcriptomes demonstrated

enrichment for IFN type I response gene signature in myeloma PC in >700 MM patients at diagnosis while proliferative but not IFN type I gene signatures were dominant in relapsed disease myeloma PC and in MMCL.²¹

The physiological roles of ZBP1 is to promote necroptosis and inflammation through interaction with RIPK3 in response to pathogen or cellular dsRNA.^{47,10,12} While interaction of ZBP1 with IRF3 and TBK1 has been previously shown in an ectopic expression system,^{17,40} whether it regulates type I IFN response has been disputed.¹⁸ Here we confirmed direct and functional interactions of endogenous ZBP1-IRF3-TBK1 in myeloma cells that highlight ZBP1 as a physical platform that directs activation of TBK1 and IRF3.

While transcriptional activation by phosphorylation of IRF3 in response to inflammatory stimuli is expected to be transient, we find that IRF3 is constitutively phosphorylated in myeloma cells both primary and cell lines. This is not unique to MM since constitutively phosphorylated IRF3 has been reported in several ZBP1-negative cancer lines³⁹ but not functionally investigated although a pro-proliferative effect of IRF3 has been reported in acute myeloid leukaemia cells at cellular level.⁴⁸ Importantly, we demonstrate that IRF3 binds to transcriptionally active regions of the genome and it directly regulates genes that promote cell cycle progression in myeloma cells. Accordingly, IRF3 depletion in myeloma cells leads to cell cycle arrest and apoptosis.

We also show that TBK1 depletion results in cell cycle arrest and apoptosis in myeloma cells. Although this cellular effect is likely linked to downstream regulation of cell cycle genes by pIRF3, other mechanisms are also possible since TBK1 is a pleiotropic kinase.⁴⁹

IRF4, the lineage-defining transcription factor in PC development,³⁴ establishes an aberrant transcriptional circuitry with MYC that renders myeloma PC highly dependent on an oncogenic programme that includes activation of cell cycle amongst other pathways.⁴¹ Here, based on IRF3 binding to the super-enhancer and promoter of IRF4 and the fact that depletion of IRF3 (also ZBP1) results in significant *IRF4* downregulation we demonstrate direct transcriptional activation of IRF4 by IRF3. Indeed, since as little as 50% reduction in *IRF4* expression levels is toxic to myeloma cells,⁴¹ the >50% reduction in *IRF4* mRNA induced by IRF3-depletion would be expected to contribute significantly to myeloma cell death. Our genome-wide and sequential ChIP assays demonstrate and validate extensive co-occupancy of IRF3 and IRF4 in the myeloma regulatory genome including at the super-enhancer of IRF4, and the genes involved in cell cycle control being amongst the targets of the IRF3-IRF4 synergy.

In summary, our data show that like other NA sensors, ZBP1 can regulate cellular pathways critical for cancer biology. We show a constitutively active ZBP1-IRF3 axis that is co-opted into promoting proliferative pathways in myeloma PC and regulating expression of the critical myeloma oncogene IRF4. Guided by our initial delineation of the structural requirements of the ZBP1-IRF3 interaction in myeloma cells,

disruption of the ZBP1-IRF3 axis will offer an opportunity for targeted and relatively selective therapeutic intervention in MM.

References

1. Palumbo A, Anderson K. Multiple myeloma. *N Engl J Med*. 2011;364(11):1046-1060.
2. Morgan GJ, Walker BA, Davies FE. The genetic architecture of multiple myeloma. *Nat Rev Cancer*. 2012;12(5):335-348.
3. Manier S, Salem KZ, Park J, Landau DA, Getz G, Ghobrial IM. Genomic complexity of multiple myeloma and its clinical implications. *Nat Rev Clin Oncol*. 2017;14(2):100-113.
4. Shi W, Liao Y, Willis SN, et al. Transcriptional profiling of mouse B cell terminal differentiation defines a signature for antibody-secreting plasma cells. *Nat Immunol*. 2015;16(6):663-673.
5. Ha SC, Kim D, Hwang H-Y, Rich A, Kim Y-G, Kim KK. The crystal structure of the second Z-DNA binding domain of human DAI (ZBP1) in complex with Z-DNA reveals an unusual binding mode to Z-DNA. *Proc Natl Acad Sci U S A*. 2008;105(52):20671-20676.
6. Schwartz T, Behlke J, Lowenhaupt K, Heinemann U, Rich A. Structure of the DLM-1–Z-DNA complex reveals a conserved family of Z-DNA-binding proteins. *Nat Struct Biol*. 2001;8(9):761-765.
7. Maelfait J, Liverpool L, Bridgeman A, Ragan KB, Upton JW, Rehwinkel J. Sensing of viral and endogenous RNA by ZBP1/DAI induces necroptosis. *EMBO J*. 2017;36(17):2529-2543.
8. Thapa RJ, Ingram JP, Ragan KB, et al. DAI Senses Influenza A Virus Genomic RNA and Activates RIPK3-Dependent Cell Death. *Cell Host Microbe*. 2016;20(5):674-681.

9. Sridharan H, Ragan KB, Guo H, et al. Murine cytomegalovirus IE3-dependent transcription is required for DAI/ZBP1-mediated necroptosis. *EMBO Rep.* 2017;18(8):1429-1441.
10. Upton JW, Kaiser WJ, Mocarski ES. DAI/ZBP1/DLM-1 complexes with RIP3 to mediate virus-induced programmed necrosis that is targeted by murine cytomegalovirus vIRA. *Cell Host Microbe.* 2012;11(3):290-297.
11. Newton K, Wickliffe KE, Maltzman A, et al. RIPK1 inhibits ZBP1-driven necroptosis during development. *Nature.* 2016;540(7631):129-133.
12. Lin J, Kumari S, Kim C, et al. RIPK1 counteracts ZBP1-mediated necroptosis to inhibit inflammation. *Nature.* 2016;540(7631):124-128.
13. Jiao H, Wachsmuth L, Kumari S, et al. Z-nucleic-acid sensing triggers ZBP1-dependent necroptosis and inflammation. *Nature.* 2020;580(7803):391-395.
14. Tanaka Y, Chen ZJ. STING specifies IRF3 phosphorylation by TBK1 in the cytosolic DNA signaling pathway. *Sci Signal.* 2012;5(214):ra20.
15. Ablasser A, Goldeck M, Cavlar T, et al. cGAS produces a 2',5'-linked cyclic dinucleotide second messenger that activates STING. *Nature.* 2013;498(7454):380-384.
16. Mankan AK, Schmidt T, Chauhan D, et al. Cytosolic RNA:DNA hybrids activate the cGAS-STING axis. *EMBO J.* 2014;33(24):2937-2946.
17. Takaoka A, Wang Z, Choi MK, et al. DAI (DLM-1/ZBP1) is a cytosolic DNA sensor and an activator of innate immune response. *Nature.* 2007;448(7152):501-505.
18. Ishii KJ, Kawagoe T, Koyama S, et al. TANK-binding kinase-1 delineates innate and adaptive immune responses to DNA vaccines. *Nature.* 2008;451(7179):725-729.

19. Yang D, Liang Y, Zhao S, et al. ZBP1 mediates interferon-induced necroptosis. *Cell Mol Immunol.* 2020;17:356-368.
20. Kuriakose T, Man SM, Malireddi RKS, et al. ZBP1/DAI is an innate sensor of influenza virus triggering the NLRP3 inflammasome and programmed cell death pathways. *Sci Immunol.* 2016;1(2):aag2045.
21. Sarin V, Yu K, Ferguson ID, et al. Evaluating the efficacy of multiple myeloma cell lines as models for patient tumors via transcriptomic correlation analysis. *Leukemia.* 2020;34(10):2754–2765.
22. Dobin A, Davis CA, Schlesinger F, et al. STAR: ultrafast universal RNA-seq aligner. *Bioinformatics.* 2013;29(1):15-21.
23. Patro R, Duggal G, Love MI, Irizarry RA, Kingsford C. Salmon provides fast and bias-aware quantification of transcript expression. *Nat Methods.* 2017;14(4):417-419.
24. Love MI, Huber W, Anders S. Moderated estimation of fold change and dispersion for RNA-seq data with DESeq2. *Genome Biol.* 2014;15(12):550.
25. Ritchie ME, Phipson B, Wu D, et al. limma powers differential expression analyses for RNA-sequencing and microarray studies. *Nucleic Acids Res* 2015;43(7):e47.
26. Zhang Y, Liu T, Meyer CA, et al. Model-based analysis of ChIP-Seq (MACS). *Genome Biol.* 2008;9(9):R137.
27. Ramírez F, Ryan DP, Grüning B, et al. deepTools2: a next generation web server for deep-sequencing data analysis. *Nucleic Acids Res.* 2016;44(W1):W160-165.
28. Thorvaldsdóttir H, Robinson JT, Mesirov JP. Integrative Genomics Viewer (IGV): high-performance genomics data visualization and exploration. *Brief Bioinform.* 2013;14(2):178-192.

29. Heinz S, Benner C, Spann N, et al. Simple combinations of lineage-determining transcription factors prime cis-regulatory elements required for macrophage and B cell identities. *Mol Cell*. 2010;38(4):576-589.
30. Wang S, Sun H, Ma J, et al. Target analysis by integration of transcriptome and ChIP-seq data with BETA. *Nat Protoc*. 2013;8(12):2502-2515.
31. Subramanian A, Tamayo P, Mootha VK, et al. Gene set enrichment analysis: a knowledge-based approach for interpreting genome-wide expression profiles. *Proc Natl Acad Sci U S A*. 2005;102(43):15545-15550.
32. Kuleshov MV, Jones MR, Rouillard AD, et al. Enrichr: a comprehensive gene set enrichment analysis web server 2016 update. *Nucleic Acids Res*. 2016;44(W1):W90-97.
33. Cattoretti G, Shaknovich R, Smith PM, Jäck H-M, Murty VV, Alobeid B. Stages of germinal center transit are defined by B cell transcription factor coexpression and relative abundance. *J Immunol*. 2006;177(10):6930-6939.
34. Ochiai K, Maienschein-Cline M, Simonetti G, et al. Transcriptional Regulation of Germinal Center B and Plasma Cell Fates by Dynamical Control of IRF4. *Immunity*. 2013;38(5):918-929.
35. Buehler E, Chen Y-C, Martin S. C911: A Bench-Level Control for Sequence Specific siRNA Off-Target Effects. *PLoS One*. 2012;7(12):e51942.
36. Zuber J, McJunkin K, Fellmann C, et al. Toolkit for evaluating genes required for proliferation and survival using tetracycline-regulated RNAi. *Nat Biotechnol*. 2011;29(1):79-83.
37. Laganà A, Perumal D, Melnekoff D, et al. Integrative network analysis identifies novel drivers of pathogenesis and progression in newly diagnosed multiple myeloma. *Leukemia*. 2018;32(1):120-130.
38. Kuiper R, Broyl A, de Knecht Y, et al. A gene expression signature for high-risk multiple myeloma. *Leukemia*. 2012;26(11):2406-2413.

39. Muvaffak A, Pan Q, Yan H, et al. Evaluating TBK1 as a Therapeutic Target in Cancers with Activated IRF3. *Mol Cancer Res.* 2014;12(7):1055-1066.
40. Wang Z, Choi MK, Ban T, et al. Regulation of innate immune responses by DAI (DLM-1/ZBP1) and other DNA-sensing molecules. *Proc Natl Acad Sci U S A.* 2008;105(14):5477-5482.
41. Shaffer AL, Emre NCT, Lamy L, et al. IRF4 addiction in multiple myeloma. *Nature.* 2008;454(7201):226-231.
42. Zheng R, Wan C, Mei S, et al. Cistrome Data Browser: expanded datasets and new tools for gene regulatory analysis. *Nucleic Acids Res.* 2019;47(D1):D729-D735.
43. Jin Y, Chen K, De Paepe A, et al. Active enhancer and chromatin accessibility landscapes chart the regulatory network of primary multiple myeloma. *Blood.* 2018;131(19):2138-2150.
44. Kesavardhana S, Malireddi RKS, Burton AR, et al. The Z α 2 domain of ZBP1 is a molecular switch regulating influenza-induced PANoptosis and perinatal lethality during development. *J Biol Chem.* 2020;295(24): 8325-8330.
45. Yang D, Liang Y, Zhao S, et al. ZBP1 mediates interferon-induced necroptosis. *Cell Mol Immunol.* 2020;17(4):356-368.
46. Hose D, Rème T, Hielscher T, et al. Proliferation is a central independent prognostic factor and target for personalized and risk-adapted treatment in multiple myeloma. *Haematologica.* 2011;96(1):87-95.
47. Rebsamen M, Heinz LX, Meylan E, et al. DAI/ZBP1 recruits RIP1 and RIP3 through RIP homotypic interaction motifs to activate NF-kappaB. *EMBO Rep.* 2009;10(8):916-922.
48. Tian W-L, Jiang Z-X, Wang F, et al. IRF3 is involved in human acute myeloid leukemia through regulating the expression of miR-155. *Biochem Biophys Res Commun.* 2016;478(3):1130-1135.

49. Pillai S, Nguyen J, Johnson J, Haura E, Coppola D, Chellappan S. Tank binding kinase 1 is a centrosome-associated kinase necessary for microtubule dynamics and mitosis. *Nat Commun.* 2015;6(1):1-14.
50. Quinlan AR, Hall IM. BEDTools: a flexible suite of utilities for comparing genomic features. *Bioinformatics.* 2010;26(6):841-842.

Figure legends

Figure 1: Restricted and constitutive ZBP1 expression in normal and myeloma plasma cells

(A) *ZBP1* mRNA expression as assessed in 4 MMCL and in the erythromyeloid cell line K562 by qPCR (n=3; data shown as mean \pm standard error of mean-SEM).

(B) ZBP1 expression in indicated MMCL as assessed by immunoblotting using GAPDH as loading control. Two main isoforms \sim 48 and \sim 40 kDa are detected in MMCL.

(C, D) ZBP1 mRNA and protein expression in 6 myeloma patient-derived bone marrow PC purified for CD138+ marker using CD138 immunomagnetic microbeads, and U266 MMCL shown as control.

(E) Immunohistochemistry on paraffin-embedded tonsil tissue section: Panel on the left depicts low and high magnification of a germinal center where expression of PAX5 and ZBP1 is mutually exclusive in most parts indicating ZBP1 expression in plasma cells that are negative for PAX5. Panel on the right depicts sub-epithelial tonsillar plasma cells showing co-expression of IRF4 (MUM.1) and ZBP1.

(F) Immunohistochemistry for ZBP1 expression in paraffin-embedded bone marrow tissue section of two MM patients.

Figure 2: ZBP1 is required for optimal T cell-dependent humoral immune responses in mice

(A) *Zbp1* mRNA levels as assessed by qPCR in FACS-purified splenic GCB (B220⁺CD19⁺GL7⁺CD95⁺) and PC (B220^{lo}CD138⁺) from *Zbp1*^{-/-} (KO) mice or their wildtype (WT) littermates immunised with just alum (control) or alum-NP-KLH (NP-

KLH) on day 10 post-immunization. Lack of *Zbp1* mRNA confirms *Zbp1*-deficiency in *Zbp1*^{-/-} mice. (n=3)

(B, C) Flow-cytometric identification of splenic GCB cells as B220⁺CD19⁺GL7⁺CD95⁺ and GCB frequency in *Zbp1*^{-/-} mice and their WT littermates immunised with NP-KLH or alum-only control on day 10 post-immunization (B) and GCB cell fold difference between WT and *Zbp1*^{-/-} mice after NP-KLH immunization normalised to median frequency of control animals (C). Numbers in the flow cytometry plots represent % frequency. (n=11 mice/group)

(D, E) Flow-cytometric identification of splenic PC as B220^oCD138⁺ and PC frequency in *Zbp1*^{-/-} mice and their WT littermates in control and NP-KLH-immunised animals on day 10 post-immunization (D) and PC fold difference between WT and *Zbp1*^{-/-} mice after NP-KLH immunization normalised to median frequency of control animals (E). Numbers in the flow cytometry plots represent % frequency. (n=11 mice/group)

(F) NP-KLH-specific IgG responses in *Zbp1*^{-/-} mice and their WT littermates in control- and NP-KLH-immunised animals on day 10 post-immunization. IgG Ab relative levels (left panels) after NP-KLH immunization and their fold differences normalised to median Ab levels of control animals (right panels). (n=6 mice/group)

(G) NP-KLH-specific IgM responses in *Zbp1*^{-/-} mice and their WT littermates in control- and NP-KLH-immunised animals on day 10 post-immunization. IgM Ab relative levels (left panels) after NP-KLH immunization and their fold differences normalised to median Ab levels of control animals (right panels). (n=6 mice/group)

The error bars of all the cumulative data indicate mean ± SEM. Two-tailed unpaired t-test was applied to determine the P values. * p ≤ 0.05, ** p ≤ 0.01, *** p ≤ 0.001,

**** $p \leq 0.0001$, ns- not significant ($p > 0.05$). The number of experiments performed or animals used for the study are indicated separately in each figure legend.

Figure 3: ZBP1 is required for myeloma cell proliferation and survival

(A) %GFP+ cells after transduction with GFP-encoding, *ZBP1*-targeting shRNA1 (sh1) or 2 (sh2) or shRNA3 (sh3) or appropriate scramble control (scr) lentiviral constructs in U266 and H929 cells. All the time points were normalised to day 3 %GFP expression levels for each shRNA or scr control shown. (n=3)

(B) %GFP+ cells after the transduction with *ZBP1*-targeting shRNA1 (sh1) or 2 (sh2) or appropriate scramble control (scr) lentiviral constructs in dexamethasone sensitive MM.1S and its resistant derivative MM.1R cells. All the time points were normalised to day 3 %GFP expression levels for each shRNA or scr control shown. (n=3)

(C) %GFP+ cells after the transduction of K562 and HeLa cells, that do not express *ZBP1*, with *ZBP1*-targeting sh1 or sh2 or appropriate scr control. The %GFP+ cells were normalised to day 3 %GFP expression levels for all the time points for each shRNA or scr control shown. (n=3)

(D, E) Photographs of tumors explanted at sacrifice from control (i.e., non-Dox-treated) or Dox-treated animals engrafted with H929 myeloma cells transduced with Dox-inducible sh1 or sh2 targeting *ZBP1* (D). Subcutaneous tumor volume of H929 or MM.1S over a period of up to 4 weeks in control or Dox-treated animals (D, E). (n=4-5 mice/group)

(F) RNA-seq was performed with poly(A) tail-enriched RNA from FACS-purified GFP+ live cells of scr or shRNA-transduced cells. Venn diagram showing number of commonly and differentially (up- and down-regulated) expressed genes based on

log₂ fold change to scramble control with cut-off adjusted P-value (p adj) <0.05 among the two *ZBP1*-depleted transcriptomes of MMCL H929 and MM.1S and both anti-ZBP1 sh1 or sh2. (n=2)

(G) Heatmap shows the expression patterns of the top 289 commonly and differentially expressed genes, based on log₂ fold change to scramble control with cut off p adj <0.05, shared by the two *ZBP1*-depleted MMCL H929 and MM.1S and both anti-ZBP1 sh1 or sh2.

(H) Enrichr pathway enrichment analysis of the shared 270 genes that are commonly downregulated between two MMCL treated with anti-*ZBP1* shRNA1 or shRNA2 as compared to scramble control.

(I) A representative histogram shows depletion of ZBP1 by anti-ZBP1 shRNA1 or shRNA2 induces cell cycle arrest in MMCL H929 as compared to scramble control, and its cumulative data shown for MMCL H929 and MM.1S cells. Analysis was performed on GFP+ cells on day 4 post-transduction. (n=3)

(J) A representative histogram shows anti-ZBP1 shRNA1- or shRNA2-mediated ZBP1 depletion induces cell cycle arrest as compared to scr control in MM patient-derived bone marrow myeloma cells purified for CD138+ marker, and its quantitative data. Flow cytometry plot on top shows gating strategy for GFP+ population in transduced cells. Analysis was performed on GFP+ cells on day 4 post-transduction. (n=3 MM BM samples)

The error bars of all the cumulative data indicate mean ± SEM. Two-tailed unpaired t-test was applied to determine the P values. * p≤ 0.05, ** p≤ 0.01, *** p≤0.001, ns- not significant (p> 0.05). The number of experiments performed are indicated separately in each figure legend.

Figure 4: ZBP1 as a scaffold for IRF3 constitutive activation by TBK1

(A) Immunoblotting analysis of pIRF3/IRF3 expression in myeloma (MM.1S and H929) and non-myeloma cell lines (K562; Jurkat; HL60: acute myeloid leukemia; DG75: B lineage; AR230: chronic myeloid leukemia; GM1271: EBV-transformed B cell lineage).

(B) Immunoblotting for pIRF3/IRF3 expression in MM patient-derived bone marrow PC purified for CD138+ using CD138 immunomagnetic microbeads.

(C, D) Immunoblotting against IRF3 and ZBP1 in MM.1S cells following co-immunoprecipitation with anti-ZBP1 (C), or anti-IRF3 (D) or corresponding isotype control antibodies.

(E) Immunoblotting against TBK1 and ZBP1 in MM.1S cells following co-immunoprecipitation with anti-ZBP1 or its corresponding isotype control antibodies.

(F) Immunoblotting for pIRF3/IRF3 expression in anti-ZBP1 shRNA1 or shRNA2 or scr transduced MM.1S cells on day 4 post-transduction (left), and imageJ quantification shows profound reduction in pIRF3 but not in total IRF3 levels in anti-ZBP1 sh1- or sh2-transduced cells as compared to scr control cells (right). The protein lysates were prepared from the cells with >90% transduction efficiency.

(G) Immunoblotting for pIRF3/IRF3 expression on day 4 following anti-*TBK1* shRNA1 (sh1) or 2 (sh2) or scr transduction in MM.1S cells. The protein lysates were prepared from the cells with >90% transduction efficiency.

(H) %GFP+ cells after transduction with *IRF3*-targeting shRNA1 or shRNA2 or scr control in MMCL H929 and MM.1S cells. All the time points were normalised to day 3 %GFP expression levels for each shRNA shown. (n=3)

(I) A representative flow-cytometric histogram of cell cycle in MMCL transduced with anti-*IRF3* shRNA1 or shRNA2 or scr control. Analysis was performed on GFP+ cells day 4 post-transduction and its cumulative data for H929 shows cell cycle arrest in anti-*IRF3* sh1- or sh2-transduced H929 cells. (n=3)

The error bars of all the cumulative data indicate mean \pm SEM. Two-tailed unpaired t-test was applied to determine the P values. * $p \leq 0.05$, ** $p \leq 0.01$, *** $p \leq 0.001$. The number of experiments performed for the study are indicated separately in each figure legend.

Figure 5: IRF3 regulates cell cycle genes in myeloma cells

(A) RNA-seq was performed with poly(A) tail-enriched RNA from FACS-purified GFP+ live cells of scr or shRNA-transduced cells. Venn diagram shows number of commonly up- and down-regulated genes among top 50% differentially expressed genes, based on log2 fold change to scramble control with cut-off $p \text{ adj} < 0.05$, of *ZBP1*-depleted and *IRF3*-depleted transcriptomes in MM.1S cells. (n=2)

(B) Heatmap shows the expression patterns of the top 132 commonly expressed genes among the top 50% differentially expressed genes of *ZBP1*-depleted and *IRF3*-depleted transcriptomes in MM.1S cells.

(C) Enrichr pathway enrichment analysis for the shared 109 genes that are commonly downregulated upon *ZBP1*- or *IRF3*-depletion in MM.1S cells.

(D) Transcription factor motif analysis of IRF3 ChIP-seq shows enrichment for IRF3-bound genomic regions in MM.1S cells. (IRF3 ChIP-seq; n=2).

(E) Metagene (top) and heatmap (bottom) representation of IRF3 genome-wide binding as assessed by IRF3 ChIP-seq in MM.1S cells along with indicated histone

marks, RNA Polymerase II (Pol II) binding and chromatin accessibility as assessed by ATAC-seq. Genomic feature annotation for each peak in the heatmap is shown on the left and the small color bar (below) indicates the genomic regions for 27868 binding regions annotated. IRF3 binding is observed in genomic regions marked for active transcription i.e., with increased chromatin accessibility, activating chromatin marks (H3K27ac, H3K4me1/3) and Pol II binding.

(F) Venn diagram showing number of genes predicted to be directly regulated (activated or repressed) by IRF3 in MM.1S cells as assessed by integration of IRF3 cistrome, IRF3 binding within 2kb distance to TSS, and *IRF3*-depleted transcriptome with cut off $p \text{ adj} < 0.05$ using BETA-plus software.

(G) IGV browser snapshots of IRF3 and Pol II binding, chromatin accessibility and histone mark enrichment at regulatory areas of several genes promoting cell cycle progression and cell proliferation. The red block on the top indicates 5kb genome size.

Figure 6: IRF3 co-operates with IRF4 and regulates cell cycle genes in myeloma cells

(A, B) IGV browser snapshots of IRF3 and IRF4 co-binding at the promoter and super-enhancer of *IRF4* as assessed by ChIP-seq (A) and \log_2 fold change of *IRF4* expression ($p \text{ adj} < 0.05$) assessed by RNA-seq after depletion of indicated mRNA/protein in relation to scr control in MM.1S cells (B).

(C) Heatmaps of IRF3 and IRF4 genome wide bindings, and common binding regions of IRF3 and IRF4 (intersection) as their binding regions are intersected by Bedtools Intersect.⁵⁰ Number of binding regions are shown within the brackets.

(D) Venn diagram showing number of genomic regions of IRF3 and IRF4 co-binding with gene regulatory potential as assessed by integration of whole transcriptome of *IRF3*-depleted MM.1S cells with IRF3- or IRF4-cistrome alone or IRF3 and IRF4 co-binding regions (intersection) in MM.1S cells. Here IRF4 genome-wide binding regions with very low scores were omitted and only top 50% binding regions with highest scores were used.

(E) Number of genes predicted to be directly co-regulated (repressed or activated) by IRF3 and IRF4 binding. The co-binding (intersection) regions were integrated with *IRF3*-depleted transcriptome by shRNA1 and shRNA2 in MM.1S cells.

(F) Enrichr pathway enrichment analysis for common genes predicted to be activated by IRF3-IRF4 co-binding.

(G) Primary ChIP-qPCR against IRF3 (left) followed by re-ChIP-qPCR against IRF4 (right). Position of amplicons is shown as horizontal coloured lines in Figure 6A.

(H) Primary ChIP-qPCR against IRF4 (left) followed by re-ChIP-qPCR against IRF3 (right). Position of amplicons is shown as horizontal coloured lines in Figure 6A.

Figure 1

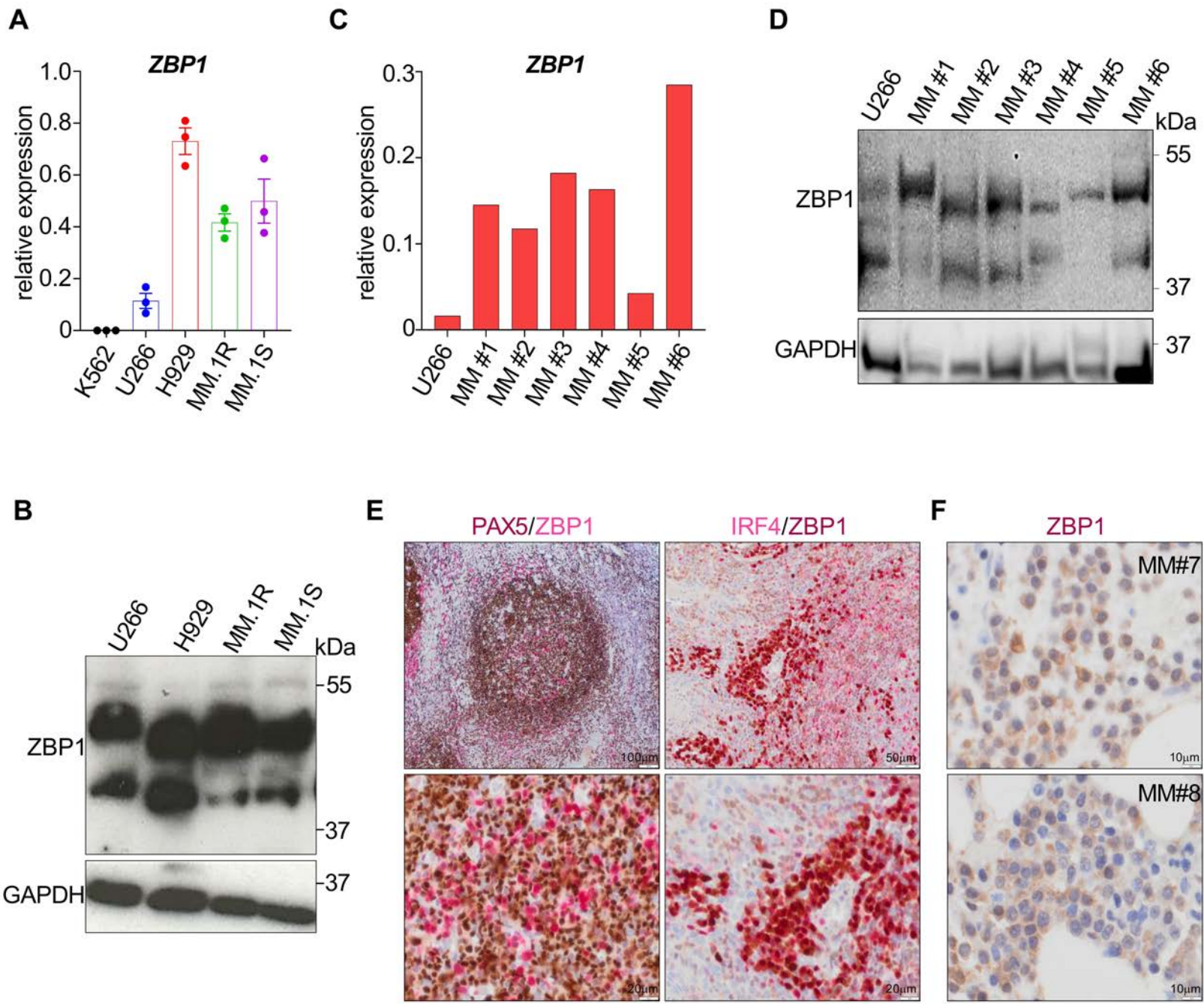


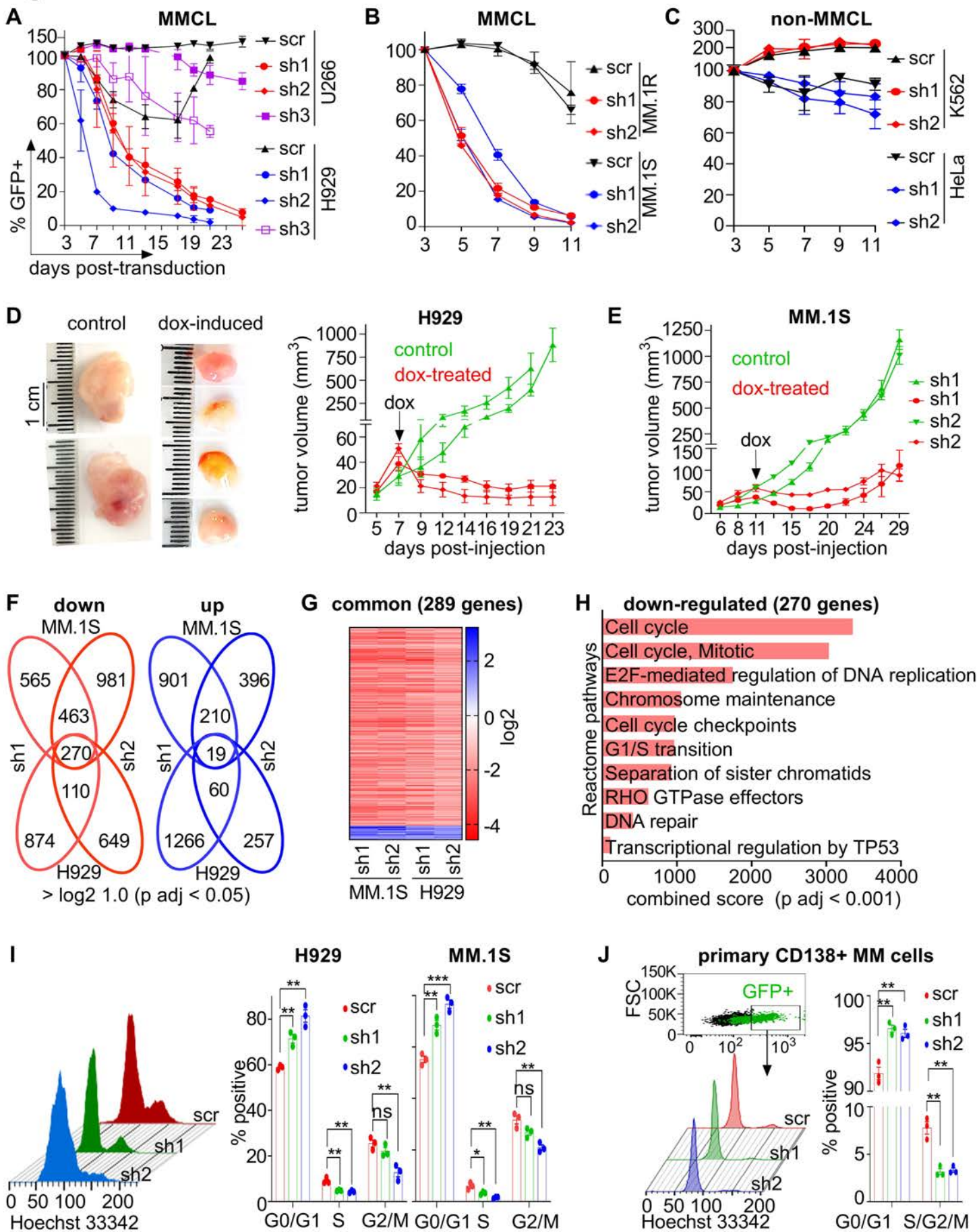
Figure 3

Figure 4

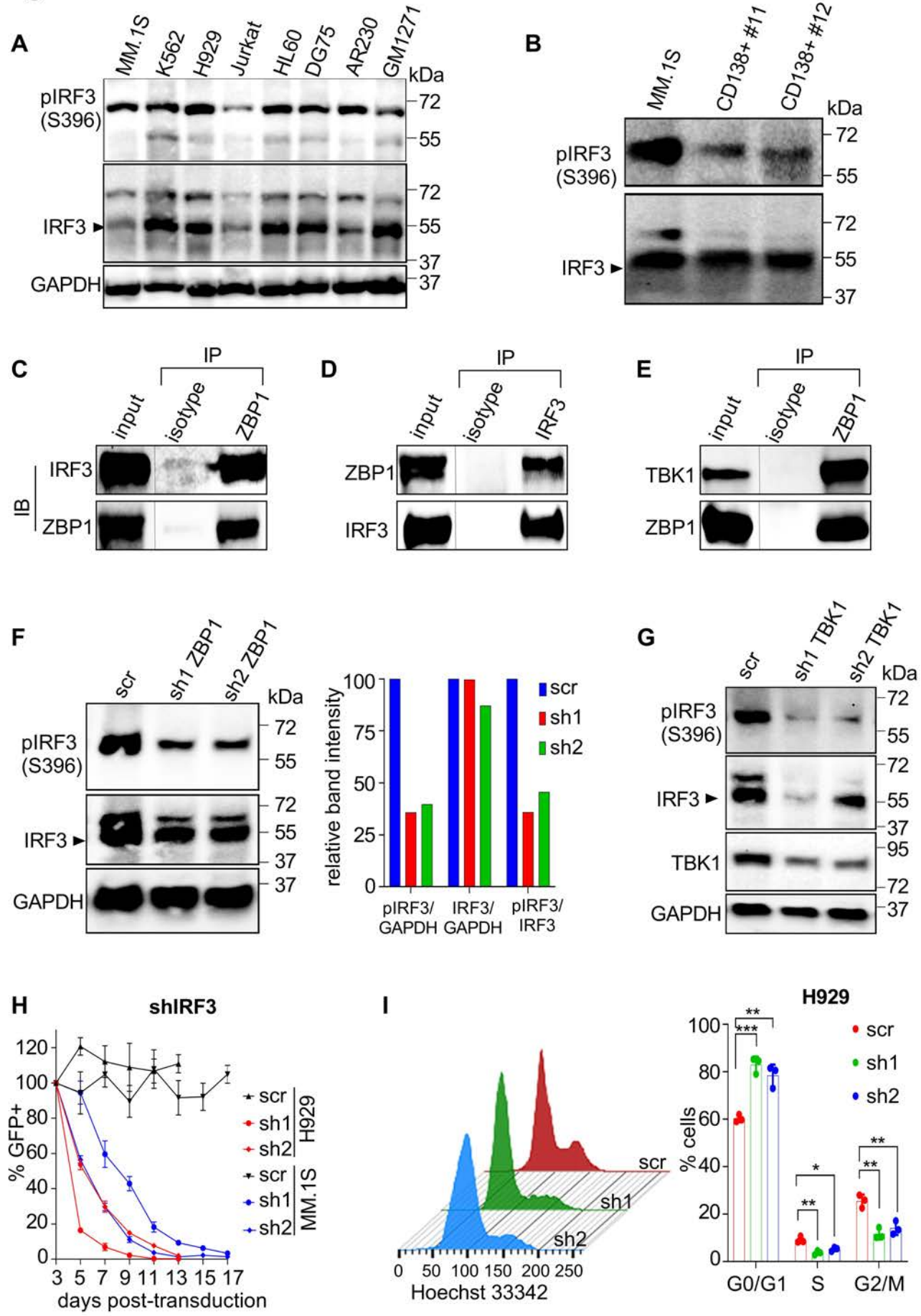


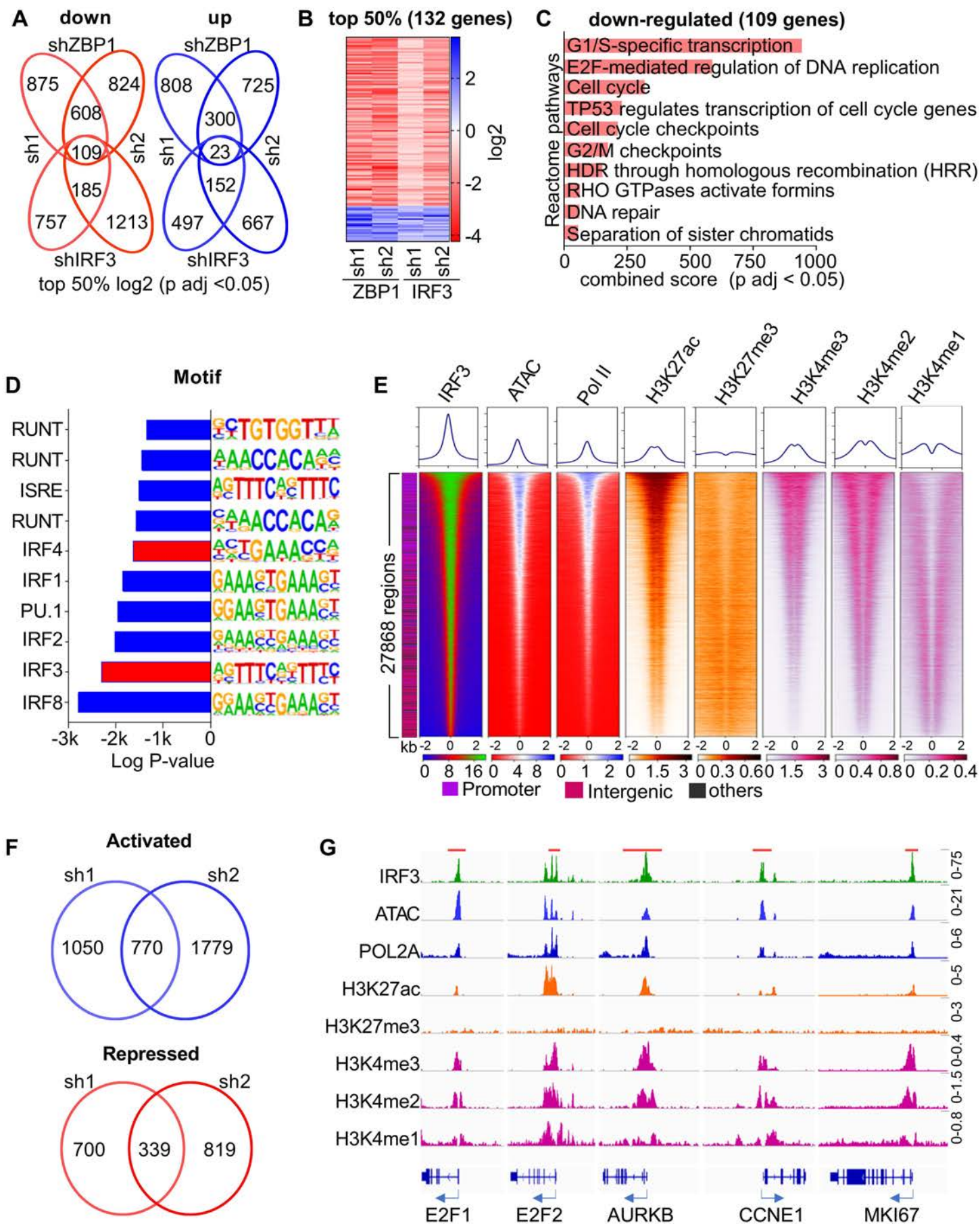
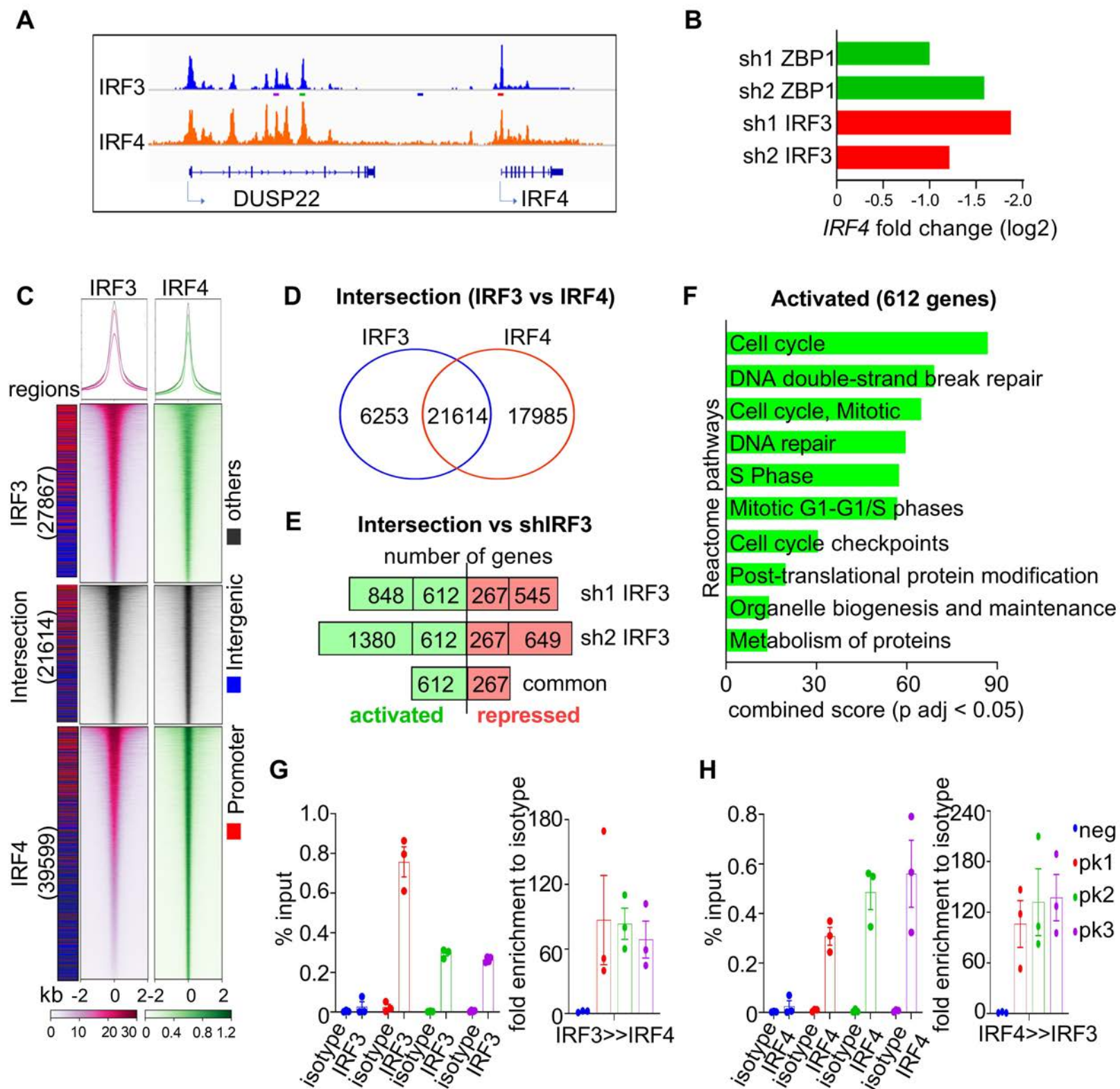
Figure 5

Figure 6



The innate sensor ZBP1-IRF3 axis regulates cell proliferation in multiple myeloma

Ponnusamy K et al.,

Supplementary methods

Cloning and lentiviral transduction

The puromycin selection gene was replaced with green fluorescent protein (eGFP) cDNA in Lentiviral pLKO.1 plasmid (Sigma). shRNA oligos (Sigma) were annealed by temperature ramp from 100°C to 25°C and cloned into pLKO.1 vector between AgeI and EcoRI sites. Doxycycline-inducible shRNAs were established using retroviral TRMPVIR vector (kind gift from Scott Lowe, Addgene plasmid #27994) as previously described.¹ ZBP1-full cDNA construct was kindly gifted by Stefan Rothenburg, University of California, USA.² The ZBP1 cDNA was amplified using forward (Forw): GGAATTCATGGCCCAGGCTCCTGCT and reverse (Rev): TAGCGGCCGCCTAAATCCCACCTCCCCA primers from pEGFPN.1 vector cloned into LeGO-iG2-IRES-EGFP vector (Addgene plasmid #27341) between EcoRI and NotI sites followed by 5 repeats of strep-tag II (TGGAGCCATCCGCAGTTTGAAAAA) sequences insertion between BamHI and EcoRI sites. ZBP1 ΔRHIM vector was constructed by amplifying strep-tagII-ZBP1 using forward: CCGGAATTAGGATCCATGTGGAGCCATCCG and reverse: TAGCGGCCGCCTAGGCTGACTTTGCTCTTC from LeGO-strep-tagII-ZBP1 full vector. The genetic rescue experiment was performed by co-expression of ZBP1 cDNA with silent mutation at shRNA1 binding regions 5'-CAAGAGGGAGCTCAA**TCAGGTATTATATAGAATGAAG**AAGGAGTTGAAAGTCTCCCT-3' (here gray indicates sh1 ZBP1 target site and bold indicates mutated sequences) using LeGO-iC2 (mCherry) plasmid (addgene #27345) and anti-ZBP1 shRNA1 in MM.1S cells. All viral particles were produced by calcium phosphate co-transfection of pRSV.REV, pMDLgpRRE and pMD2.VSVG (lentiviral) plasmids in HEK293T cells and concentrated by ultracentrifugation at 23,000 rpm for 100 minutes at 4°C. Myeloma and non-myeloma cells were treated with 8µg/ml polybrene (Sigma) and transduced with lentivirus by spinoculation at 2000 rpm, 37°C for 1hr followed by replacement of polybrene-media with appropriate culture media 24hr post-spinoculation.

shRNA sequences (5'-3')

scramble (scr): GGCCCTCCATCACAGTCTATA
sh1 ZBP1: CCAAGTCCTCTACCGAATGAA
sh2 ZBP1: GCACAATCCAATCAACATGAT
sh3 ZBP1: GCGGATCAATAGGTCAGGAAA
sh1 IRF3: GATGAGCTACGTGAGGCATGT
sh2 IRF3: CCCTTCATTGTAGATCTGATT
sh1 TBK1: GCAGAACGTAGATTAGCTTAT
sh2 TBK1: GCGGCAGAGTTAGGTGAAATT
sh1* ZBP1 seed control: CCAAGTCCTCCTGCGAATGAA

TRMPVIR-sh1 ZBP1 (5'-3')

TCGAGAAGGTATATTGCTGTTGACAGTGAGCGCCAAGTCCTCTACCGAATGAAATAGTGAA
GCCACAGATGTATTTCAATTCGGTAGAGGACTTGGTGCCTACTGCCTCGG

TRMPVIR-sh2 ZBP1 (5'-3')

TCGAGAAGGTATATTGCTGTTGACAGTGAGCGGCACAATCCAATCAACATGATTAGTGAAG
CCACAGATGTAATCATGTTGATTGGATTGTGCTGCCTACTGCCTCGG

qPCR primers (5'-3')

following primers used for ChIP and ChIP-re-ChIP

Negative: ACAGCCTAGCCCATGGATTT (Forw) and CAGCGTCCCTCATCCAGTTC (Rev)

Peak 1: TCTCAGTTTCACCGCTCGAT (Forw) and TCCTCTCTGGTATCAGCCTCA (Rev)

Peak 2: TCTGACCGTGCCCACTTTAG (Forw) and AACCTCCAACACCTGTGACT (Rev)

Peak 3: TGTTTGAAGCCAACCCAGAT (Forw) and CGCTCTTACACACCCGACTG (Rev)

E2F1: GTCTCGACTGCACCGACTTC (Forw) and GATCCGAATTTTCGCGGCAC (Rev)

E2F2: GTCTCGACTGCACCGACTTC (Forw) and GATCCGAATTTTCGCGGCAC (Rev)

MCM2: CTCCGTGTCCCTTCTGGTCG (Forw) and ACGATCCTCTCCGCCACTAC (Rev)

MCM3: AATCTCTCTGAGCCTCCCGC (Forw) and GTTCGGAAGTTTTTCGCGCC (Rev)

MCM4: CCCTAGCCAACGCTAGAGGA (Forw) and CCCGTGCGTAAACCAGAAGTA (Rev)

MCM5: GTTTTTCCCGCGAAACTCGG (Forw) and CCAACTACACCCGAAATCCA (Rev)

Taqman probe for mouse *Zbp1*: Mm01247052_m1

Human *ZBP1*: GCCAACAACGGGAGGAAGA (Forw); ATCTTCTGGGCGGTAAATCGT (Rev)
Human *E2F1*: GGA CTCTTCGGAGAACTTTCA (Forw); TGGTGGTGGTGACACTATGG (Rev)
Human *Ki-67*: CGTCCCAGTGGGAAGAGTTGT (Forw); CGACCCCGCTCCTTTTGATA (Rev)
Human *FOXM1*: TCTTTCTTTGTTTATCAGTGCTGC (Forw); CCCAGGCTGGATTTCTTCC
(Rev)

Antibodies for Co-IP

anti-ZBP1 (ThermoFisher Scientific; catalog number: PA5-20455), anti-V5-Tag (ThermoFisher Scientific; catalog number: 37-7500), anti-IRF3 (BioLegend; clone number: 12A4A35).

Total cell lysis buffer

250mM NaCl, 1.5mM MgCl₂, 20mM HEPES pH 7.4, 0.5mM EDTA, 1% IGEPAL CA-630, 1% Triton X-100, 0.1% SDS, 10mM of PMSF (Sigma) supplemented with 1x halt protease & phosphatase Inhibitor cocktail (Fisher scientific).

Antibodies for immunoblot

anti-ZBP1 (1:1000; ThermoFisher Scientific; catalog number: PA5-20455), anti-ZBP1 (1:1000; SantCruz Biotech; sc-67259), anti-IRF3 (1:500; BioLegend; clone number: 12A4A35), anti-TBK1 (1:1000; SantCruz Biotech; sc-52957), anti-pTBK1(ser172) (1:250; Cell Signalling Technolog; catalog number: 5483), anti-V5-tag (1:500; Cell Signalling Technology; catalog number:13202S), anti-pIRF3(S396) (1:500; ThermoFisher Scientific; Catalog number: 720012), GAPDH (1:2000; SantCruz Biotech; sc-47724).

Immunization

Zbp1^{-/-} animals,³ already cross-bred to C57BL/6 animals for 4-5 generations were obtained from Manolis Pasparakis, Institute of Genetics, Cologne, Germany. They were further cross-bred with wild type C57BL/6 mice for another three generations and their littermates used to study T-cell dependent humoral immune response to 4-Hydroxy-3-nitrophenylacetyl hapten conjugated to Keyhole Limpet Hemocyanin (NP-KLH) antigen (Santacruz Biotech). 6mg/kg NP-KLH prepared in Imject™ Alum Adjuvant (Thermoscientific) 3:1 ratio and injected intraperitoneally into 10-12 weeks old age-

matched *Zbp1*^{-/-} and wild type littermates. On day 4 post-immunization, 4mg/kg NP-KLH alone injected as booster dose and after 10 days post-immunization, blood samples were collected, and spleen was harvested. Single cell suspension of spleen cells were stained for B220 (BioLegend; clone: RA3-6B2), CD19 (BioLegend; clone: 6D5), CD95 (eBioscience; clone number: 15A7), GL7 (BioLegend; clone:GL7), CD138 (BioLegend; clone: 281-2) and analyzed for germinal center activated B cells (GCB), plasma cell (PC) development. GCB (B220⁺ CD19⁺ GL7⁺ CD95⁺) and PC (B220^{lo}CD138⁺) spleen cells were sorted using (FACS Aria), and total RNA was isolated and quantified *Zbp1* mRNA levels as described in qPCR methods. A standard ELISA method was used to quantify NP-KLH-specific IgG or IgM antibodies. Diluted (1:1000) serum samples used to detect levels of IgG by anti-IgG-HRP antibody (Bio-Techne) or IgM by anti-IgM-HRP antibody (Sigma) on 100µg/ml NP-KLH-coated plates. The antibody levels of immunized mice sera were normalized to their appropriate control alum-only immunized mice sera.

ChIP-seq and ChIP-re-ChIP

MM.1S cells were cross-linked with 1% formaldehyde (Alfa Aesar) at 10⁶ cells/ml density for 15min at room temperature with gentle mixing followed by addition of 0.125M Glycine to final volume for 5min at room temperature with gentle mixing. Cells were washed thrice with ice cold 1x PBS with 10mM phenylmethylsulfonyl fluoride (PMSF) and 10⁸ cells were lysed with hypotonic lysis buffer (10 mM Hepes-KOH, pH 7.8, 10 mM KCl, 0.1 mM EDTA, and 0.1% IGEPAL CA-630) for 15minutes on ice followed by centrifugation at 5000g for 5min. Further the cell pellet was lysed in nuclear lysis buffer (1% SDS, 50mM Tris-HCl pH 8.0, 10mM EDTA pH 8.0, 300mM NaCl supplemented with 1x halt protease & phosphatase Inhibitor cocktail (Fisher scientific) for 15min on ice. The lysate was diluted 10 times with dilution buffer (0.01% SDS, 1 % Triton X-100, 1mM EDTA, 50mM Tris-HCl pH 8.0, 150mM NaCl) and sonicated to shear the chromatin DNA up to 500bp size. The lysates were precleared with 50 µl protein A/G magnetic beads (Life Technologies) and then IRF3-bound chromatins were pulled overnight, rotating at 4°C with either 5µg IRF3 antibody (BioLegend, clone:12A4A35) or equivalent isotype control conjugated with protein A/G magnetic beads. Immunoprecipitated beads were washed twice with wash buffer A (0.1% SDS,

1% TritonX-100, 1mM EDTA, 10mM Trish-HCl pH 8.0, 150mM NaCl), buffer B (0.1% SDS, 1% TritonX-100, 1mM EDTA, 10mM Trish-HCl pH 8.0, 500mM NaCl) and buffer C (0.25M LiCl, 1% IGEPAL CA-630, 1% sodium deoxycholate, 1mM EDTA, 10mM Tris-HCl pH 8.0) for 5min, rotating at 4°C. The CHIP complex was treated with 10mg/ml RNase A, 20mg/ml proteinase K and reverse crosslinked with a buffer containing 1% SDS, 50mM Tris HCl pH 8.0, 4M NaCl, 1mM EDTA at 65°C overnight. CHIP DNA was collected with Ampure XP beads (Beckman) and quantified using Qubit High Sensitivity DNA kit (Life Technologies). 1ng of CHIP DNA was taken to prepare library using NEBNext kit for Illumina (New England Biolabs) following manufacturer's instructions and the quality or fragment size was assessed using the Bioanalyser High Sensitivity DNA kit (Agilent). 2nM of 400-500bp DNA library was sequenced using Illumina NextSeq500 platform to obtain paired-end 150bp reads.

For CHIP-reChIP, above protocol to pull IRF3 or IRF4-bound chromatin using IRF3 antibody (BioLegend, clone:12A4A35) or IRF4 antibody (BioLegend, clone: IRF4.3E4) and their equivalent isotype control respectively was followed. The chromatin was eluted in 1% SDS with 1x halt protease & phosphatase Inhibitor cocktail (Fisher Scientific) followed by 10 times dilution with elution buffer and repeated CHIP with the appropriate antibody. The CHIP-reChIP DNA was quantified using Qubit High Sensitivity DNA kit (Life Technologies) and quantified specific DNA fragments by qPCR.

Immunohistochemistry

Immunohistochemistry was undertaken on one-micron formalin-fixed paraffin-embedded tissue sections on Leica Bond III automated immunohistochemistry stainer. Prior to the procedure, paraffin sections were placed in oven preheated to 60°C for 30 minutes. Ready to use antibodies were used for PAX5 (clone number: PA0552; 15 minutes incubation) and MUM.1 (IRF4) (clone number: PA0129; 15 minutes incubation) antigens. Antibodies for ZBP1 (Sigma-Aldrich; catalogue number: HPA041256; 20 minutes incubation), CD3e (clone: NCC-L-CD3-565; 20 minutes incubation) and CD21 (clone: NCC-L-CD21-269; 20 minutes incubation) were diluted 1:100, 1:100 and 1:25 respectively prior to incubation. Heat induced epitope retrieval was undertaken for 20 minutes (PAX5 (EDTA buffer), MUM.1 (EDTA buffer), ZBP1 (citrate buffer) and CD21 (citrate buffer)) and 30 minutes (CD3e (citrate buffer)).

Signal detection for single immunostains was performed using Bond Polymer Detection Kit (clone number: DS9800) with DAB (brown colour) as the chromogen. For double immunostains, the sections were initially stained for CD3e, CD21, MUM.1 or PAX5 antigens as for single immunostaining protocol. This was followed by a sequential step for staining for ZBP1 antigen, where the ZBP1 signals were detected using Bond Polymer Refine Red Detection Kit (Red signals; catalogue number: DS9390).

RNA-seq and ChIP-seq data analysis

For RNA sequencing analysis, reads were aligned and transcripts were quantified using STAR (v2.5.3a),⁴ for shRNAs targeting *ZBP1* in MM.1S and H929 cells; related to figure 2, against GRCh38 release 79 or with Salmon (v0.12.0),⁵ for shRNAs targeting *ZBP1* or *IRF3* in MM.1S; related to figure 4, against GRCh38 Gencode v28 transcript annotations. Differential expression analysis was performed in R (R Core Team, 2020 (<https://www.R-project.org/>)) with DESeq2 (v1.24.0) from STAR output or Salmon output using tximport (v1.12.3), and limma-voom for processing CCLE data with cut off $p \text{ adj} < 0.05$.^{4,6} IRF3 ChIP sequencing reads were aligned with BWA MEM (v0.7.15) to GRCh38 genome (Gencode v28) with standard settings. QC and duplicate marking were performed with Picard (v2.6.0) and samtools (v1.2). Tracks were generated with Deeptools (v3.3.1),⁷ and peaks were called with MACS2 (v2.1.1).⁸ Motif enrichment was performed with Homer (v4.10).⁹ The peaks were visualized using Integrative Genomes Browser (IGV) (v2.5.2).¹⁰ Binding and Expression Target Analysis (BETA)-plus package (v1.0.7)¹¹ was used to integrate IRF3 cistrome, with the peaks within 2kb distance to TSS, and a complete transcriptome of *IRF3*-depleted MM.1S cells with cut off $p \text{ adj} < 0.05$. Bigwig and BED files of ATAC-seq and Pol II, H3K27ac, H3K27me3, H3K4me3, H3K4me2, H3K4me1 and IRF4 ChIP-seq files of MM.1S cells were collected from Cistrome Data Browser.¹²

Bedtools (v2.25.0) Intersect¹³ was used to identify the common genome-wide binding of IRF3 and IRF4 factors. Deeptools computeMatrix and plotHeatmap (v3.4.1)⁷ with 2kb distance in reference to center of the region were used to visualize genome-wide binding of histone marks, Pol II, with IRF3, and IRF4 transcription factors. Homer (v4.10)⁹ was used for annotation of the genomic regions that are plotted in the

heatmap. Gene Set Enrichment Analysis (GSEA) (v4.0.3) software¹⁴ was used for pathway annotation of differentially regulated genes with $p \text{ adj} < 0.05$ to analyse the pathways of Hallmark gene sets. Enrichr online web tool¹⁵ was used for pathways enrichment analysis of differentially regulated genes from RNA-seq and output of BETA-plus for integration of ChIP-seq and RNA-seq data. Significant pathways enriched with $p \text{ adj} < 0.05$ were selected to create the figures and listed in the tables.

Statistical analysis

Data graph and statistical analysis were performed using GraphPad Prism 8.0 software under institute licence. All experiments were repeated at least three times except for RNA-seq and ChIP-seq which were performed in replicates. Fold changes for *in vivo* data that were obtained in different time points were calculated by comparing the immunized groups to median value of control group. Comparison of two groups were performed using two-tailed unpaired Student t-test. All the information on sample size, replicates, statistical method and significance are indicated in the figure legends. GraphPad Prism 8.0 or Morpheus (<https://software.broadinstitute.org/morpheus>) was used for heatmap creation with log₂ transformed values of RNA-seq data.

References

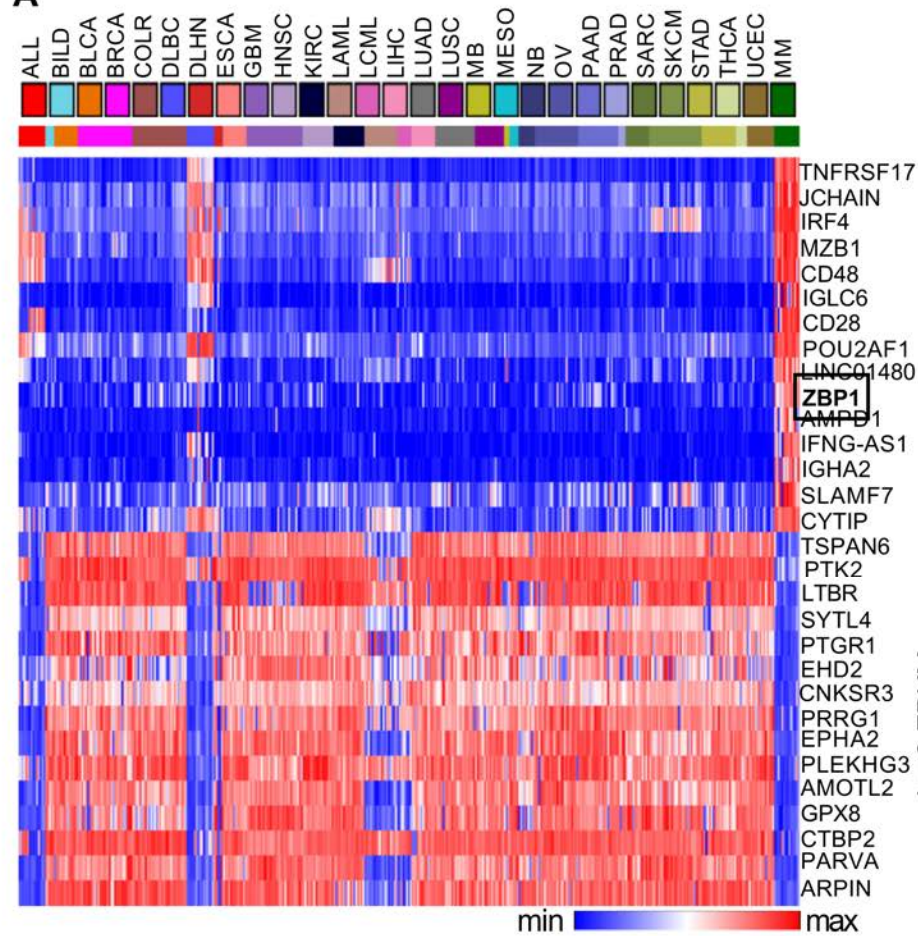
1. Zuber J, McJunkin K, Fellmann C, et al. Toolkit for evaluating genes required for proliferation and survival using tetracycline-regulated RNAi. *Nat Biotechnol* 2011;29(1):79–83.
2. Deigendesch N, Koch-Nolte F, Rothenburg S. ZBP1 subcellular localization and association with stress granules is controlled by its Z-DNA binding domains. *Nucleic Acids Res* 2006;34(18):5007–5020.
3. Ishii KJ, Kawagoe T, Koyama S, et al. TANK-binding kinase-1 delineates innate and adaptive immune responses to DNA vaccines. *Nature* 2008;451(7179):725–729.
4. Dobin A, Davis CA, Schlesinger F, et al. STAR: ultrafast universal RNA-seq aligner. *Bioinformatics* 2013;29(1):15–21.

5. Patro R, Duggal G, Love MI, Irizarry RA, Kingsford C. Salmon provides fast and bias-aware quantification of transcript expression. *Nat Methods* 2017;14(4):417–419.
6. Love MI, Huber W, Anders S. Moderated estimation of fold change and dispersion for RNA-seq data with DESeq2. *Genome Biol* 2014;15(12):550.
7. Ramírez F, Ryan DP, Grüning B, et al. deepTools2: a next generation web server for deep-sequencing data analysis. *Nucleic Acids Res* 2016;44(W1):W160-165.
8. Zhang Y, Liu T, Meyer CA, et al. Model-based analysis of ChIP-Seq (MACS). *Genome Biol* 2008;9(9):R137.
9. Heinz S, Benner C, Spann N, et al. Simple combinations of lineage-determining transcription factors prime cis-regulatory elements required for macrophage and B cell identities. *Mol Cell* 2010;38(4):576–589.
10. Thorvaldsdóttir H, Robinson JT, Mesirov JP. Integrative Genomics Viewer (IGV): high-performance genomics data visualization and exploration. *Brief Bioinform* 2013;14(2):178–192.
11. Wang S, Sun H, Ma J, et al. Target analysis by integration of transcriptome and ChIP-seq data with BETA. *Nat Protoc* 2013;8(12):2502–2515.
12. Zheng R, Wan C, Mei S, et al. Cistrome Data Browser: expanded datasets and new tools for gene regulatory analysis. *Nucleic Acids Res* 2019;47(D1):D729–D735.
13. Quinlan AR, Hall IM. BEDTools: a flexible suite of utilities for comparing genomic features. *Bioinformatics* 2010;26(6):841–842.
14. Subramanian A, Tamayo P, Mootha VK, et al. Gene set enrichment analysis: a knowledge-based approach for interpreting genome-wide expression profiles. *Proc Natl Acad Sci U S A* 2005;102(43):15545–15550.

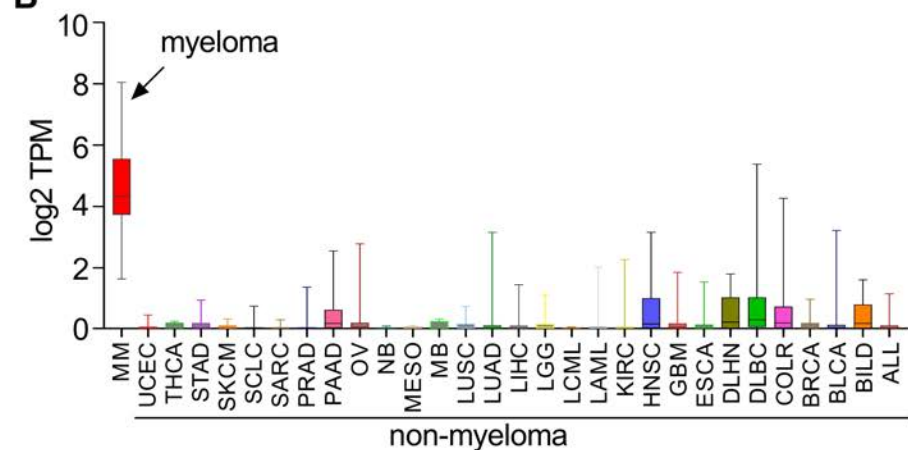
15. Kuleshov MV, Jones MR, Rouillard AD, et al. Enrichr: a comprehensive gene set enrichment analysis web server 2016 update. *Nucleic Acids Res* 2016;44(W1):W90-97.

Supplementary Figure S1

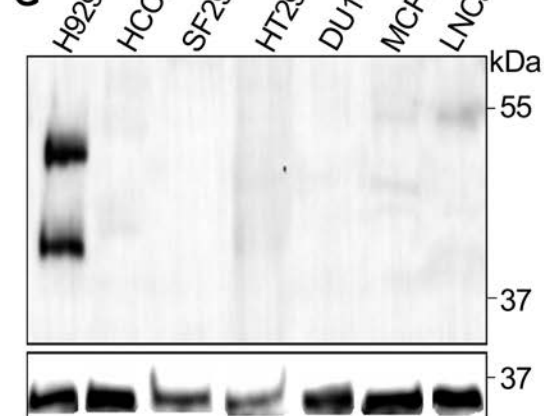
A



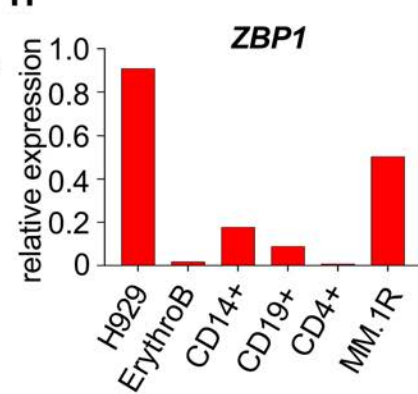
B



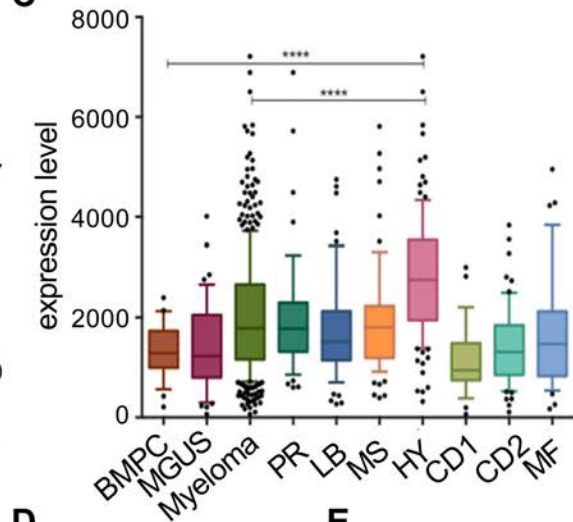
G



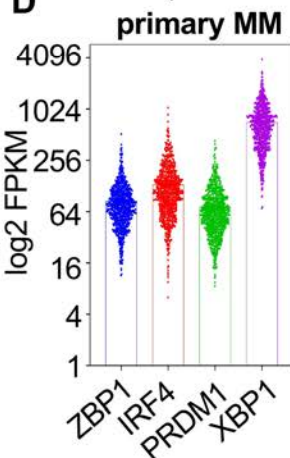
H



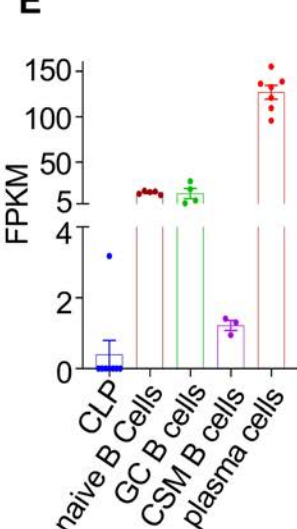
C



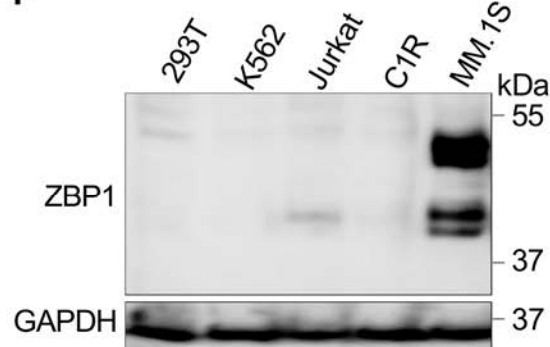
D



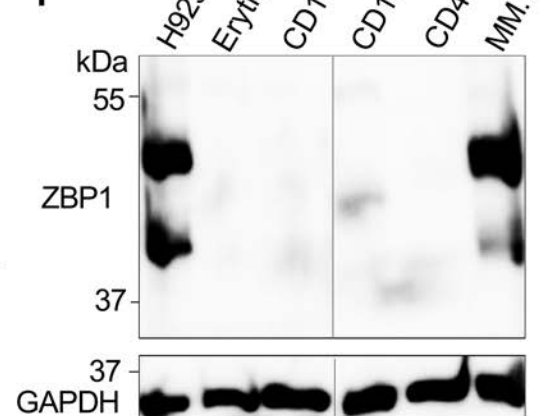
E



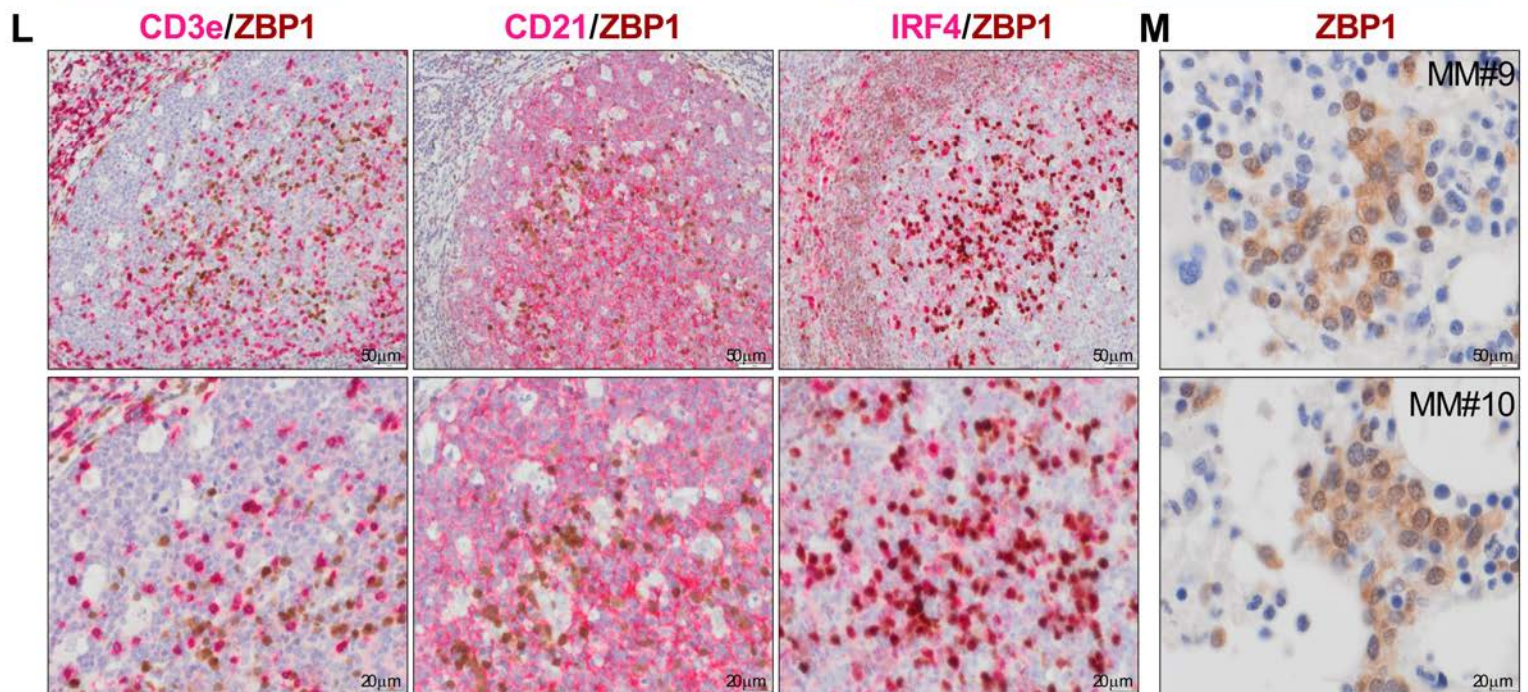
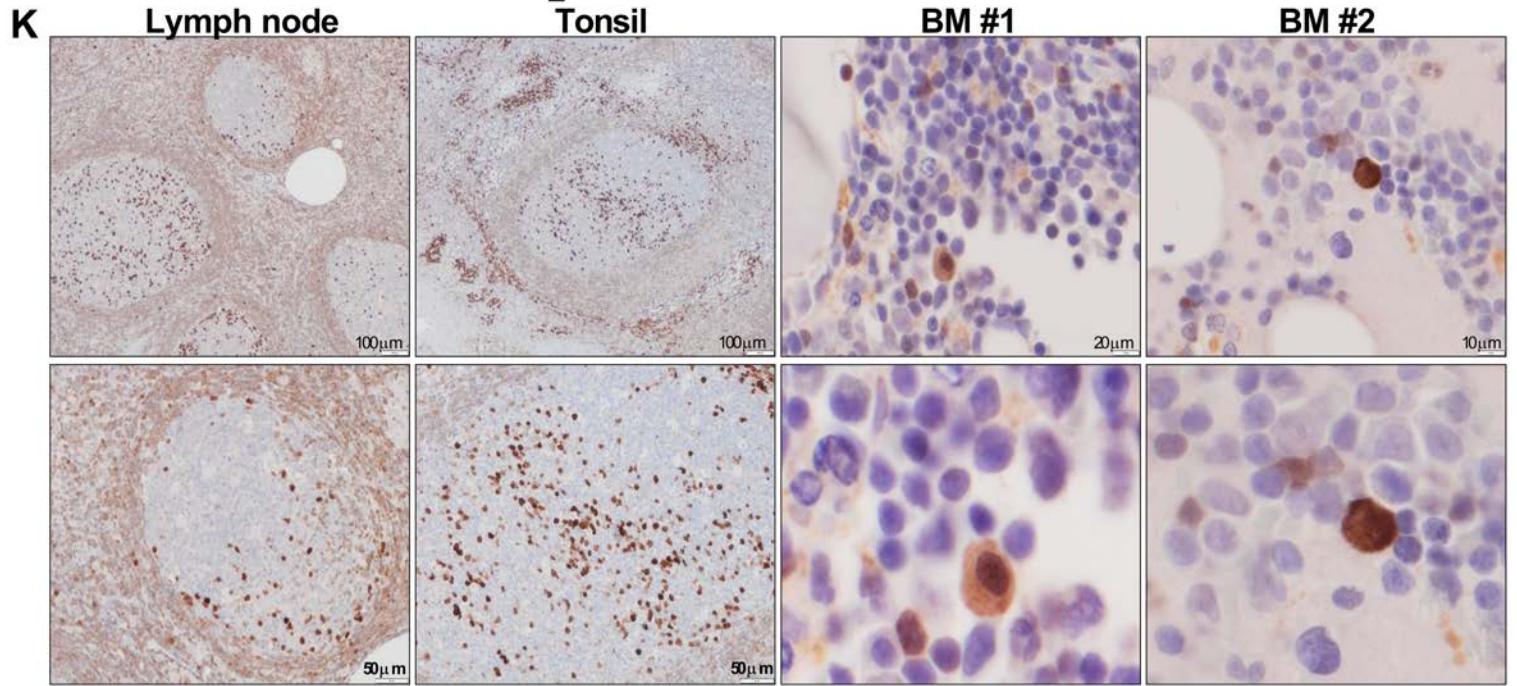
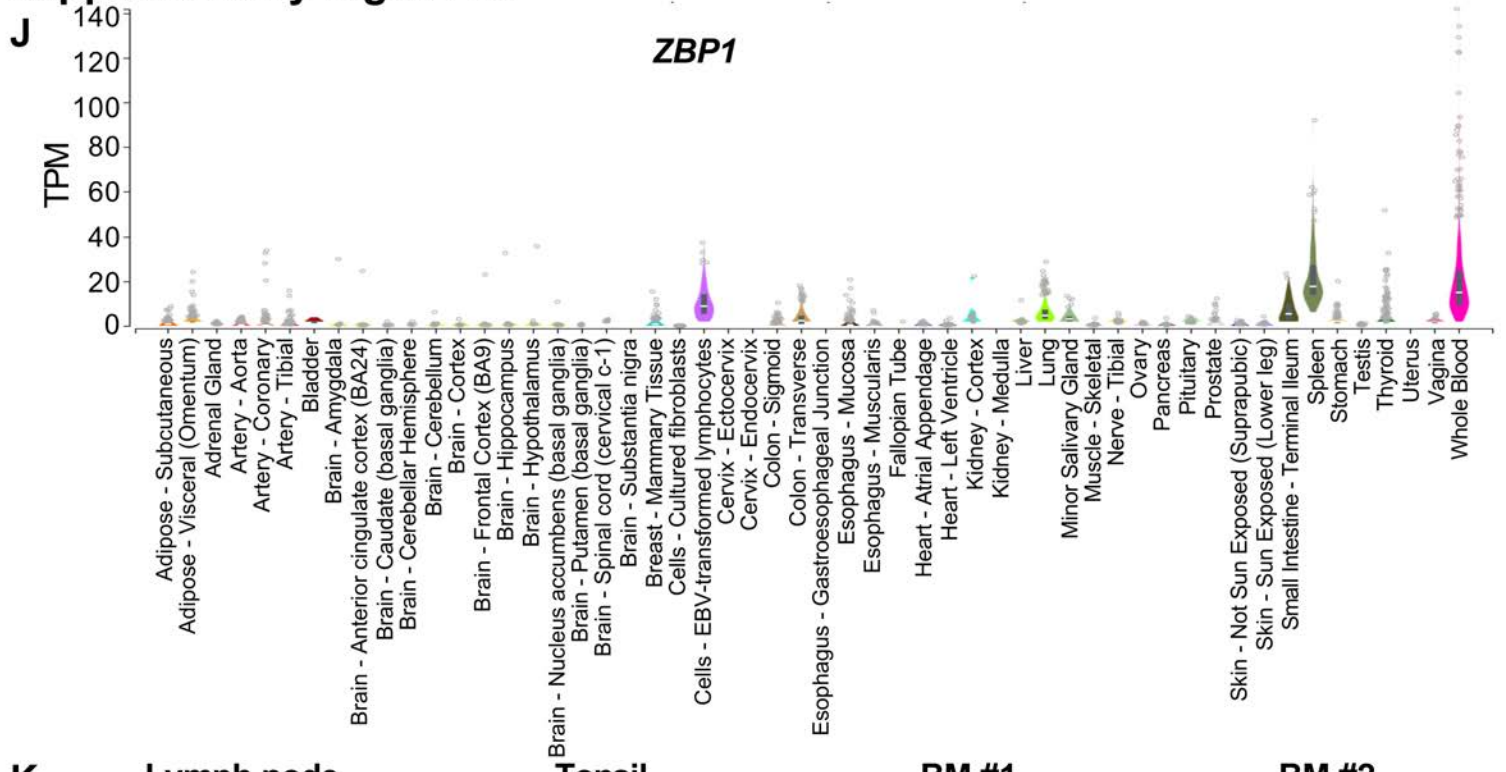
F



I



Supplementary Figure S1



Supplementary Figure S1 (related to Figure 1)

(A) Heat map showing the top 30 differentially expressed genes between 27 MM and >800 non-myeloma cancer cell lines (raw data collected from the Cancer Cell Line Encyclopedia Portal (CCLE)). *ZBP1* is boxed. ALL: Acute Lymphoblastic B Cell Leukaemia, BILD: Biliary Tract Carcinoma, BLCA: Bladder Carcinoma, BRCA: Breast Carcinoma, COLR: Colorectal Carcinoma, DLBC: Burkitt Lymphoma, DLHN: Lymphoma Hodgkin, ESCA: Squamous Cell Carcinoma, GBM: glioma HighGrade, HNSC: Upper Aerodigestive Tract, KIRC: Clear Cell Renal Cell Carcinoma, LAML: Acute Myeloid Leukaemia, LCML: Blast Phase Chronic Myeloid Leukaemia, LIHC: Hepatocellular Carcinoma, LGG: Glioma, LUAD: Lung Non-Small Cell Carcinoma, LUSC: Lung Squamous Cell Carcinoma, MB: Medulloblastoma, MESO: Mesothelioma, NB: Neuroblastoma, OV: Ovary Carcinoma, PAAD: Pancreas Carcinoma, PRAD: Prostate Carcinoma, SARC: Ewings Sarcoma, SCLC: Lung Small Cell, SKCM: Skin Melanoma, STAD: Stomach Gastric Carcinoma, THCA: Thyroid Carcinoma, UCEC: Endometrium Carcinoma, MM: Plasma Cell Myeloma.

(B) mRNA expression levels of *ZBP1* in >800 cancer cell lines (non-myeloma) including 27 MMCL (myeloma) from CCLE data sets. Box-whiskers plot shows minimum to maximum log₂ TPM values. Elaborated form of all the cell line names shown in *Online Supplementary Figure S1A* legend.

(C) mRNA expression level of *ZBP1* in GSE4581 data set. Expression of *ZBP1* is not different between normal, MGUS and myeloma PC. However, in the hyperdiploid group expression of *ZBP1* is significantly higher than normal and total myeloma PC. BMPC (n=22), normal bone marrow PC; MGUS (n=44); Myeloma (n=414). Molecular subgroups: PR: proliferative; LB: lytic bone; MS: over-expression of MMSET in t(4;14); HY: hyperdiploid; CD1 and CD2: Cyclin D1 and D2 over-expression groups; MF: MAF over-expression in t(14;16).

(D) mRNA expression levels of *ZBP1* in purified myeloma PC (n=767 MM patients) compared to PC-lineage defining transcription factors *IRF4*, *XBP1* and *PRDM1* from MMRF data sets. Bar graph shows the mean values.

(E) *ZBP1* mRNA expression in human common lymphoid progenitors (CLP), naïve, class switched memory (CSM) and germinal centre (GC) B cells as well as tonsillar plasma cells (data from the Blueprint DCC Portal; data shown as mean ± SEM).

(F, G) Immunoblot shows lack of *ZBP1* expression in non-myeloma hematopoietic cell lines K562 (erythromyeloid), Jurkat (T cell lymphoblastic) and C1R (EBV-transformed B cell) cells, and 293T cells, and solid tumor cell lines HCC95 (squamous cell lung carcinoma), SF295 (glioblastoma), HT29 (colon adenocarcinoma), DU145 and LNCaP (prostate carcinoma) and MCF7 (breast cancer).

(H, I) *ZBP1* mRNA and protein expression as assessed by qPCR (H) and immunoblotting (I) respectively in FACS-purified primary human bone marrow erythroblasts (ErythroB), peripheral blood CD14⁺ monocytes, CD19⁺ B cells, CD4⁺ T cells. The MMCL H929 and MM.1S are shown as positive controls.

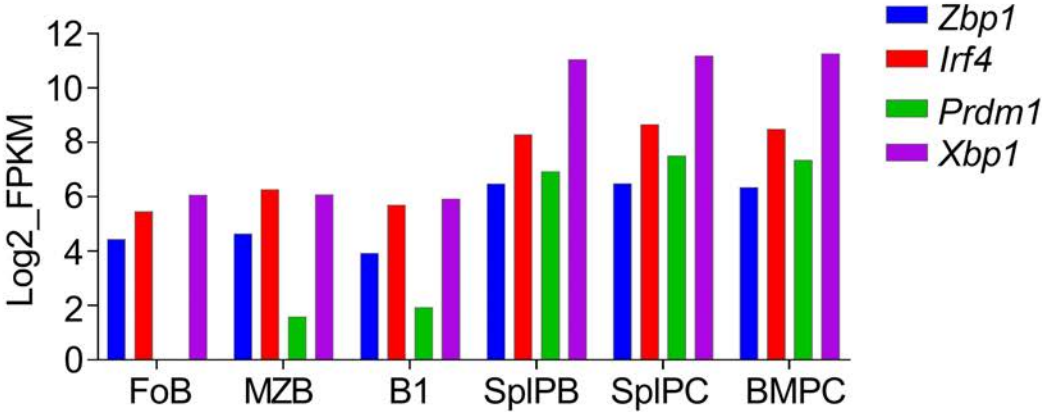
(J) *ZBP1* mRNA expression in 53 healthy human tissues. *ZBP1* expression is only detected in organs with lymphoid tissue (data obtained from the GTEx Portal).

(K) *ZBP1* expression in lymph nodes, tonsil, and healthy bone marrow as assessed by immunohistochemistry on paraffin-embedded tissue section. Within lymph nodal and tonsillar germinal centres, *ZBP1* expression is mostly restricted to PCs. Germinal centre B cells are mostly negative. *ZBP1* is also strongly expressed in PCs outside the follicles. There is weaker *ZBP1* expression in mantle cells and other interfollicular B cells. *ZBP1* expression is mostly restricted to PCs in normal bone marrow (BM#1 & BM#2).

(L) *ZBP1* expression in tonsillar germinal centres co-stained with CD3e (T cells), CD21 (follicular dendritic cells) or MUM.1 (IRF4) as identified by immunohistochemistry on paraffin-embedded tonsil tissue section. *ZBP1* is not expressed in CD3e⁺ T cells or CD21⁺ follicular dendritic cells, but is co-expressed with IRF4 (MUM.1)⁺ PCs.

(M) *ZBP1* expression in bone marrow tissue sections of another two MM patients.

Supplementary Figure S2

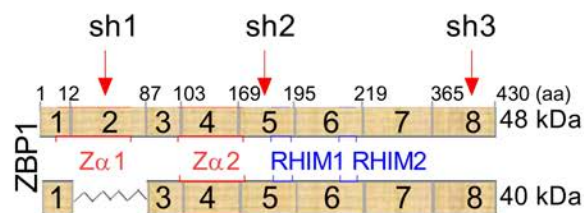


Supplementary Figure S2 (related to Figure 2)

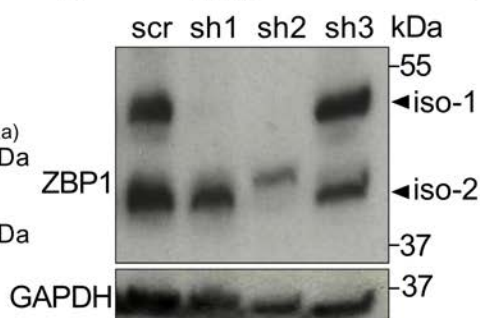
Zbp1 mRNA expression levels in murine follicular B cells (FoB), marginal-zone B cells (MZB), B1, splenic plasmablasts (splPB) and splenic and bone marrow plasma cells (splPC, BMPC) compared to PC-lineage defining transcription factors (data were reanalysed from previously published RNA-seq experiments by Shi et al., REF. #4).

Supplementary Figure S3

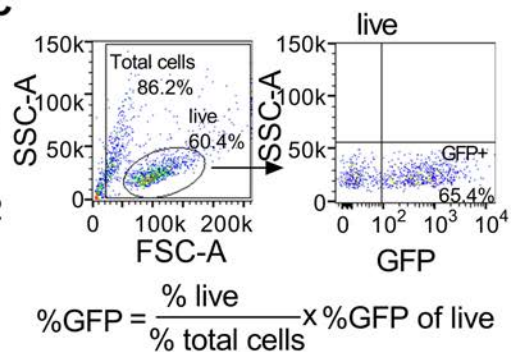
A shRNA target site on ZBP1



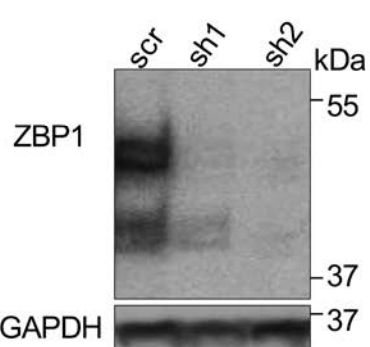
B H929



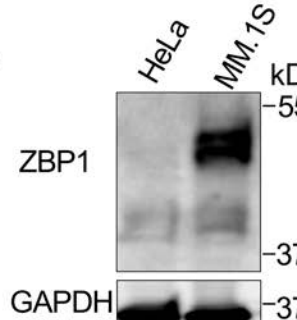
C



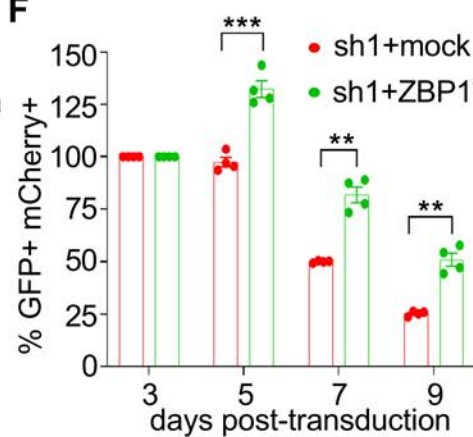
D MM.1S



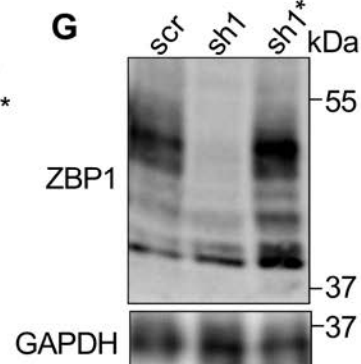
E



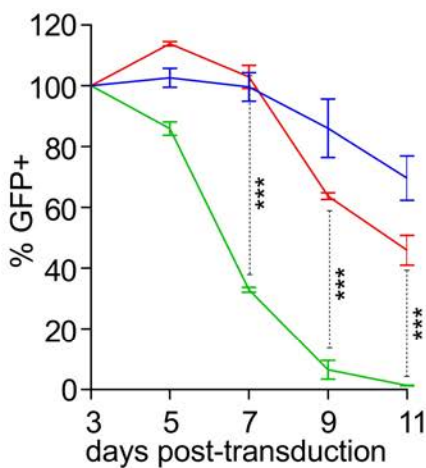
F



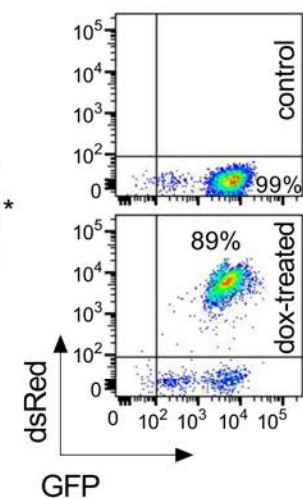
G



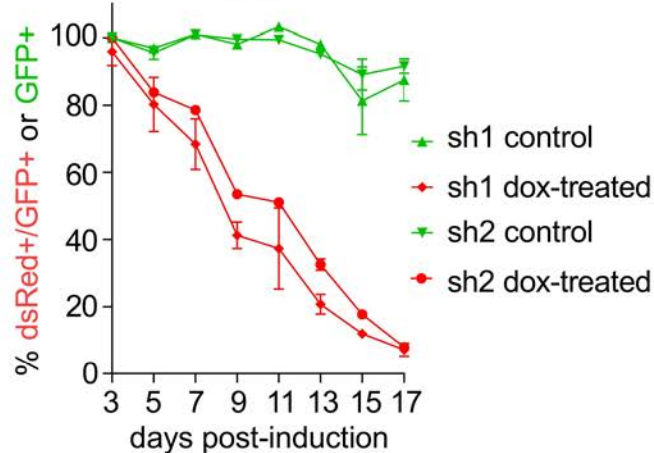
H



I

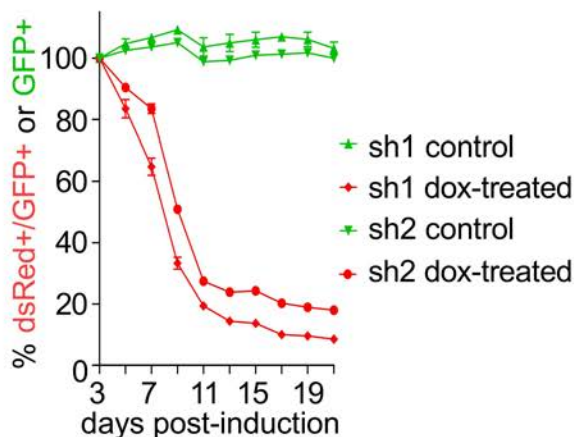


H929

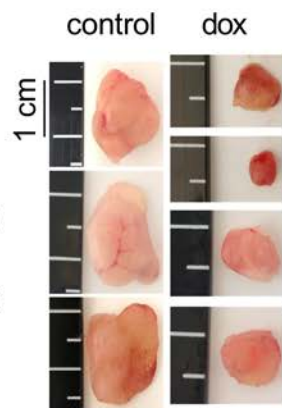


J

MM.1S



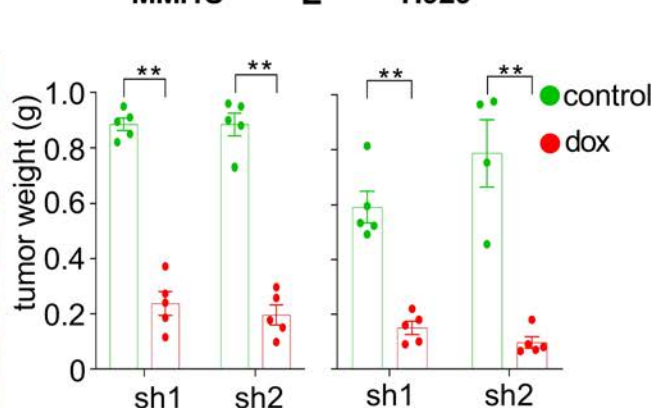
K



MM.1S

L

H929



Supplementary Figure S3 (Related to Figure 3)

(A) Schematic of *ZBP1* mRNA exonic structure, positions of Z α 1, Z α 2 and RHIM domains and shRNA1 (sh1)-, shRNA2 (sh2)- and shRNA3 (sh3)-targeting sites with reference to the two main ~48 and ~40 kDa ZBP1 isoforms are shown.

(B) Immunoblotting shows shRNA1- or shRNA2-mediated depletion of ZBP1 isoforms in MMCL H929 cells on day 4 post-transduction with sh1 or sh2 or sh3 or scr control that had >90% transduction efficiency. GAPDH is shown as loading control. Two ZBP1 isoforms i.e isoform 1 (iso-1) and isoform 2 (iso-2) are indicated.

(C) Typical example of gating strategies of flow cytometry plots (top) and applied formula (bottom) for calculation of the %GFP+ cells to analyse cytostatic effects of shRNA- or scramble-transduced cells. Live cells were determined by negative for DAPI staining.

(D) Immunoblotting for ZBP1 in MMCL MM.1S cells on day 4 post-transduction with sh1 or sh2 or scr control that had >90% transduction efficiency. GAPDH is shown as loading control.

(E) Immunoblotting for ZBP1 expression in the epithelial cancer cell line HeLa.

(F) %GFP+ cells after co-transduction of MM.1S myeloma cells with *ZBP1*-targeting sh1 with empty vector (mock) or *ZBP1*-targeting sh1 with *ZBP1* cDNA with silent mutation at sh1 seed annealing sequences (*ZBP1**). (n=4)

(G) ZBP1 expression assessed by immunoblotting in MM.1S cells transduced with shRNA1 targeting ZBP1 (sh1), 'seed' shRNA1 control (sh1*) or scr control.

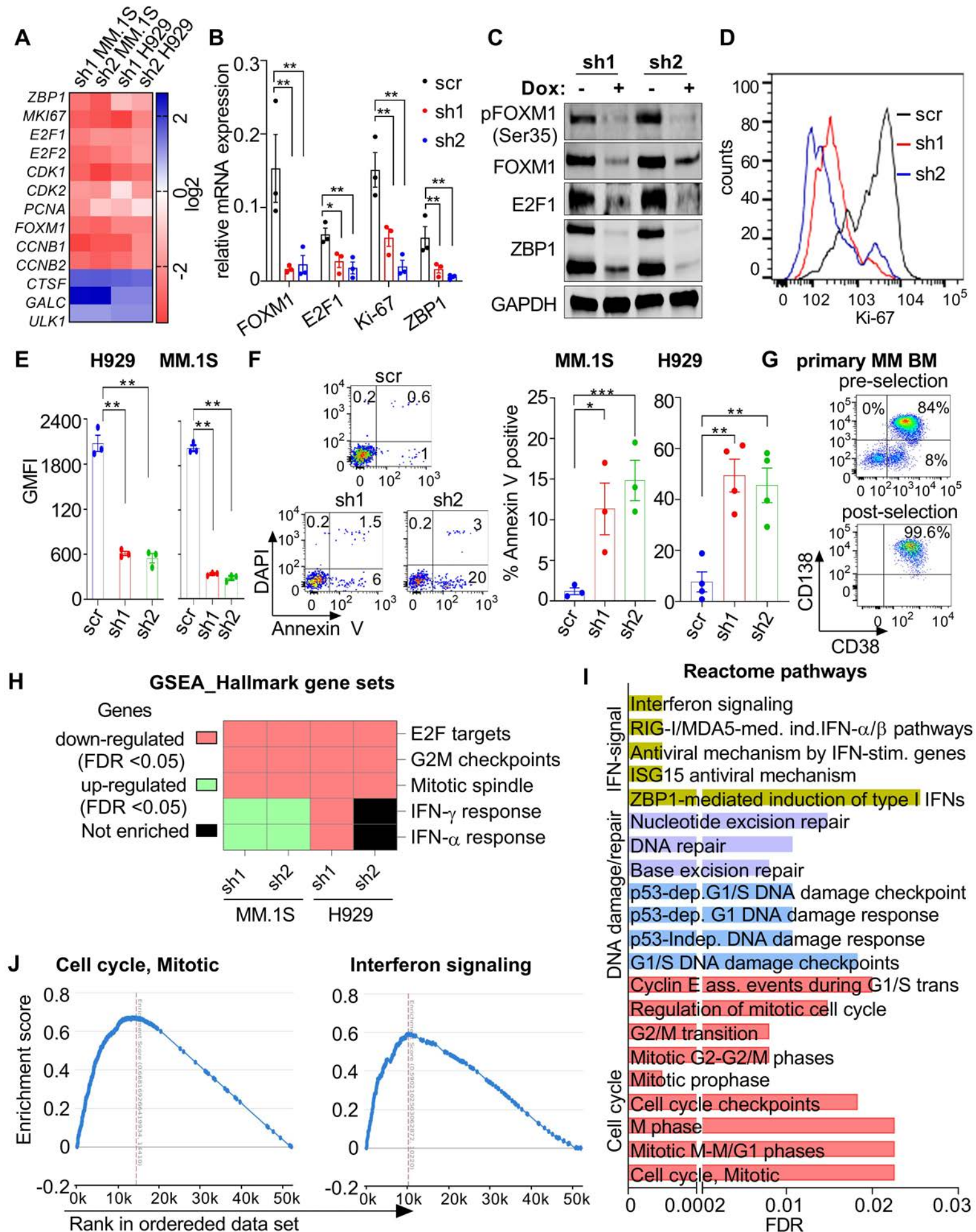
(H) %GFP+ cells after transduction with ZBP1-targeting sh1, 'seed' shRNA1 (sh1*) control or scr control in MM.1S cells. The %GFP+ cells were normalised to day 3 %GFP expression levels for all the time points for each shRNA or scr control shown. (n=3)

(I, J) Representative flow-cytometric analysis of doxycycline inducible shRNA targeting ZBP1 in MMCL before and after dox treatment. Transduced cells are GFP+, and express dsRed+ after dox-treatment. Quantitative data for %GFP+ or %GFP+dsRed+ H929 (I) and MM.1S (J) myeloma cells without and with dox treatment *in vitro*. (n=3)

(K, L) Photographs of tumors explanted at sacrifice from control (i.e., non-dox-treated) or dox-treated animals engrafted with MMCL MM.1S transduced with dox-inducible shRNA1 or shRNA2 targeting ZBP1. Tumor weight at sacrifice in animals engrafted with MM.1S (K) and H929 (L) myeloma cells transduced with anti-ZBP1 shRNAs for control or dox-treated.

The error bars of all the cumulative data indicate mean \pm SEM. Two-tailed unpaired t-test was applied to determine the P values. ** $p \leq 0.01$, *** $p \leq 0.001$. The number of experiments performed for the study are indicated separately in each figure legend.

Supplementary Figure S4



Supplementary Figure S4 (Related to Figure 3)

(A) Heatmap showing log₂-fold change in expression of key cell cycle genes from RNA-seq data after sh1- or sh2-mediated ZBP1 depletion in MM.1S and H929 cells (p adj <0.05).

(B) Expression of cell cycle genes *FOXM1*, *E2F1*, *Ki-67* validated at mRNA level using qPCR on day 4 post-transduction with anti-ZBP1 sh1 or sh2 or scr control in MM.1S cells.

(C) Immunoblotting for indicated cell cycle proteins following dox-induction of inducible anti-ZBP1 sh1 or sh2 in MM.1S myeloma cells. Protein lysates were prepared from FACS-purified GFP+dsRed+ or GFP+ live cells on day 3 after dox-treatment or control respectively.

(D, E) A representative flow-cytometric histogram of Ki-67 expression in MM.1S cells (D) and its cumulative data shows reduction of cell proliferation marker Ki-67 in anti-ZBP1 sh1- or sh2-transduced cells as compared to scramble control cells on day 4 post-transduction in MMCL H929 and MM.1S (E). (n=3)

(F) Flow-cytometric analysis of Annexin V staining and its cumulative data shows apoptosis induction following ZBP1-depletion in MMCL MM.1S and H929. (n=3)

(G) Representative flow-cytometric example of MM patient-derived bone marrow myeloma PC purity before and after CD138+ selection using CD138 immunomagnetic microbeads.

(H) Gene set enrichment analysis with reference to Molecular Signatures Database v7.1 Hallmark gene sets for transcriptomes of ZBP1-depleted MM.1S and H929 MMCL.

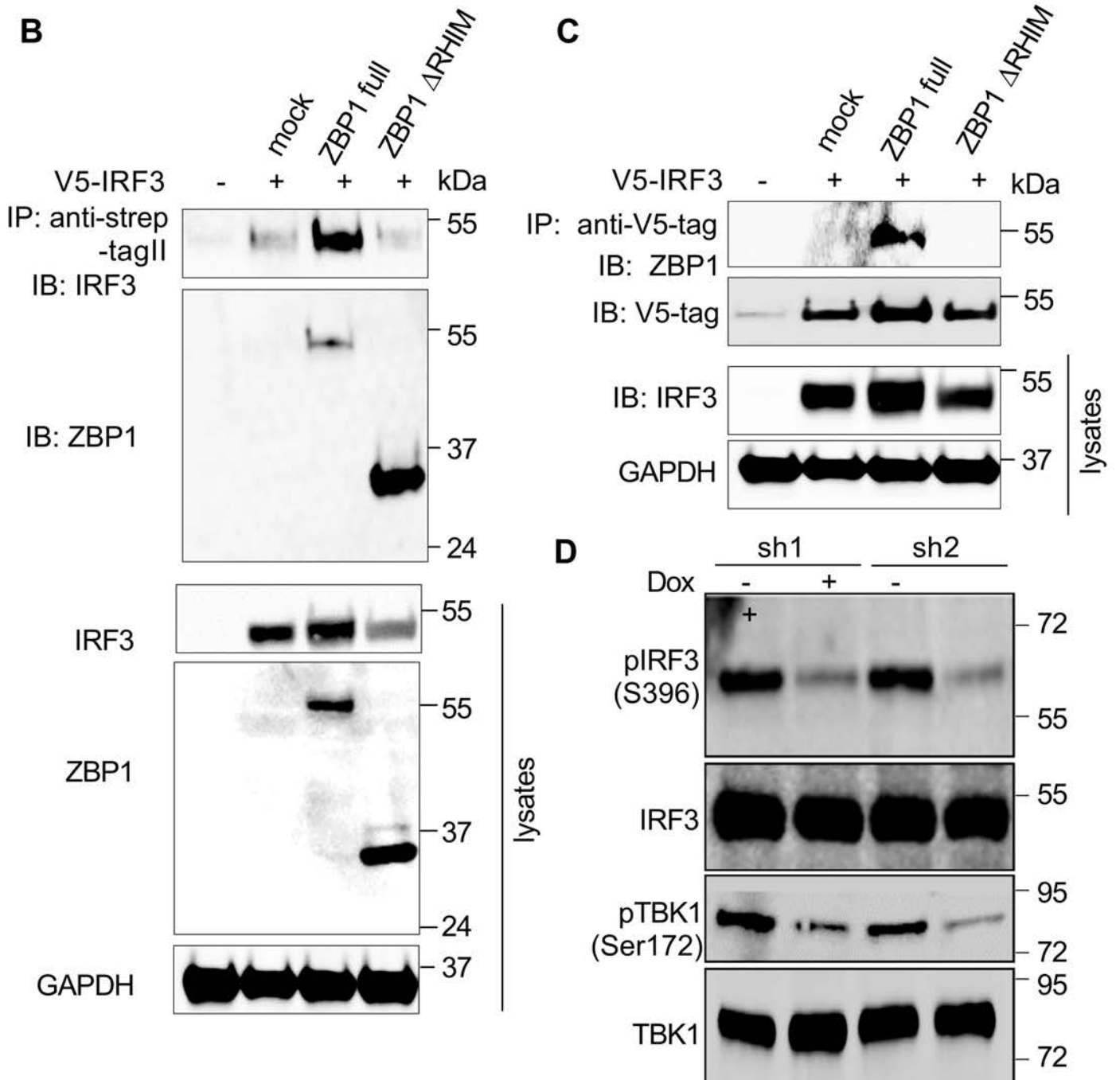
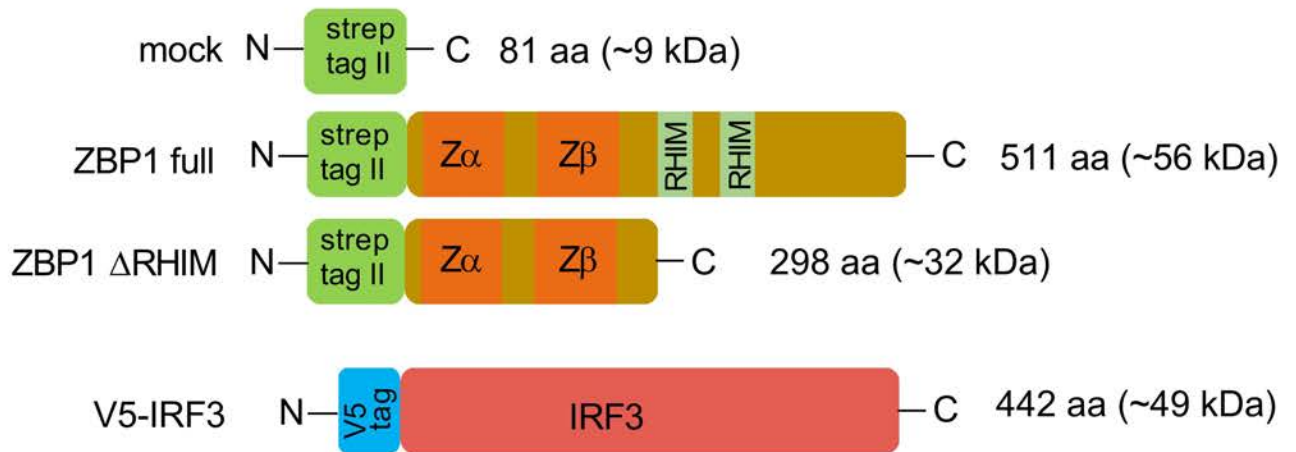
(I) GSEA of highest 5% vs lowest 90% ZBP1-expressing myeloma PC. Analysis was performed using RNA-seq transcriptomes of purified myeloma PC (n=767 patients) and the inbuilt GSEA tool in the multiple myeloma research foundation (MMRF) research gateway portal.

(J) GSEA example of reactome pathway for cell cycle, mitotic genes enriched in the top 5% ZBP1-expressing cohort as compared to lowest 90% ZBP1-expressing myeloma PC cells.

The error bars of all the cumulative data indicate mean ± SEM. Two-tailed unpaired t-test was applied to determine the P values. * p≤0.05, ** p≤0.01, *** p≤0.001. The number of experiments performed for the study are indicated separately in figure legends.

Supplementary Figure S5

A Structures of tagged-ZBP1 and -IRF3



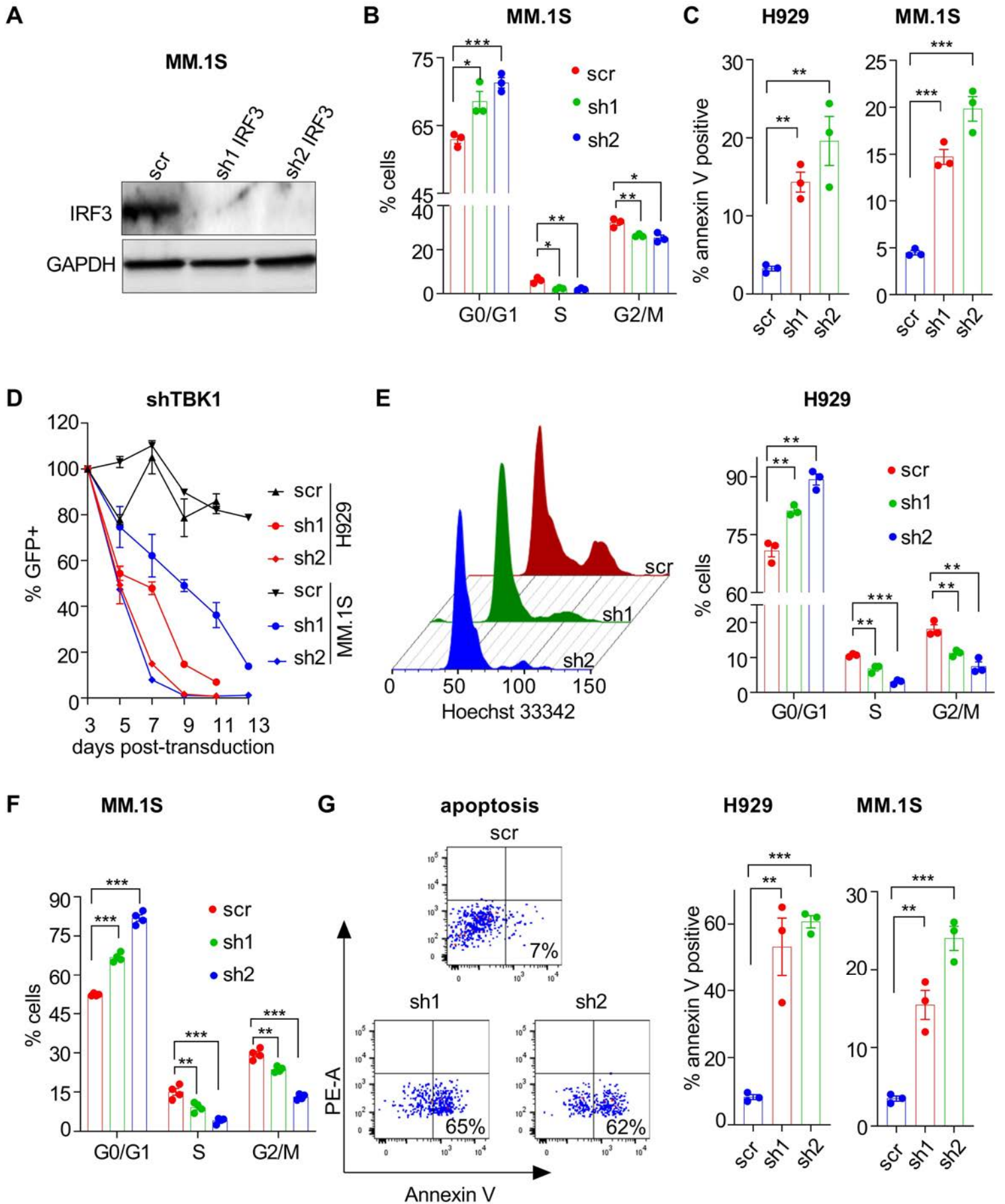
Supplementary Figure S5 (Related to Figure 4)

(A) Schematic illustration of V5-tagged IRF3 and strep-tag II-tagged full length ZBP1 and its deletion mutant. RHIM, RIP homotypic interaction motif.

(B, C) Strep-tag II ZBP1-full, ZBP1- Δ RHIM and mock GFP-expressing cDNA constructs, were transiently co-expressed with V5-tagged IRF3 in HEK293T cells. Cell lysates were co-immunoprecipitated with anti-V5 antibody or anti-strep-tag magnetic beads followed by immunoblotting with anti-ZBP1 or -IRF3 antibody. IRF3 can be readily co-immunoprecipitated with only full length ZBP1.

(D) Immunoblot for pIRF3/IRF3 and pTBK1/TBK1 following dox-induction of inducible anti-ZBP1 sh1 or sh2 in MM.1S cells. Lysates were prepared from FACS-purified GFP+dsRed+ or GFP+ live cells on day 3 after dox-treatment or control respectively.

Supplementary Figure S6



Supplementary Figure S6 (Related to Figure 4)

(A) Immunoblot for IRF3 in MM.1S cells on day 4 post-transduction with scr or IRF3-targetting shRNA1 or shRNA2. Lysates were prepared from the cells with >90% transduction efficiency.

(B) Flow-cytometric analysis of cell cycle in MM.1S cells on GFP+ cells day 4 post-transduction with scr or anti-IRF3 shRNA1 or shRNA2. (n=3)

(C) Annexin V staining for flow cytometric-based assessment of apoptosis in H929 and MM.1S cells on day 4 post-transduction with scr or anti-IRF3 shRNA1 or shRNA2. (n=3)

(D) %GFP+ cells after transduction with scr control or shRNA1 or shRNA2 targeting TBK1 in H929 and MM.1S cells. All the time points were normalised to day 3 %GFP expression levels for each shRNA shown. (n=3)

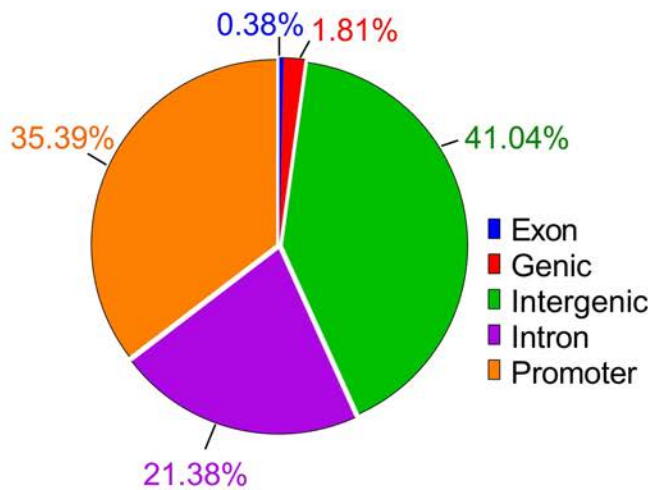
(E, F) A representative flow-cytometric histogram for cell cycle analysis in GFP+ cells day 4 post-transduction with *TBK1*-depleting shRNA1 or shRNA2 or scr control and its quantitative data show cell cycle arrest in H929 (E) and MM.1S (F) cells. (n=3-4)

(G) Annexin V staining for flow cytometric-based assessment of apoptosis in MMCL H929 and MM.1S cells on day 4 post-transduction with *TBK1*-depleting shRNA1 or shRNA2 or scr control. (n=3)

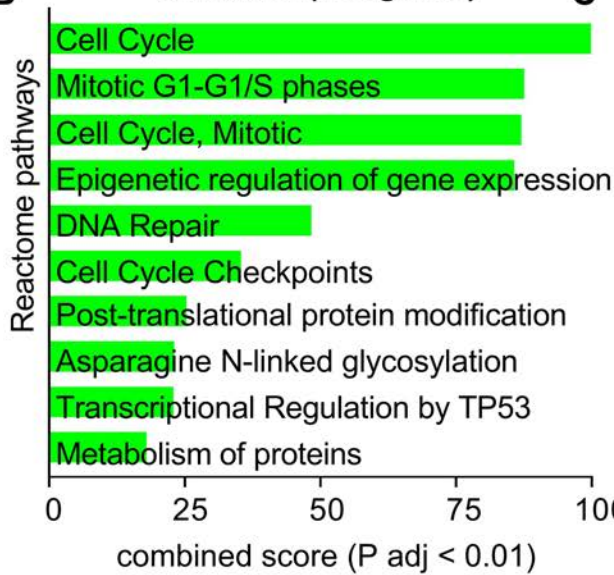
The error bars of all the cumulative data indicate mean \pm SEM. Two-tailed unpaired t-test was applied to determine the P values. * $p \leq 0.05$, ** $p \leq 0.01$, *** $p \leq 0.001$. The number of experiments performed for the study are indicated separately in each figure legend.

Supplementary Figure S7

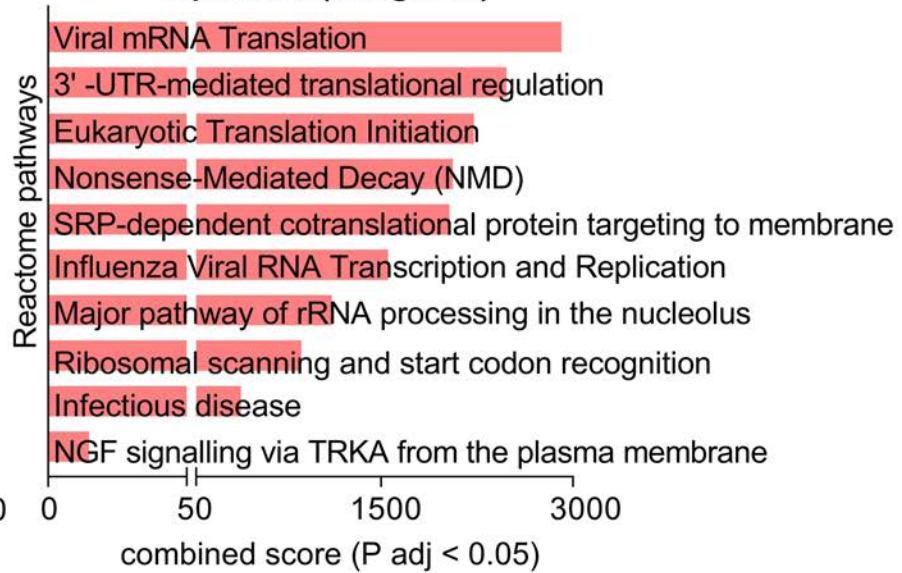
A IRF3 genome-wide binding



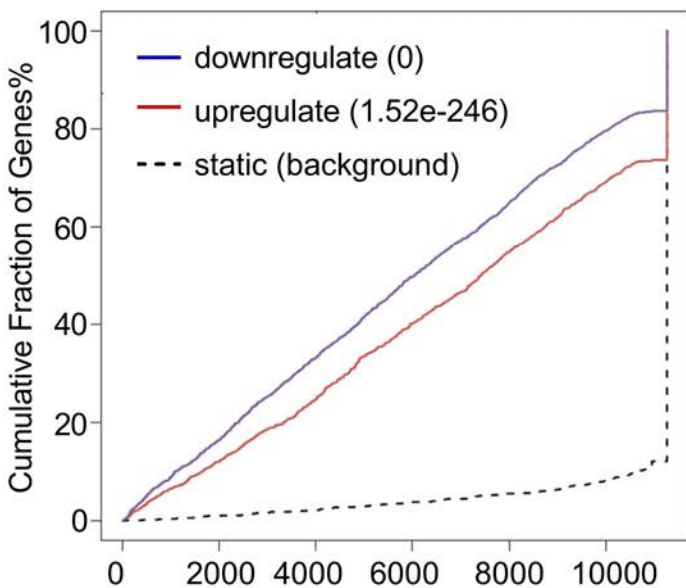
B activated (770 genes)



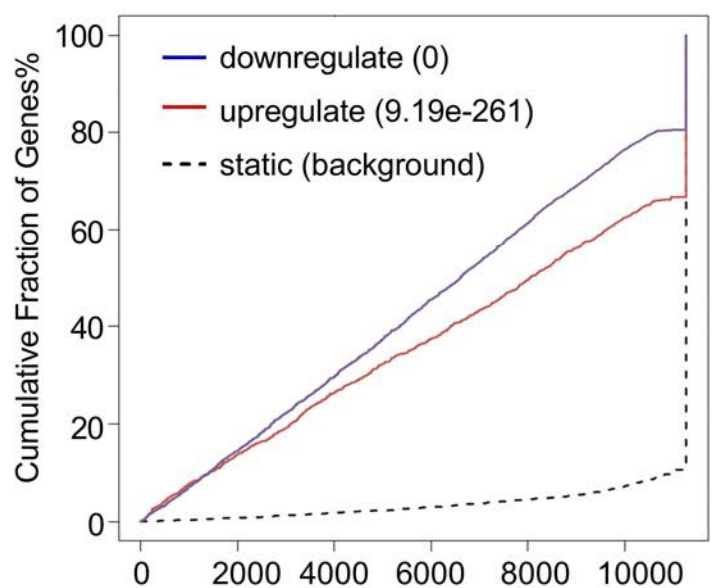
C repressed (339 genes)



D sh1 IRF3

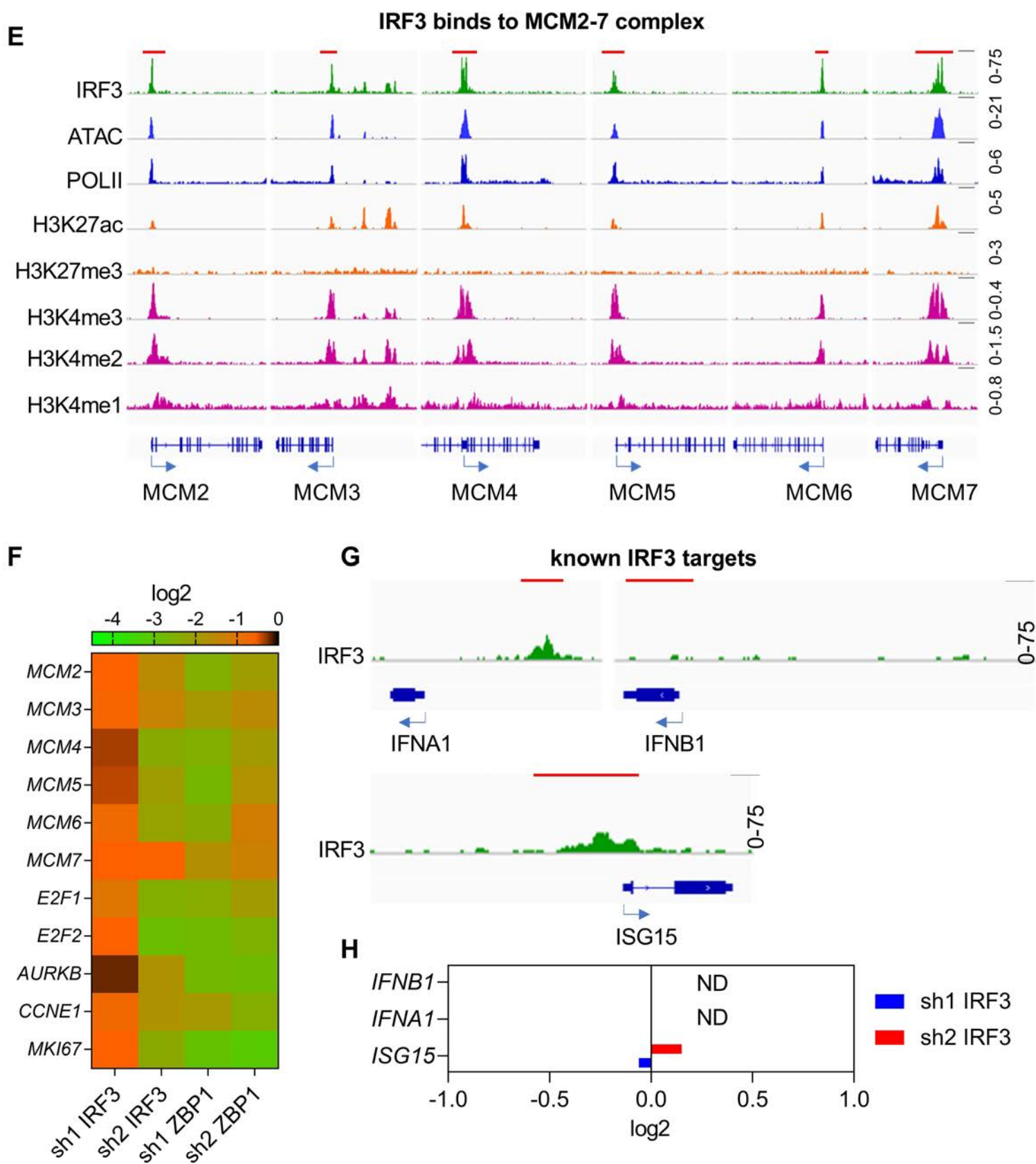


sh2 IRF3



Rank of genes based on Regulatory Potential Score (from high to low)

Supplementary Figure S7



Supplementary Figure S7 (Related to Figure 5)

(A) Annotation of IRF3 genome wide binding according to genomic features. ~35% and ~41% of IRF3 binding observed in promoter and intergenic genomic regions respectively.

(B, C) Enrichr pathway enrichment analysis of the 770 and 339 genes predicted to be directly activated (B) and repressed (C) by IRF3 binding to their regulatory areas.

(D) Regulatory potential prediction models display significant activating (blue) and repressive (red) function of IRF3 in MM.1S cells. Models derived from BETA-plus analysis, after integrating the IRF3 cistrome with *IRF3*-depleted transcriptome for anti-IRF3 shRNA1 or shRNA2.

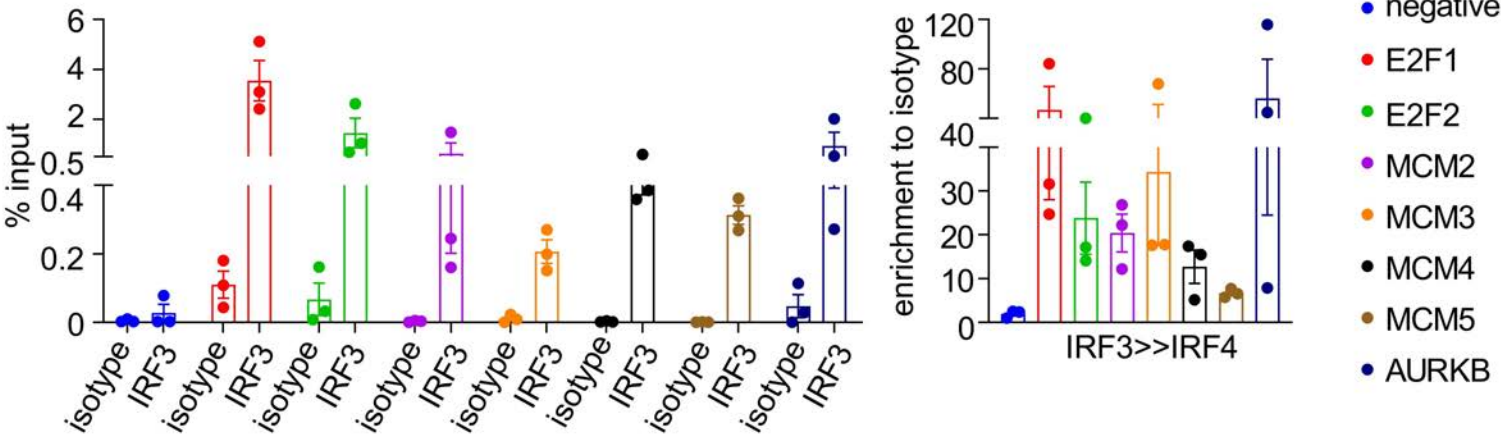
(E) IGV browser snapshots of IRF3 and Pol II binding, chromatin accessibility and histone mark enrichment at regulatory areas of several genes promoting cell cycle progression and cell proliferation. The red block on the top indicates 5kb genomic size.

(F) Heatmap shows the downregulation of MCM2-7 complex at mRNA levels in indicated mRNA-depleted RNA-seq data (p adj <0.05).

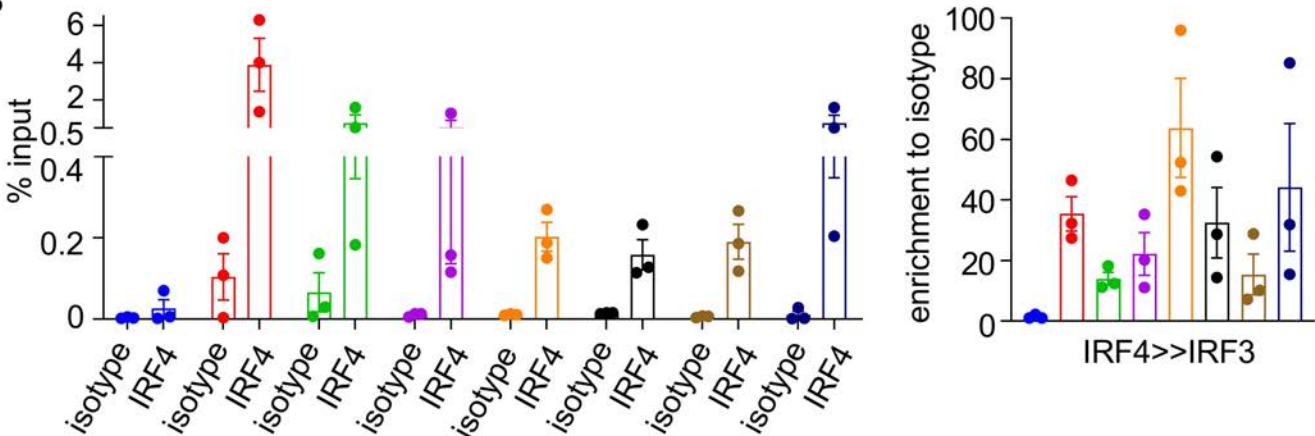
(G, H) IRF3 binding to IFN type I pathway genes (G), the red block on the top indicates 1kb genomic size, and mRNA expression changes of indicated genes (H). Note neither *IFNA1* nor *IFNB1* is expressed before or after IRF3 depletion in MM.1S cells.

Supplementary Figure S8

A



B



Supplementary Figure S8 (Related to Figure 6)

(A, B) qPCR of IRF3 ChIP or IRF3 to IRF4 ChIP-re-ChIP (A) and qPCR of IRF4 ChIP or IRF4 to IRF3 ChIP-re-ChIP (B) at the promoter regions of genes involved in cell cycle regulation.

Supplementary Table S1. Differentially expressed genes that are common in both H929 and MM.1S cells and in both shRNAs (log2 fold change >1.0 and p adj <0.05)

down-regulated							up-regulated
NEDD1	NCAPD3	CHTF18	TTK	CDC25C	BIRC5	CENPA	IGHA1
SLC1A4	KCNQ5	GINS1	RFC5	KIF15	ORC6	CDCA5	GALC
SURF4	CENPK	DCLRE1B	CENPE	FANCI	RFC3	CDCA8	SNAP91
C17orf96	RPL39L	KIF11	RFC2	ZBP1	E2F2	NEIL3	ZBTB18
UBALD2	C21orf58	WDHD1	KIAA1524	RAD51AP	CDCA3	CDCA2	PLEKHA1
RCN2	CENPO	FAM72B	ZWINT	KIF4A	FEN1	RRM2	LRRN2
GPI	FANCM	MIS18A	KIF22	PTTG1	MYB	DEPDC1B	IGHA2
TBL1X	SUV39H2	SMC2	FANCB	HMMR	GINS2	CCNB1	KIF13A
NUDT8	PDSS1	BRCA1	CKAP2L	KIF2C	ORC1	CDC20	SATB1
SLIT3	IQGAP3	C4orf46	STIL	FAM72A	SPC25	DLGAP5	PPIC
NEDD9	CENPU	PRIM1	FANCG	NUSAP1	BRI3BP	KIF20A	PLEKHH1
ADCY3	OIP5	CENPM	MCM6	POLA1	C16orf59	CDKN3	ZBTB10
MFSD2A	PRC1	PLCXD1	CDC6	DTL	SKA1	CENPW	TMEM132B
KNTC1	GGH	CLSPN	E2F1	RAD54L	ESPL1	UBE2C	CTSF
ME2	DUT	MELK	SUV39H1	MAD2L1	CDT1	FAM111B	TMEM232
MYH15	MCM8	CCDC150	CHEK2	FBXO5	SHCBP1	CDC25A	NR2F2
ACBD7	BRCA2	FAM64A	WDR76	NCAPG	DDIAS	MCM10	TMEM74B
YBX1	KIAA1161	NUP35	MND1	GSG2	TRAIP	BLM	LINC01176
DPF1	FANCD2	SPDL1	BUB1B	ERCC6L	CDK1	UHRF1	ULK1
HNRNPUL1	SASS6	CHAF1B	TCF19	PARPBP	KIF23	PLK1	
APOBEC3B	RAD18	POLA2	POC1A	KIF18A	AURKA	GTSE1	
ZNF367	ZGRF1	CKS1B	NDC80	TUBA1C	ARHGAP1	CENPH	
CNTN1	MCM3	UBE2S	RRM1	SPAG5	EXO1	KIF18B	
YBX1P1	PTMA	SLCO4A1	CHAF1A	TK1	NEK2	CCNF	
C12orf75	NRGN	NCAPG2	KIF20B	DSCC1	INCENP		
NDC1	ANKRD18	ANLN	TUBB	SGO2	HJURP		
RTKN2	DIAPH3	EME1	H2AFX	MYBL2	NCAPH		
POLQ	LRRC8C	POLE2	HMGB2	NUF2	KIFC1		
LYAR	TMPO	NCAPD2	PBK	CENPI	TROAP		
AQP3	TCOF1	DHFR	GINS4	TONSL	PRR11		
CHEK1	C17orf53	WDR62	KIAA0101	CCNA2	TUBA1B		
H2AFZ	ANP32B	KNL1	FAM72D	FAM83D	MKI67		
NUDT1	DMC1	ATAD2	AUNIP	MCM5	SKA3		
FBXO43	SGO1	BRIP1	KIF14	CDC45	UNG		
MMS22L	CIT	MTFR2	TOP2A	ASPM	PKMYT1		
RANBP1	HELLS	UBE2T	MCM2	FOXM1	ESCO2		
PRPF38A	DONSON	LMNB1	PLK4	RECQL4	TPX2		
YBX1P10	C1orf112	STMN1	MCM4	TACC3	RAD51		
FAM72C	PSMC3IP	RACGAP1	SPC24	CCNB2	XRCC2		
MIR1244-2	MSH2	ASF1B	RFC4	TUBBP1	CEP55		
CENPP	DEPDC1	CKS2	PTMAP5	AURKB	TRIP13		

Supplementary Table S2. Reactome pathways_Enrichr pathway enrichment analysis of the 270 common genes downregulated in both MM.1S and H929 cells treated with anti-ZBP1 shRNAs

Name of the enriched pathways (Homo sapiens)	Overlap	Adj P-value	Odds Ratio	Combined Score
Cell Cycle_R-HSA-1640170	111/566	8.91E-98	14.527	3352.79
Cell Cycle, Mitotic_R-HSA-69278	95/462	2.25E-84	15.232	3034.86
DNA strand elongation_R-HSA-69190	18/32	4.48E-24	41.667	2427.56
Unwinding of DNA_R-HSA-176974	10/12	6.71E-16	61.728	2410.61
Mitotic Prometaphase_R-HSA-68877	36/107	2.88E-38	24.922	2302.45
Activation of ATR in response to replication stress_R-HSA-176187	19/37	2.29E-24	38.038	2246.47
Activation of the pre-replicative complex_R-HSA-68962	16/30	6.64E-21	39.506	2003.07
Resolution of Sister Chromatid Cohesion_R-HSA-2500257	32/99	3.05E-33	23.943	1929.67
G1/S-Specific Transcription_R-HSA-69205	11/17	1.50E-15	47.93	1831.33
E2F mediated regulation of DNA replication_R-HSA-113510	16/33	4.92E-20	35.915	1747.48
M Phase_R-HSA-68886	50/268	8.22E-40	13.82	1329.89
RHO GTPases Activate Formins_R-HSA-5663220	29/114	8.24E-27	18.843	1228.52
Phosphorylation of Emi1_R-HSA-176417	5/6	5.60E-08	61.728	1221.09
DNA Replication_R-HSA-69306	27/105	4.24E-25	19.048	1162.93
Condensation of Prometaphase Chromosomes_R-HSA-2514853	7/11	7.92E-10	47.138	1153.01
Chromosome Maintenance_R-HSA-73886	23/86	6.54E-22	19.811	1052.26
Mitotic Metaphase and Anaphase_R-HSA-2555396	35/174	1.24E-28	14.9	1039.99
S Phase_R-HSA-69242	28/124	1.87E-24	16.726	992.391
Synthesis of DNA_R-HSA-69239	24/97	5.55E-22	18.328	977.428
Mitotic Anaphase_R-HSA-68882	34/173	1.57E-27	14.558	974.934
Cell Cycle Checkpoints_R-HSA-69620	35/182	5.56E-28	14.245	970.72
G1/S Transition_R-HSA-69206	26/112	4.44E-23	17.196	961.438
Mitotic G1-G1/S phases_R-HSA-453279	29/136	1.46E-24	15.795	942.258
Polo-like kinase mediated events_R-HSA-156711	8/16	4.15E-10	37.037	932.413
G2/M DNA replication checkpoint_R-HSA-69478	4/5	3.00E-06	59.259	927.032
Cyclin B2 mediated events_R-HSA-157881	4/5	3.04E-06	59.259	927.032
Separation of Sister Chromatids_R-HSA-2467813	32/162	5.44E-26	14.632	924.796
E2F-enabled inhibition of pre-replication complex formation_R-HSA-113507	6/10	2.84E-08	44.444	914.853
G2/M Checkpoints_R-HSA-69481	30/150	1.56E-24	14.815	883.889
Leading Strand Synthesis_R-HSA-69109	7/14	6.54E-09	37.037	820.487
Polymerase switching_R-HSA-69091	7/14	6.66E-09	37.037	820.487
Polymerase switching on the C-strand of the telomere_R-HSA-174411	7/14	6.78E-09	37.037	820.487
CDC6 association with the ORC:origin complex_R-HSA-68689	6/11	5.54E-08	40.404	800.287

Cyclin A/B1 associated events during G2/M transition_R-HSA-69273	9/22	2.03E-10	30.303	785.311
Telomere C-strand (Lagging Strand) Synthesis_R-HSA-174417	9/22	2.08E-10	30.303	785.311
Homologous DNA Pairing and Strand Exchange_R-HSA-5693579	13/42	3.00E-13	22.928	748.394
Telomere C-strand synthesis initiation_R-HSA-174430	4/6	8.11E-06	49.383	718.801
DNA replication initiation_R-HSA-68952	4/6	8.20E-06	49.383	718.801
Kinesins_R-HSA-983189	13/44	5.63E-13	21.886	699.358
Presynaptic phase of homologous DNA pairing and strand exchange_R-HSA-5693616	12/39	3.36E-12	22.792	687.007
Lagging Strand Synthesis_R-HSA-69186	8/20	3.33E-09	29.63	679.727
Nucleosome assembly_R-HSA-774815	14/52	2.55E-13	19.943	655.432
Deposition of new CENPA-containing nucleosomes at the centromere_R-HSA-606279	14/52	2.63E-13	19.943	655.432
M/G1 Transition_R-HSA-68874	18/82	1.85E-15	16.26	616.625
DNA Replication Pre-Initiation_R-HSA-69002	18/82	1.92E-15	16.26	616.625
RHO GTPase Effectors_R-HSA-195258	36/255	2.93E-24	10.458	614.343
Activation of NIMA Kinases NEK9, NEK6, NEK7_R-HSA-2980767	4/7	1.77E-05	42.328	580.703
HDR through Homologous Recombination (HRR)_R-HSA-5685942	15/64	2.50E-13	17.361	570.378
Extension of Telomeres_R-HSA-180786	9/28	2.29E-09	23.81	556.076
Resolution of D-loop Structures through Synthesis-Dependent Strand Annealing (SDSA)_R-HSA-5693554	8/26	3.01E-08	22.792	467.079
Homology Directed Repair_R-HSA-5693538	20/118	6.59E-15	12.555	459.744
Resolution of D-loop Structures through Holliday Junction Intermediates_R-HSA-5693568	9/32	7.48E-09	20.833	458.353
Resolution of D-Loop Structures_R-HSA-5693537	9/33	9.82E-09	20.202	438.268
Signaling by Rho GTPases_R-HSA-194315	39/367	7.65E-22	7.8716	416.493
DNA Repair_R-HSA-73894	33/285	1.55E-19	8.577	407.105
HDR through Homologous Recombination (HR) or Single Strand Annealing (SSA)_R-HSA-5693567	18/112	5.01E-13	11.905	382.139
Regulation of DNA replication_R-HSA-69304	14/75	5.16E-11	13.827	378.627
DNA Double-Strand Break Repair_R-HSA-5693532	21/145	2.99E-14	10.728	376.244
HDR through Single Strand Annealing (SSA)_R-HSA-5685938	9/37	2.83E-08	18.018	370.636
PCNA-Dependent Long Patch Base Excision Repair_R-HSA-5651801	6/19	2.56E-06	23.392	370.176
G0 and Early G1_R-HSA-1538133	7/25	6.10E-07	20.741	359.605
G2/M DNA damage checkpoint_R-HSA-69473	14/78	8.86E-11	13.295	356.539
Association of licensing factors with the pre-replicative complex_R-HSA-69298	5/15	1.83E-05	24.691	337.425
Assembly of the pre-replicative complex_R-HSA-68867	12/67	2.78E-09	13.267	307.028
Recognition of DNA damage by PCNA-containing replication complex_R-HSA-110314	7/28	1.38E-06	18.519	305.024
Fanconi Anemia Pathway_R-HSA-6783310	8/35	3.58E-07	16.931	302.829

Telomere Maintenance_R-HSA-157579	11/59	9.22E-09	13.81	300.722
Resolution of AP sites via the multiple-nucleotide patch replacement pathway_R-HSA-110373	6/22	6.41E-06	20.202	299.949
Regulation of TP53 Activity through Phosphorylation_R-HSA-6804756	14/89	5.13E-10	11.652	290.603
COPI-dependent Golgi-to-ER retrograde traffic_R-HSA-6811434	13/81	2.00E-09	11.888	279.533
Removal of licensing factors from origins_R-HSA-69300	12/72	6.20E-09	12.346	274.831
Inhibition of replication initiation of damaged DNA by RB1/E2F1_R-HSA-113501	4/12	2.15E-04	24.691	274.648
Chk1/Chk2(Cds1) mediated inactivation of Cyclin B:Cdk1 complex_R-HSA-75035	4/12	2.17E-04	24.691	274.648
Regulation of mitotic cell cycle_R-HSA-453276	13/85	3.39E-09	11.329	259.251
APC/C-mediated degradation of cell cycle proteins_R-HSA-174143	13/85	3.46E-09	11.329	259.251
Condensation of Prophase Chromosomes_R-HSA-2299718	8/41	1.30E-06	14.453	239.275
Orc1 removal from chromatin_R-HSA-68949	11/70	5.33E-08	11.64	231.184
Switching of origins to a post-replicative state_R-HSA-69052	11/70	5.41E-08	11.64	231.184
Processing of DNA double-strand break ends_R-HSA-5693607	12/81	2.23E-08	10.974	228.72
Golgi Cisternae Pericentriolar Stack Reorganization_R-HSA-162658	4/14	4.14E-04	21.164	220.96
Removal of the Flap Intermediate_R-HSA-69166	4/14	4.18E-04	21.164	220.96
Resolution of Abasic Sites (AP sites)_R-HSA-73933	7/35	6.47E-06	14.815	219.484
Base Excision Repair_R-HSA-73884	7/35	6.55E-06	14.815	219.484
SUMOylation of DNA replication proteins_R-HSA-4615885	8/44	2.24E-06	13.468	215.111
Mitotic G2-G2/M phases_R-HSA-453274	19/175	1.15E-10	8.0423	213.395
Meiotic recombination_R-HSA-912446	9/54	8.32E-07	12.346	210.066
DNA Damage Bypass_R-HSA-73893	8/46	3.07E-06	12.882	201.076
Processive synthesis on the lagging strand_R-HSA-69183	4/15	5.48E-04	19.753	200.313
Depolymerisation of the Nuclear Lamina_R-HSA-4419969	4/15	5.54E-04	19.753	200.313
Termination of translesion DNA synthesis_R-HSA-5656169	6/30	3.96E-05	14.815	190.577
G2/M Transition_R-HSA-69275	18/173	7.94E-10	7.7071	188.67
G2 Phase_R-HSA-68911	2/5	0.01932	29.63	187.796
Translesion synthesis by REV1_R-HSA-110312	4/16	7.11E-04	18.519	182.664
Gap-filling DNA repair synthesis and ligation in GG-NER_R-HSA-5696397	5/23	1.77E-04	16.103	182.574
Mitotic Prophase_R-HSA-68875	13/107	5.03E-08	8.9997	179.527
Nuclear Envelope Breakdown_R-HSA-2980766	8/51	6.66E-06	11.619	171.674
Golgi-to-ER retrograde transport_R-HSA-8856688	13/110	6.61E-08	8.7542	171.61
Translesion synthesis by POLI_R-HSA-5656121	4/17	8.96E-04	17.429	167.429
Translesion synthesis by POLK_R-HSA-5655862	4/17	9.03E-04	17.429	167.429

Activation of APC/C and APC/C:Cdc20 mediated degradation of mitotic proteins_R-HSA-176814	10/75	1.30E-06	9.8765	163.412
APC-Cdc20 mediated degradation of Nek2A_R-HSA-179409	5/25	2.66E-04	14.815	161.528
Recruitment of NuMA to mitotic centrosomes_R-HSA-380320	3/11	0.00436	20.202	159.608
TP53 Regulates Transcription of Genes Involved in G2 Cell Cycle Arrest_R-HSA-6804114	4/18	0.00113	16.461	154.165
Regulation of TP53 Activity_R-HSA-5633007	15/151	5.04E-08	7.3584	146.888
Assembly of the ORC complex at the origin of replication_R-HSA-68616	2/6	0.02812	24.691	146.706
Phosphorylation of the APC/C_R-HSA-176412	4/19	0.00136	15.595	142.531
Translesion Synthesis by POLH_R-HSA-110320	4/19	0.00137	15.595	142.531
Translesion synthesis by Y family DNA polymerases bypasses lesions on DNA template_R-HSA-110313	6/37	1.41E-04	12.012	139.079
Factors involved in megakaryocyte development and platelet production_R-HSA-983231	14/141	1.59E-07	7.3549	137.62
AURKA Activation by TPX2_R-HSA-8854518	9/72	8.88E-06	9.2593	133.835
Meiosis_R-HSA-1500620	10/85	3.98E-06	8.7146	133.643
Inactivation of APC/C via direct inhibition of the APC/C complex_R-HSA-141430	4/20	0.00165	14.815	132.256
Inhibition of the proteolytic activity of APC/C required for the onset of anaphase by mitotic spindle checkpoint components_R-HSA-141405	4/20	0.00166	14.815	132.256
APC/C:Cdc20 mediated degradation of mitotic proteins_R-HSA-176409	9/74	1.11E-05	9.009	128.076
Mitotic Telophase/Cytokinesis_R-HSA-68884	3/13	0.00724	17.094	125.993
Mitotic Spindle Checkpoint_R-HSA-69618	4/21	0.002	14.109	123.126
Regulation of APC/C activators between G1/S and early anaphase_R-HSA-176408	9/79	1.84E-05	8.4388	115.219
SUMO E3 ligases SUMOylate target proteins_R-HSA-3108232	10/96	1.14E-05	7.716	109.44
APC/C:Cdc20 mediated degradation of Cyclin B_R-HSA-174048	4/23	0.00285	12.882	107.647
Transcriptional Regulation by TP53_R-HSA-3700989	23/348	1.05E-08	4.8957	105.782
Nuclear Pore Complex (NPC) Disassembly_R-HSA-3301854	5/34	0.00114	10.893	101.815
SUMOylation_R-HSA-2990846	10/101	1.77E-05	7.3341	100.55
Regulation of PLK1 Activity at G2/M Transition_R-HSA-2565942	9/87	4.04E-05	7.6628	98.3472
MHC class II antigen presentation_R-HSA-2132295	10/103	2.06E-05	7.1917	97.2915
RHO GTPases activate CIT_R-HSA-5625900	3/16	0.01346	13.889	93.4529
TP53 Regulates Transcription of Cell Cycle Genes_R-HSA-6791312	6/48	6.02E-04	9.2593	92.9528
Dual Incision in GG-NER_R-HSA-5696400	5/39	0.00209	9.4967	82.3788
Intra-Golgi and retrograde Golgi-to-ER traffic_R-HSA-6811442	13/179	1.64E-05	5.3797	74.2846

APC:Cdc20 mediated degradation of cell cycle proteins prior to satisfaction of the cell cycle checkpoint_R-HSA-179419	7/72	7.13E-04	7.2016	70.9443
Recruitment of mitotic centrosome proteins and complexes_R-HSA-380270	7/79	0.00123	6.5635	60.7414
Centrosome maturation_R-HSA-380287	7/79	0.00124	6.5635	60.7414
Loss of proteins required for interphase microtubule organization?from the centrosome_R-HSA-380284	6/69	0.00399	6.4412	51.5046
Loss of Nlp from mitotic centrosomes_R-HSA-380259	6/69	0.00403	6.4412	51.5046
Cdc20:Phospho-APC/C mediated degradation of Cyclin A_R-HSA-174184	6/71	0.00456	6.2598	49.0807
APC/C:Cdh1 mediated degradation of Cdc20 and other APC/C:Cdh1 targeted proteins in late mitosis/early G1_R-HSA-174178	6/71	0.00459	6.2598	49.0807
CDT1 association with the CDC6:ORC:origin complex_R-HSA-68827	5/58	0.01261	6.3857	43.4775
The role of GTSE1 in G2/M progression after G2 checkpoint_R-HSA-8852276	5/59	0.01353	6.2775	42.2533
TP53 Regulates Transcription of DNA Repair Genes_R-HSA-6796648	5/61	0.0155	6.0716	39.953
Gap-filling DNA repair synthesis and ligation in TC-NER_R-HSA-6782210	5/62	0.01655	5.9737	38.8716
Dual incision in TC-NER_R-HSA-6782135	5/63	0.01765	5.8789	37.8326
Anchoring of the basal body to the plasma membrane_R-HSA-5620912	6/97	0.02186	4.5819	28.4081
Transcription-Coupled Nucleotide Excision Repair (TC-NER)_R-HSA-6781827	5/76	0.03888	4.8733	27.3416
Generic Transcription Pathway_R-HSA-212436	24/812	0.00346	2.1894	17.8564
Membrane Trafficking_R-HSA-199991	14/420	0.01957	2.4691	15.6007

Supplementary Table S3. Gene sets enriched in indicated reactome pathways; Gene set enrichment analysis between highest 5% and lowest 90% ZBP1-expressing myeloma PC from MMRF data sets

Cell cycle, Mitotic pathway (5% ZBP1 highest/95% ZBP1 lowest); p-value <0.05

Gene	Fold-Change	Gene	Fold-Change	Gene	Fold-Change	Gene	Fold-Change	Gene	Fold-Change
PSMB9	1.4871	KIF2A	1.8556	CDC45	2.1065	CEP76	1.8712	E2F2	1.6004
MAD1L1	1.5331	PPP2R5B	1.4041	PPP1CB	1.4419	CEP192	1.7032	RCC2	1.2602
CDC27	1.4889	NUP133	1.4911	CDC23	1.8488	PSMD10	1.5228	CLASP2	1.5275
DHFR	2.2396	SMG6	1.4561	AAAS	1.4887	POLA1	1.7371	MAD2L1	2.2138
UPF1	1.5695	PABPC1	1.4405	PSMD5	1.6736	STAG2	1.5055	LEMD3	1.7028
DBF4	1.5907	CSNK2A2	1.4326	NUP188	1.7266	EMD	1.3580	LEMD2	1.3773
PAFAH1B1	1.4217	PRKACA	1.4529	FGFR1OP	1.7308	CENPI	2.3121	PSMD2	1.5048
PSMB1	1.3729	FBXW11	1.7771	PSMD8	1.5519	NUP93	2.9343	PSMD1	1.7307
CDK11A	1.5529	NDE1	1.6296	MAPK1	1.4982	CENPT	1.4832	CDK1	2.6002
NCAPD2	1.8065	MCM2	2.1519	NUP62	1.6856	PSMD7	1.4589	NIPBL	1.6964
PSMC4	1.4382	CLASP1	1.4175	MCM5	1.6225	CCP110	1.5745	ANAPC10	1.6061
POLA2	1.9113	NUP37	1.5488	EP300	1.4826	CEP152	1.8193	PSMD6	1.4762
MNAT1	1.5902	MCM6	1.6880	RANGAP1	1.5512	RAB2A	1.3231	PSMC3	1.6954
VRK2	1.4907	DYNC1I2	1.5534	POLE2	2.1134	PPP2CB	1.4167	DCTN2	1.3089
NUP160	1.7894	POLD3	1.7212	PSMC6	1.5377	DCTN1	1.5079	RAD21	1.5428
CENPQ	1.7299	PPP2R5C	2.0603	PSMA3	1.3713	CSNK2B	1.3568	ORC5	1.7811
RFC1	1.5251	RBL1	1.6509	VRK1	1.6120	CCNE1	2.8558	PTTG1	2.3277
TUBG2	1.7389	NDC80	2.6181	PSMC1	1.4951	PSMB8	1.5490	RFC4	1.7710
CCDC99	2.0297	XPO1	1.7806	PSMB5	1.6025	FZR1	1.7622	AURKB	2.2140
PSMA4	1.8814	PDS5B	1.7431	PSMA6	1.3897	LIG1	2.0206	CKAP5	1.9196
OFD1	1.4891	SEH1L	1.6445	PSME2	2.0096	PPP2R1A	1.5547	FEN1	1.8576
TPR	1.4568	ZW10	1.5717	GIN51	2.4646	RPA3	1.5353	UBB	1.4233
RFC2	1.5440	PSMC5	1.5845	NINL	2.0324	PSMA2	1.7327	UBE2E1	1.8591
ANAPC4	1.4572	AURKA	2.2797	MYBL2	2.1013	POLD2	1.7996	RAB8A	1.9369
SDCCAG8	1.3201	DYNLL1	1.5333	E2F4	1.3965	SMC3	1.6431	TK2	1.5051
CUL1	1.4648	ANAPC5	1.4418	RAE1	1.8403	PSMB3	1.4316	BUB1	1.9658
PPP1R12A	1.4814	BIRC5	2.3403	PSMA7	1.4842	PSMD3	1.4378	YWHAG	1.6476
WAPAL	1.4903	NUDC	1.5497	CDC25B	1.6696	NUP88	1.5362	ESCO2	2.2478
PPP2R2A	1.5342	AC005522	1.5583	CSNK2A1	1.5780	PSMD11	1.4532	CDT1	2.1051
POLD1	1.7550	ORC6	1.6600	PSMB10	1.8780	YWHAE	1.6662	PPP2R3B	1.5977
MCM10	2.3261	PSME1	1.6085	MAPRE1	1.4897	SMG5	1.4840	GOLGA2	1.3450
CSNK1E	2.0310	NUP50	1.6554	E2F1	1.9224	CEP290	1.4597	PSME4	1.3869
NCAPG	2.7609	CENPK	2.3389	TUBGCP4	1.8073	CENPF	2.2820	SMC1A	1.5176
TFDP1	1.7336	CDK2	1.4745	KIF23	2.7584	CDCA8	2.1978	BLZF1	1.3958
CEP164	1.6417	B9D2	1.6184	HAUS2	1.9239	KIF2C	2.0871	NSL1	1.4647
NUP98	1.6126	NUP85	1.6810	CASC5	2.1613	PPP2R5E	1.3319	SGOL2	2.0688
PSMD9	1.5436	PSMF1	1.3795	RAB1A	1.2818	SKA1	2.3352	NUMA1	1.6932
FOXM1	1.9684	MCM8	1.8459	ACTR1A	1.3089	CKS1B	1.7487	PMF1	1.4223
RFC5	1.5372	MAX	1.3485	CENPO	1.8710	MIS12	1.3494	TAOK1	1.5894

NUP107	1.5405	CEP250	1.6576	DNA2	2.0971	GORASP2	1.2554	CDC25C	2.7255
MCM3	1.6645	PSMB2	1.5110	HNRNPD	1.4698	CDKN2C	2.8599	PPP2R2D	1.4223
E2F3	1.6310	TUBGCP3	1.5015	ANAPC7	1.7019	CCNA2	2.2648	CEP57	1.6834
GMNN	1.5895	NUP214	1.4859	DYNC1H1	1.5666	UBA52	1.3111	ZWILCH	2.0847
PPP2R5D	1.5528	PKMYT1	2.2989	NUP54	1.4714	UBC	1.3084	BANF1	1.6035
CEP72	2.5335	TUBA4A	1.6656	CENPE	2.1971	PSMD4	1.3970	RBBP4	1.4429
KIF20A	2.3693	AKAP9	1.4463	NUPL1	1.5884	CSNK1D	1.4392	POLD4	1.5026
LMNB1	1.5896	TUBGCP6	1.5703	NEDD1	1.4451	CENPN	1.5782	CEP135	1.5430
SKP1	1.5850	ARPP19	1.6462	ESCO1	1.6331	CENPM	1.8241	NUP35	1.8293
SFI1	1.5152	PSMA1	1.6834	AZI1	1.8267	DTX4	1.9829	PSMC2	1.6349
PPP2CA	1.5444	SGOL1	2.1607	ANAPC11	1.3963	OPTN	1.4410	APITD1	1.4492
NUP155	1.6571	MAU2	1.7459	PSMB6	1.4180	LIN52	1.3587	BTRC	1.4553
SMC4	1.7443	CDC16	1.7948	POM121	1.5740	TSGA14	1.6168	RAB1B	1.4195
CEP70	1.5142	TUBGCP2	1.4465	PLK4	2.0560	JUB	2.1347	SPC24	2.8021
TFDP2	1.6773	GINS2	1.9837	ITGB3BP	1.5486	NOTCH1	1.5324	UBE2C	2.3297
NCBP2	1.7441	TUBG1	1.5996	LIN54	1.3963	RBL2	1.3176	MCM7	1.7598
GORASP1	1.6034	PSME3	1.6705	PSMA5	1.3614	CDC25A	1.6678	PSMD12	1.3773
EIF4G1	1.2793	NUP210	1.9129	TUBB	1.5565	ORC1	1.6739	CENPH	2.3717
CENPA	2.6487	TOP2A	2.4631	NUF2	2.4157	NEK7	1.3550	SPC25	2.8236
PSMD14	1.6613	RPA1	1.6638	RPS27A	1.5769	PLK1	2.0148	POLE	1.6972
ORC2	1.7562	PCNA	1.8155	CENPC1	1.5717	PSMB4	1.2740	ANAPC1	1.8709
ORC4	1.5471	RFC3	2.4969	CENPP	2.2472	FBXO5	1.4423	RB1	1.2758
ALMS1	1.4602	E2F5	2.1627	SKP2	1.8895	NUP153	1.3129	ANKLE2	1.4157
HDAC1	1.6277	CCNB1	2.4833	CDCA5	2.7618	RPS27	1.3030	TUBGCP5	2.0138
SMG7	1.5866	CDK7	1.6379	TUBB2C	1.4552	RRM2	2.0190	TYMS	2.3005
NEK2	2.2585	CCNH	1.5221	ERCC6L	3.5825	SEC13	1.1966	BUB3	2.0045
RPA2	1.7383	ORC3	1.5953	HDAC8	1.6230	MCM4	1.5934	CDC26	1.5027
STAG1	1.4168	CDK4	1.3966	GINS4	2.0177	CDC7	1.5877	PSMA8	2.4742
CNTRL	1.7719	ESPL1	2.2798	CDKN2A	2.0161	ENSA	1.2900	NUP205	1.7608
NEK9	1.6387	BORA	1.6790	PPP1CC	1.6710	CDC6	1.5429	BUB1B	2.5061
NUP43	1.7715	ODF2	1.8022	CEP78	1.7475	CDC20	1.7116	ANAPC2	1.6573
PRIM1	1.6096	NUPL2	1.7165	CEP63	1.5045	PPP1R12	1.2742	CCNB2	2.3397
CENPL	1.6877	CDK5RAP2	1.7837	LIN9	1.8396	AHCTF1	1.2943	SSNA1	1.5519
MASTL	1.5319	SMC2	2.0005	KNTC1	1.6467	NDEL1	1.1977	PCNT	1.5748
TMPO	1.5175	PSMB7	1.6388	PSMD13	1.6110	PCM1	1.2334	DYRK1A	1.4218
NCAPH	2.4510	NCBP1	1.7537	INCENP	1.9233	UBE2D1	1.2827	ZWINT	2.2172
KIF18A	2.1386	MYC	2.1254	SKA2	1.7172	USO1	1.1754	PPP2R1B	1.8480
PDS5A	1.5427	DCTN3	1.6122	DSN1	1.7053	CDKN1B	1.2572	MLF1IP	1.8244

Interferon Signaling pathway (5% ZBP1 highest/95% ZBP1 lowest); p-value <0.05

Gene	Fold-Change	Gene	Fold-Change	Gene	Fold-Change	Gene	Fold-Change	Gene	Fold-Change
IFNA17	15.513	CAMK2G	1.6568	ITGB3	1.6369	KPNA4	1.3309	NUP62	1.6856
IFNA8	10.747	EIF4A2	1.7911	EIF4G3	1.6245	DDX58	2.1343	IRF1	1.6817
IFNA7	8.4985	EIF4A1	1.6722	EIF2AK2	1.6181	IRF3	1.8063	UBA7	1.6756
IFNA14	4.5365	RNASEL	1.5408	IFITM2	1.6173	USP41	2.3186	PTPN2	1.6734
IFNA4	4.2438	NUP205	1.7608	RPS27A	1.5769	ARIH1	1.7096	MX2	1.6644

IFNB1	3.9058	HERC5	1.566	SUMO1	1.5739	IRF5	1.9069	NUP155	1.6571
IFIT2	2.6502	NCAM1	2.705	NUP37	1.5488	JAK2	1.6943	SEH1L	1.6445
CAMK2B	2.2713	NUP85	1.681	PPP2CA	1.5444	PPP2CB	1.4167	PIN1	1.8299
USP18	2.1842	IFNGR2	1.5434	NUP107	1.5405	OAS1	1.7109	IRF4	2.2322
IFI35	1.8975	TLN1	1.3977	KPNA1	1.5154	OAS3	2.2781	PPM1B	1.7106
HLA-G	1.8841	NUPL1	1.5884	NUP133	1.4911	ADAR	1.4277	NUP93	2.9343
ISG20	1.8801	POM121	1.574	IRF9	1.4872	NUP214	1.4859	IFIT1	2.3023
UBE2E1	1.8591	NUP98	1.6126	PTPN11	1.4721	NUP35	1.8293	NUP188	1.7266
IP6K2	1.8488	AAAS	1.4887	STAT2	1.469	PPP2R1A	1.5547	MX1	2.3512
IFNAR1	1.8485	IRF2	1.6288	TPR	1.4568	IFNA21	3.7102	NUP153	1.3129
IFNGR1	1.847	PSMB8	1.549	KPNA2	1.4492	UBE2L6	1.9286	UBA52	1.3111
TRIM25	1.7993	TYK2	1.7651	EIF4E	1.4464	NUP210	1.9129	UBC	1.3084
NUP160	1.7894	NUP54	1.4714	EIF4A3	1.4336	EIF4E2	1.5914	PTPN6	1.2809
NEDD4	1.7797	RAE1	1.8403	GBP3	1.4251	IRF7	1.7838	EIF4G1	1.2793
NUP43	1.7715	ISG15	2.5585	UBB	1.4233	KPNB1	1.6639	MAPK3	1.2418
OAS2	1.7654	EIF4G2	1.5117	RANBP2	1.3975	PRKCD	1.8154	JAK1	1.1763
PLCG1	1.7514	IFNA10	7.5309	IFNA5	1.3942	IFNA16	3.0585	PML	2.1341
PIAS1	1.7448	NUP50	1.6554	GRB2	1.3373	KPNA5	1.6881	NUPL2	1.7165
SP100	1.7265	NUP88	1.5362	STAT1	1.3161	XAF1	1.7327	IFNAR2	1.7334
UBE2N	1.7013	KPNA3	1.758	PTPN1	1.3146	SRC	1.4247	RAP1B	1.3523
EIF4E3	1.4229	IFI27	2.2101	OASL	1.7928	SOCS3	0.2326		

Supplementary Table S4. Differentially expressed genes that are common between shZBP1 and shIRF3 in MM.1S cells (top50% log2 fold change and p adj <0.05)

down-regulated			up-regulated
THRIL	ZWINT	AMOTL1	LY86
DHCR24	TCF19	PRPS2	FCGBP
BLM	C3orf70	NASP	HLA-DQA1
RRM2	E2F1	CALM3	LINGO3
HES6	ANLN	NCAPH2	C3AR1
RAD51	LIG1	PLEKHH2	HSF4
DDIAS	GFI1	FADS1	DMBT1
CCNF	SMOC1	TSPAN33	BMF
CEP55	DPF3	EMILIN1	PARP9
AURKA	CAVIN4	MCC	NEK11
E2F8	DERA	INSIG1	MAPT
PRR11	MIS18A	LAMP5	ZBTB10
MYB	GPAT2	LRRCC1	ODAPH
EXO1	MPP1	CCSAP	FCHSD1
SKA1	AMPD1	LRP8	TMEM119
PKMYT1	CCNE1	KCNQ5	RNF207
DTL	MCM8	GNPNAT1	TMEM229B
SHCBP1	MCM3	RABL3	TP53I11
BRI3BP	ITPKA	MEI1	CPM
TONSL	HEMGN	DNMT3B	MYLK2
ERCC6L	IMPA2	HSPA4L	ALDOB
FAM111B	LRRC20	GSTCD	IL2RG
FEN1	SLC16A14	SLC39A8	CFAP70
MAD2L1	BARD1	KCNA3	
CDC45	MAL2	TIAM1	
DSCC1	CEP57L1	SCD5	
POLA1	EAF2	FRMD6	
PROB1	CYP26A1	SCN3A	
RAD51AP1	TMEFF1	CEP128	
KIF15	RELN	MCUB	
WDR76	GRB14	SIPA1	
FANCG	RHBDL3	TMC5	
CKAP2L	TMEM106C	DSN1	
CENPJ	SCD	TXNDC5	
CDC25C	ITPRIPL1	SLC17A9	
MCM6	MYORG		
TP73	SMC1A		

Supplementary Table S5. Reactome pathways_Enrichr pathway enrichment analysis of the shared 109 genes downregulated in MM.1S cells upon ZBP1 and IRF3 depletion

Name of the enriched pathways (Homo sapiens)	Overlap	Adjusted P-value	Odds Ratio	Combined Score
G1/S-Specific Transcription_R-HSA-69205	5/17	4.92E-06	53.97	943.0714
Unwinding of DNA_R-HSA-176974	4/12	4.70E-05	61.16	901.1077
DNA strand elongation_R-HSA-69190	7/32	1.80E-07	40.14	873.5304
E2F mediated regulation of DNA replication_R-HSA-113510	6/33	5.71E-06	33.36	587.6216
Resolution of D-loop Structures through Synthesis-Dependent Strand Annealing (SDSA)_R-HSA-5693554	5/26	3.36E-05	35.29	534.5948
Activation of the pre-replicative complex_R-HSA-68962	5/30	6.12E-05	30.58	440.2043
Resolution of D-loop Structures through Holliday Junction Intermediates_R-HSA-5693568	5/32	8.01E-05	28.67	403.0262
POLB-Dependent Long Patch Base Excision Repair_R-HSA-110362	2/7	0.02212	52.42	388.299
Resolution of D-Loop Structures_R-HSA-5693537	5/33	8.81E-05	27.8	386.366
Processive synthesis on the lagging strand_R-HSA-69183	3/15	0.00348	36.7	351.9814
Activation of ATR in response to replication stress_R-HSA-176187	5/37	1.41E-04	24.8	329.9524
Activation of PUMA and translocation to mitochondria_R-HSA-139915	2/8	0.02742	45.87	326.7286
Cell Cycle_R-HSA-1640170	26/566	4.91E-14	8.429	320.1011
Homologous DNA Pairing and Strand Exchange_R-HSA-5693579	5/42	2.56E-04	21.84	276.5402
G1/S Transition_R-HSA-69206	9/112	3.20E-06	14.74	270.955
Cell Cycle, Mitotic_R-HSA-69278	21/462	4.93E-11	8.34	253.3261
Lagging Strand Synthesis_R-HSA-69186	3/20	0.00778	27.52	239.2529
S Phase_R-HSA-69242	9/124	5.59E-06	13.32	232.8195
TP53 Regulates Transcription of Cell Cycle Genes_R-HSA-6791312	5/48	4.33E-04	19.11	229.098
DNA Replication_R-HSA-69306	8/105	1.65E-05	13.98	224.2559
CDC6 association with the ORC:origin complex_R-HSA-68689	2/11	0.04703	33.36	215.4542
Processive synthesis on the C-strand of the telomere_R-HSA-174414	2/11	0.04797	33.36	215.4542
Cell Cycle Checkpoints_R-HSA-69620	11/182	1.77E-06	11.09	212.8149
Telomere C-strand (Lagging Strand) Synthesis_R-HSA-174417	3/22	0.01012	25.02	210.176
Mitotic G1-G1/S phases_R-HSA-453279	9/136	9.71E-06	12.14	202.5136
HDR through Single Strand Annealing (SSA)_R-HSA-5685938	4/37	0.00262	19.84	197.2621
Presynaptic phase of homologous DNA pairing and strand exchange_R-HSA-5693616	4/39	0.00313	18.82	183.1741

Synthesis of DNA_R-HSA-69239	7/97	9.08E-05	13.24	182.8151
G2/M Checkpoints_R-HSA-69481	9/150	1.85E-05	11.01	174.3159
M/G1 Transition_R-HSA-68874	6/82	4.16E-04	13.43	162.1024
DNA Replication Pre-Initiation_R-HSA-69002	6/82	4.37E-04	13.43	162.1024
HDR through Homologous Recombination (HRR)_R-HSA-5685942	5/64	0.00165	14.33	151.4058
Extension of Telomeres_R-HSA-180786	3/28	0.01787	19.66	150.7661
Resolution of Sister Chromatid Cohesion_R-HSA-2500257	6/99	0.00113	11.12	122.1646
Mitotic Prometaphase_R-HSA-68877	6/107	0.00155	10.29	108.475
Homology Directed Repair_R-HSA-5693538	6/118	0.0026	9.33	93.21054
Assembly of the pre-replicative complex_R-HSA-68867	4/67	0.01833	10.95	83.45547
Regulation of DNA replication_R-HSA-69304	4/75	0.0262	9.786	70.36809
DNA Double-Strand Break Repair_R-HSA-5693532	6/145	0.00686	7.593	67.18344
G2/M DNA damage checkpoint_R-HSA-69473	4/78	0.02905	9.41	66.27318
HDR through Homologous Recombination (HR) or Single Strand Annealing (SSA)_R-HSA-5693567	5/112	0.01573	8.191	64.72335
RHO GTPases Activate Formins_R-HSA-5663220	5/114	0.01576	8.048	62.93194
DNA Repair_R-HSA-73894	9/285	0.00161	5.794	61.12078
Chromosome Maintenance_R-HSA-73886	4/86	0.04094	8.534	56.99652
Separation of Sister Chromatids_R-HSA-2467813	6/162	0.01146	6.796	56.04436
Regulation of TP53 Activity through Phosphorylation_R-HSA-6804756	4/89	0.04552	8.247	54.0272
Mitotic Anaphase_R-HSA-68882	6/173	0.01541	6.364	50.24109
Mitotic Metaphase and Anaphase_R-HSA-2555396	6/174	0.01547	6.327	49.75805
Transcriptional Regulation by TP53_R-HSA-3700989	9/348	0.00602	4.745	42.76202
Regulation of TP53 Activity_R-HSA-5633007	5/151	0.04459	6.076	39.80423
M Phase_R-HSA-68886	7/268	0.02379	4.793	35.03605

Supplementary Table S6. Commonly identified IRF3 target genes by integration of IRF3 binding within 2kb distance to TSS and both shRNAs-mediated *IRF3*-depleted transcriptome of MM.1S cells

Activated genes

CSRP1	SEL1L	TYRO3	KAT2B	KPNA6	FEM1B	SLC5A3	LSM10	CPOX	ARHGAP11A
AKAP2	UHRF1BP	CS	LRRC20	IRS1	CALM3	HDAC9	CDYL	NCAPG2	ZDHHC7
RRBP1	RAB3B	HDGF	NAA50	SMC6	EZR	LONP1	EYA3	CSE1L	HNRNPUL2-B
PGM1	C19orf47	SF3B3	ESRRA	PCNT	RNPEPL1	DSN1	NUS1	SUCLG1	TOMM40
LRRC59	AK2	LRIG1	CCL3	CGN	RECQL	NXPE3	CCM2	ATP6AP1	FAM111B
CCL3L1	ERC1	TBL1X	HBS1L	SIPA1	SLC25A4	LRRC57	CRY1	STAG1	PIK3AP1
NUDT3	SLC37A4	NOP9	HLA-E	MTO1	SLC39A7	PLEKHB2	NPNT	CHCHD2	RAD51AP1
SSRP1	RNF168	CERK	SLC31A1	FOXO3	MPC1	POLE3	RAP1B	GSTCD	CNOT6L
DDX21	MRPS24	YBX1	PIGX	CREBL2	MIS18A	BTAF1	MCM5	P2RX5	RAB11FIP5
ZNF275	CDC25C	EIF4H	RBBP5	ERN1	USF2	ARAP1	TMC5	LRRC8A	TMEM106C
XPO7	GOLIM4	NRN1	POLQ	TCHP	SLC25A4	CBL	UQCRCF51	CYTIP	UGT2B17
SLC38A1	TEX261	RUSC1	PRPS2	RBM3	AMOTL1	USP13	FANCI	SPATS2	SLC36A1
SCD	LAMP5	HM13	MYH10	SLK	DHCR24	WDR7	STK24	SLC25A4	SREBF1
SAMD9L	EMILIN1	NIN	FKBP4	SLC4A7	SLC39A8	COA4	UBXN2A	RAD21	TP53INP2
CASP3	FEN1	TRAM2	CDV3	PDIK1L	GLCCI1	DDOST	SPAG9	ATP10D	CKAP2L
HACD3	TPM3	SNX12	EAF2	NEK4	XIAP	PKMYT1	SLC16A14	TLN1	TRAPPC6B
TXNRD1	HIPK2	SMC5	ATP6AP2	MFN2	DPF3	KCNA3	FUCA2	SLC4A2	HNRNP2H2
RALBP1	IMMT	URB1	SKAP2	AMPD1	NOC3L	STARD4	GMPPB	MFSD6	PRADC1
MYCL	OTUD7B	ARF1	UQCRC1	GDE1	TOP3A	PRPS1	PRR15	SDF2L1	FOXRED2
ADAR	TEC	CCDC47	DENND5	CD2AP	GOLT1B	SOAT1	DDRKG1	LYAR	CDK5RAP2
MAP3K3	SLC25A5	ATP7A	PRKCI	ATP1B3	TCF19	FANCG	SNRNP25	ENDOD1	KBTBD8
MPRIIP	SYNM	PDIA4	MYO18A	MCM3	TPPP	PAPSS1	RAD51D	ITPRIPL1	SMCHD1
GLE1	IDH3A	RTN4	CCNF	MDFIC	COBLL1	TACC1	AKR1B1	VARS2	CCDC85C
DIAPH1	GOT1	NGLY1	C3orf70	MTUS1	ZNF672	PRDM1	COLGALT1	MRPL27	MCUR1
SRPK1	LRP8	NNT	NEU3	RCC2	TEX2	MACC1	ANLN	MICU1	TOR3A
MCM8	CHST15	BLOC1S5	TNPO2	GLTP	INSR	COX6B1	LMO7	RMND5B	SEPHS1
SUZ12	TIAM1	MCC	GDF11	DHFR	CLN6	ARFGEF2	SEC24A	STK26	MCM7
SLAMF7	FOXN3	SPTBN1	SMTN	E2F8	PARG	ST3GAL6	RAD51	MAD2L1	TMEM214
NF2	SNX30	IRS2	IGF2BP2	ISG20	NDRG1	WDFY1	MSH2	LRRK1	TBC1D10B
FNIP2	IDH2	FBXW4	DST	UBE3C	SRPK2	NAGA	C2orf88	ARSB	TNFRSF13B
RABL6	MICAL1	DTL	DLG5	TYMS	CD99L2	MAN1A1	CDAN1	ATG3	MRPS16
PJA2	N4BP2	MANEA	CAV1	HEMGN	TP73	LRRC8B	CYP26A1	ELK4	NDUFB10
CAP1	DENND3	TTL	OCRL	MCM2	LSS	UTP23	DCPS	HIGD1A	CEP55
BICD2	ALDH5A1	SYK	CCSAP	SKA1	HYOU1	POU2AF1	ZNF770	PSMG1	MEF2D
MAST2	TWF1	HRH2	ABCA5	SMOC1	ANKRD1	MRPL55	SERPINB6	RGS9	HNRNPUL2
IRF4	STAT2	AFG3L2	PAF1	GENE	PIGU	KIF20B	ELL	AP1S3	CCHCR1
ZNF106	DNAJC3	RAP2C	BRI3BP	ZBED4	NAB1	OTULIN	ACER3	DNMT1	ZDHHC20
TMED5	POLR2D	ABL2	SMC1A	LDLR	TCF4	GRWD1	SEC22C	CDK4	ARHGDI3
DCAF12	MTHFD2	USP1	SOD2	RBSN	GRHL1	NCAPH2	ZWINT	NANP	RFWD3
VAPA	ARFGEF3	SEMA5A	EIF4E3	DVL2	RABL3	ZDHHC23	KANSL3	XYLB	SIGMAR1
KIAA004	PM20D2	PDP2	MCM6	NASP	SHMT2	RBBP4	POLR3D	SMC2	RNASEH2A
ST6GAL1	IL10RA	UAP1L1	CKAP4	RRM2	PPHLN1	SERINC5	ACO2	GLDC	KIAA0513

BAZ1B	MTCH2	HEXA	FADS1	POLA1	MAL2	HIRIP3	DLAT	HMGN5	TMEM201
BMP6	REXO4	APEH	E2F1	CEP57	TONSL	HES6	TPD52	ATAD5	RAB11FIP4
GUSB	KIF15	UGGT2	UHRF1	PFAS	HAUS2	ANO8	CEP57L1	SULF2	SLC25A45
KIF13B	IMPA2	SVIP	KIF11	LCLAT1	NUSAP1	JAKMIP1	PHAX	STRBP	CADPS2
POLH	ABCB10	ACO1	CHAF1B	NFIL3	CCP110	AARS	BLVRB	TAF9B	ANKRD13A
SUB1	CCT8	FICD	PSMD11	RAD1	DNMBP	PASK	KIAA0232	SNX25	UBQLN2
ZBED8	KCTD9	NUAK1	CAV2	ATP2A2	HEATR5A	MAPK9	PAQR4	ALYREF	ARHGAP33
PDXK	COMTD1	MLLT3	SLC44A1	EXOC5	LANCL1	CENPJ	INPP4A	ARFRP1	AP1S2
DSCC1	PDIA6	LMO4	SPAG5	EZH2	DDIAS	DNAJC11	KLF12	NDUFA6	LGALS17A
DMXL1	EXO1	CERS6	E2F2	IDI1	BZW2	LIME1	PRKACA	SLC20A1	MRPS18C
CDT1	MSI2	AAK1	MRPS36	SLFN13	JADE1	LMNB1	KCTD1	RRAGD	HNRNPR
MCM4	GTF2A1	SP3	POM121	SHCBP1	CCL4L2	GJB2	KCNQ5	NDUFS1	HMCES
MYEOV	ZNF791	ATIC	IPO9	USP37	HMGN2	TP53INP1	NOLC1	SLC10A7	ANKRD33B
BLM	PRRG4	KIF4A	HMGB3	KANK2	PABPC4	TCP1	MPC2	CHST12	HNRNPF
POC1B	SPAG7	FDPS	LMBRD2	UBE2H	PPM1K	DEGS1	HSPA8	TMPO	SLC25A11
SKIL	ATP8B2	PHIP	TTLL5	RNGTT	ZWILCH	PAIP2B	RAB26	STIM1	RAB27A
CBX3	WDR76	XRCC6	ITPKA	BARD1	DOCK8	SLC7A5	MTHFD1	TIMM21	TNFRSF21
CDCA7L	ACAA2	NABP2	PIP5K1B	LRMP	CDC45	DONSON	CYC1	FZD5	GPATCH11
FZD3	BMP8B	AARS2	SH3RF1	SEL1L3	EBP	ZNF142	HJURP	MBD2	PSMB8-AS1
SAE1	DOCK9	HEYL	HYI	API5	ZFP91	FH	APPL1	PRKCE	TMEM109
ZNF641	ARID5B	IL6ST	STK35	GAB2	PYCR2	IPO7	SLBP	PSMC3IP	SUPT16H
LAT2	WNK1	DHRS13	AFF4	RNF103	PRKDC	TBC1D30	HS2ST1	RASGRP3	ARHGAP10
STT3A	XRCC5	STK4	FZD1	PLCB3	PRR11	MFAP3	TIMELESS	L3MBTL2	NDUFS6
SOS1	ASNSD1	HSPA4L	EML6	CENPL	ERLIN1	LIG1	MAN2A2	ARL6IP6	KATNB1
TTF2	L2HGDH	ADD2	PLEKHA7	DCK	CEP192	PAXIP1	TRIM26	SFXN5	LRRC45
NPC1	PPP6R3	DERA	ADM	H1FX	YWHAQ	FNDC3B	RAB4A	SRGAP2B	ANKRD10
MSX1	PHYH	TTLL7	VARS	CCNE1	PSMD3	GPRC5D	GIN3	ERGIC1	PGRMC2
LRRC8C	GFI1	PIGO	INSIG1	POLE	DOT1L	ZBP1	UBQLN1	XRRA1	ZMPSTE24
TRIB1	HPS3	AURKA	PNP	RCAN1	SLC38A2	TUBB	MIEF1	MLEC	DNMT3B
CDH2	THOP1	DAZAP1	DPYSL2	NCAM1	NCAPD2	PHLPP1	ZNF215	MTMR12	HNRNPAB
RTEL1	OSGIN2	ASCC3	STK39	JAKMIP	MYB	NSFL1C	GNPNAT1	DOLPP1	METTL21A
ACTB	KIF18B	SFXN4	ITGA4	CDS2	LRCH3	CKAP2	GHITM	KNOP1	SMARCA2
KIF14	MMS22L	TLR4	URB2	SFXN2	LIMD1	TAPBP	SPCS2	PRPSAP1	C16orf95
FKBP5	BBS7	JPH1	GALNT6	LIN54	PDK1	SLAIN1	MRPS18B	LRRCC1	DENND1B
RBM47	UBR7	FRMD6	ST7	NANS	PUS7L	TRIM41	SRGAP2	SLC7A1	TNFRSF17

Repressed genes

CRYBB1	IQCH	GAS5	HIF1A	RNF123	TMED4	CSTB	WDR48	PCYOX1L	TNFRSF10D
EI24	VPS9D1	SMOX	IQSEC1	NAT9	MCAT	GALNT18	DAZAP2	CSNK1G3	TMEM80
SF3B6	BIRC3	HDAC10	WNT10A	KDM3A	ARL6IP5	MFSD10	GRHL3	INAFM2	PAX8-AS1
BMF	CRTC2	MRPL10	IL27RA	RPS7	HIVEP3	LY86	PCDH1	TARBP1	ATP6V1C2
BSPRY	EML4	DNAJA1	GNAI2	POLDIP	SYTL2	CLTA	PCED1B-A	GOLM1	CDC42SE1
MIAT	IFNGR2	RPS6KA1	RPL7A	P2RX1	SLC16A3	RPS24	RPL31	TYW1	FAM86C2P
RPS28	IER5	HOOK2	KPTN	FAAH2	ARSA	DLGAP4	STK17A	NEK6	CAPRIN2
RPL8	LPIN1	PRPSAP2	RPS19	CD70	STAT4	WDR60	FTSJ3	CCR10	L3MBTL1
MAPT	LRWD1	C3AR1	RPGR	SGK1	DTX3L	IDNK	GOLGA8A	RPS3	ASB16-AS1
SYF2	NMRK1	RPL36	RPL23	FTL	NPRL3	PIP5KL1	UNC93B1	CTNNB1	MAPKAPK2

PHPT1	RCSD1	APOL2	CSK	RPL34	SLC39A4	TRMT1	POMT1	PPP1R10	LINC00893
IL2RG	PLEKHO1	RPL15	DEF6	ARL2	NARF	CASP8	RPS23	NFKB2	ARHGEF40
GNA12	RPS29	TP53I11	ZNF644	KY	NFKBIA	TRAF1	RPL17	SCNN1G	C11orf68
MKNK2	PTTG1P	RFFL	IZUMO4	DDIT4	EHD1	PIGQ	ASB13	HMOX1	GALNT10
SYNGR2	CCDC92	R3HDM4	RPL27A	TMC6	ARPC5	GALNT2	RNF207	CCDC24	APOBEC3F
JAK3	STAT6	B4GALT5	NABP1	AZIN2	RPL21	ALDH1B1	RPS27L	RPL27	THUMPD3-AS1
UBA52	LRRC1	SSBP4	ZBTB10	RPS3A	RPS8	CD86	PARP9	LUC7L3	DENND5A
PSMB5	VTI1B	ZMIZ2	IFI16	RPL35A	SOAT2	SECTM1	RPL10	RPL18A	SLC25A23
PEA15	SPPL2B	UNC119	ACADVL	APOL1	CRK	RPS9	ZNF276	KLF3	ATP6VOE1
MXI1	PLXNA3	OFD1	CLSTN1	RPL6	PRNP	BLVRA	CTDNEP1	COMT	NIPSNAP1
SCNN1B	IGF1R	ZFP36L1	MRFAP1	WASF1	GPR137	BAX	WDR73	CFAP70	SRP14-AS1
BSG	RPL22	RPS10	OGT	SUMF2	RPS21	ARPC1A	CCDC86	IKBKE	ZSCAN30
MOB3A	RGS14	AMPD3	GPR108	RPS6	FAS	ARL1	RALY-AS1	HRAS	STX16-NPEPL1
RALGDS	ELK3	C11orf1	VAMP3	PARP8	GABPB2	TSPAN31	EIF3F	NEK11	FAM171A1
PLXNB2	ERCC1	LMAN2L	OXLD1	CXXC5	GATC	RPS14	GALNT7	SLC2A11	KCNQ10T1
ECE1	NOTCH2	NRBP1	DYRK2	ARHGAP1	RPL38	RGL1	CABIN1	C1orf52	TMEM255B
SF1	TXLNB	FAU	IRF5	GNB1L	MZF1	GBP4	CCDC71L	VASP	TNFRSF10B
SNRPA1	DMWD	EIF3G	TMC8	GTF3C2	ARID5A	MAP2K3	CSNK1G2	CLPTM1	DENND6A
SLC2A1	LARS	RPL36A	BCL3	UBXN8	CYB5R1	PPFIA4	GRB2	TRADD	SYNGAP1
FJX1	SLC41A3	RPLP0	ST14	CUL7	EME2	IRF2BP2	ABHD17A	NINJ1	TMEM259
CTSA	NMI	ZNF580	ANXA4	ZMAT1	RPS15	RPL10A	ATP6V1B2	RPL37A	CDC42BPA
MR1	VPS28	ISCU	UBFD1	ICK	RPL13	ZNF467	RNF170	EIF3D	NAPA-AS1
RELL2	POLN	EPAS1	HSF4	YBX3	CC2D1A	C1RL-AS1	TGIF2	GRINA	HNRNPAO
TRIP11	CDK6	TPCN1	RHPN1	EIF4G3	LENG8	C6orf62	VEGFA	PHLDA3	

Supplementary Table S7. Reactome pathways_Enrichr pathway enrichment analysis of the 770 genes predicted to be directly activated by IRF3 binding to their regulatory areas

Name of the enriched pathways (Homo sapiens)	Overlap	Adjusted P-value	Odds Ratio	Combined Score
Unwinding of DNA_R-HSA-176974	9/12	1.79E-08	19.48	468.9
DNA strand elongation_R-HSA-69190	12/32	4.14E-07	9.74	201.0831
G1/S-Specific Transcription_R-HSA-69205	8/17	1.16E-05	12.22	199.2733
Activation of the pre-replicative complex_R-HSA-68962	11/30	1.83E-06	9.524	178.5999
Pyruvate metabolism and Citric Acid (TCA) cycle_R-HSA-71406	13/48	3.48E-06	7.035	124.5455
Citric acid cycle (TCA cycle)_R-HSA-71403	7/19	2.99E-04	9.569	118.7075
IRS activation_R-HSA-74713	3/5	0.01784	15.58	117.3632
Cell Cycle_R-HSA-1640170	65/566	4.39E-12	2.983	99.87958
Resolution of D-loop Structures through Synthesis-Dependent Strand Annealing (SDSA)_R-HSA-5693554	8/26	3.00E-04	7.992	99.4886
Activation of ATR in response to replication stress_R-HSA-176187	10/37	7.77E-05	7.02	97.6146
E2F mediated regulation of DNA replication_R-HSA-113510	9/33	2.40E-04	7.084	90.13903
Mitotic G1-G1/S phases_R-HSA-453279	23/136	6.71E-07	4.393	87.58288
Cell Cycle, Mitotic_R-HSA-69278	54/462	2.67E-10	3.036	87.0802
G1/S Transition_R-HSA-69206	20/112	2.03E-06	4.638	85.77785
Signal attenuation_R-HSA-74749	4/10	0.01419	10.39	81.81775
S Phase_R-HSA-69242	21/124	2.03E-06	4.399	80.76056
DNA Replication_R-HSA-69306	18/105	1.25E-05	4.453	71.86397
POLB-Dependent Long Patch Base Excision Repair_R-HSA-110362	3/7	0.04371	11.13	70.53198
M/G1 Transition_R-HSA-68874	15/82	4.55E-05	4.751	69.16752
DNA Replication Pre-Initiation_R-HSA-69002	15/82	4.86E-05	4.751	69.16752
Resolution of D-Loop Structures_R-HSA-5693537	8/33	0.0015	6.297	66.13454
Synthesis of DNA_R-HSA-69239	16/97	7.73E-05	4.284	59.84078
DNA Double-Strand Break Repair_R-HSA-5693532	21/145	2.05E-05	3.762	58.5392
Assembly of the pre-replicative complex_R-HSA-68867	12/67	5.10E-04	4.652	54.40799
IRF3-mediated induction of type I IFN_R-HSA-3270619	4/13	0.03282	7.992	53.88441
The citric acid (TCA) cycle and respiratory electron transport_R-HSA-1428517	21/153	4.79E-05	3.565	52.19291
Resolution of D-loop Structures through Holliday Junction Intermediates_R-HSA-5693568	7/32	0.00731	5.682	49.09321
DNA Repair_R-HSA-73894	32/285	9.61E-06	2.916	48.36416
Early Phase of HIV Life Cycle_R-HSA-162594	4/14	0.04018	7.421	47.76672
HDR through Homologous Recombination (HRR)_R-HSA-5685942	11/64	0.00156	4.464	46.55633
Regulation of DNA replication_R-HSA-69304	12/75	0.00155	4.156	43.65912
Homologous DNA Pairing and Strand Exchange_R-HSA-5	8/42	0.0073	4.947	42.8895

G2/M Checkpoints_R-HSA-69481	19/150	3.60E-04	3.29	40.04601
Synthesis of substrates in N-glycan biosynthesis_R-HSA-44	10/63	0.00611	4.123	36.71012
Cholesterol biosynthesis_R-HSA-191273	5/23	0.04087	5.647	36.43604
Cell Cycle Checkpoints_R-HSA-69620	21/182	4.76E-04	2.997	35.38072
Presynaptic phase of homologous DNA pairing and strand exchange_R-HSA-5693616	7/39	0.02082	4.662	34.28883
Homology Directed Repair_R-HSA-5693538	15/118	0.00236	3.302	32.8438
Sialic acid metabolism_R-HSA-4085001	6/33	0.03831	4.723	30.85951
Regulation of TP53 Activity through Phosphorylation_R-HSA-6804756	12/89	0.00665	3.502	30.78408
Orc1 removal from chromatin_R-HSA-68949	10/70	0.01299	3.711	29.73416
Switching of origins to a post-replicative state_R-HSA-69052	10/70	0.01333	3.711	29.73416
AURKA Activation by TPX2_R-HSA-8854518	10/72	0.01486	3.608	28.07016
Removal of licensing factors from origins_R-HSA-69300	10/72	0.01521	3.608	28.07016
Regulation of cholesterol biosynthesis by SREBP (SREBF)_R-HSA-1655829	8/55	0.03296	3.778	25.59725
Post-translational protein modification_R-HSA-597592	42/521	3.74E-04	2.094	25.31411
HDR through Homologous Recombination (HR) or Single Strand Annealing (SSA)_R-HSA-5693567	13/112	0.01432	3.015	23.78714
Biosynthesis of the N-glycan precursor (dolichol lipid-linked oligosaccharide, LLO) and transfer to a nascent protein_R-HSA-446193	10/78	0.02488	3.33	23.75895
SUMOylation_R-HSA-2990846	12/101	0.01708	3.086	23.44182
Asparagine N-linked glycosylation_R-HSA-446203	24/259	0.00327	2.407	23.08093
Transcriptional Regulation by TP53_R-HSA-3700989	30/348	0.0018	2.239	22.95018
Loss of proteins required for interphase microtubule organization?from the centrosome_R-HSA-380284	9/69	0.03412	3.388	22.59023
Loss of Nlp from mitotic centrosomes_R-HSA-380259	9/69	0.03473	3.388	22.59023
Mitotic Prometaphase_R-HSA-68877	12/107	0.02593	2.913	20.60454
SUMO E3 ligases SUMOylate target proteins_R-HSA-310	11/96	0.03264	2.976	20.13795
Mitotic G2-G2/M phases_R-HSA-453274	17/175	0.01527	2.523	19.50638
Sphingolipid metabolism_R-HSA-428157	9/74	0.04999	3.159	19.49119
Regulation of PLK1 Activity at G2/M Transition_R-HSA-2	10/87	0.04516	2.986	18.77097
Regulation of TP53 Activity_R-HSA-5633007	15/151	0.0236	2.58	18.5986
Metabolism of proteins_R-HSA-392499	69/1074	0.00122	1.669	17.99519
Epigenetic regulation of gene expression_R-HSA-212165	12/115	0.04069	2.71	17.45593
G2/M Transition_R-HSA-69275	16/173	0.03196	2.402	16.39538
HIV Infection_R-HSA-162906	19/222	0.03	2.223	15.3561
Metabolism_R-HSA-1430728	105/190	0.00503	1.429	13.04787

Enrichr pathway enrichment analysis of the 339 genes predicted to be directly repressed by IRF3 binding to their regulatory areas

Name of the enriched pathways (Homo sapiens)	Overlap	Adjusted P-value	Odds Ratio	Combined Score
--	---------	------------------	------------	----------------

Formation of a pool of free 40S subunits_R-HSA-72689	42/96	6.6E-46	25.81	2874.639
3' -UTR-mediated translational regulation_R-HSA-157279	42/106	2.4E-44	23.38	2481.838
L13a-mediated translational silencing of Ceruloplasmin expression_R-HSA-156827	42/106	3E-44	23.38	2481.838
GTP hydrolysis and joining of the 60S ribosomal subunit_R-HSA-72706	42/107	3.2E-44	23.16	2447.439
Peptide chain elongation_R-HSA-156902	39/84	3.3E-44	27.39	2913.375
Viral mRNA Translation_R-HSA-192823	39/84	4.9E-44	27.39	2913.375
Eukaryotic Translation Termination_R-HSA-72764	39/87	7.2E-44	26.45	2766.136
Selenocysteine synthesis_R-HSA-2408557	39/87	8.2E-44	26.45	2766.136
Nonsense Mediated Decay (NMD) independent of the Exon Junction Complex (EJC)_R-HSA-975956	39/89	1.8E-43	25.85	2674.693
Eukaryotic Translation Elongation_R-HSA-156842	39/89	2E-43	25.85	2674.693
Eukaryotic Translation Initiation_R-HSA-72613	42/114	4.1E-43	21.74	2227.01
Cap-dependent Translation Initiation_R-HSA-72737	42/114	4.4E-43	21.74	2227.01
Selenoamino acid metabolism_R-HSA-2408522	40/111	1.5E-40	21.26	2051.558
Nonsense Mediated Decay (NMD) enhanced by the Exon Junction Complex (EJC)_R-HSA-975957	39/106	5.4E-40	21.71	2063.111
Nonsense-Mediated Decay (NMD)_R-HSA-927802	39/106	5.8E-40	21.71	2063.111
SRP-dependent cotranslational protein targeting to membrane_R-HSA-1799339	39/107	7.8E-40	21.5	2034.399
Translation_R-HSA-72766	42/151	2.4E-37	16.41	1457.546
Influenza Life Cycle_R-HSA-168255	40/136	1.3E-36	17.35	1511.003
Influenza Viral RNA Transcription and Replication_R-HSA-168273	39/128	2.3E-36	17.98	1554.129
Influenza Infection_R-HSA-168254	40/147	3.8E-35	16.05	1342.074
Major pathway of rRNA processing in the nucleolus_R-HSA-6791226	40/166	7.3E-33	14.22	1112.89
rRNA processing_R-HSA-72312	40/180	2.2E-31	13.11	980.9076
Metabolism of amino acids and derivatives_R-HSA-71291	43/335	1.6E-23	7.573	429.397
Infectious disease_R-HSA-5663205	43/348	7.1E-23	7.29	402.021
Formation of the ternary complex, and subsequently, the 43S complex_R-HSA-72695	19/50	1.6E-19	22.42	1062.841
Translation initiation complex formation_R-HSA-72649	19/57	2.7E-18	19.67	874.6005
Ribosomal scanning and start codon recognition_R-HSA-72702	19/57	2.9E-18	19.67	874.6005
Activation of the mRNA upon binding of the cap-binding complex and eIFs, and subsequent binding to 43S_R-HSA-72662	19/58	3.9E-18	19.33	852.1469
Disease_R-HSA-1643685	51/725	2.4E-16	4.15	165.6816
Metabolism of proteins_R-HSA-392499	58/1074	1.7E-13	3.186	106.1788
Gene Expression_R-HSA-74160	66/1631	1.1E-09	2.387	58.50422
Metabolism_R-HSA-1430728	65/1908	1.7E-06	2.01	34.50708
Regulation of necroptotic cell death_R-HSA-5675482	5/14	0.00011	21.07	272.6659
RIPK1-mediated regulated necrosis_R-HSA-5213460	5/16	0.00022	18.44	224.7141

Regulated Necrosis_R-HSA-5218859	5/16	0.00023	18.44	224.7141
Death Receptor Signalling_R-HSA-73887	7/48	0.00065	8.604	95.389
Dimerization of procaspase-8_R-HSA-69416	4/11	0.00096	21.45	227.8933
Regulation by c-FLIP_R-HSA-3371378	4/11	0.00098	21.45	227.8933
CASP8 activity is inhibited_R-HSA-5218900	4/11	0.00101	21.45	227.8933
Toll-Like Receptors Cascades_R-HSA-168898	11/140	0.00105	4.635	48.70507
TRIF-mediated TLR3/TLR4 signaling_R-HSA-937061	9/97	0.00143	5.474	55.4238
Toll Like Receptor 3 (TLR3) Cascade_R-HSA-168164	9/97	0.00146	5.474	55.4238
MyD88-independent TLR3/TLR4 cascade_R-HSA-166166	9/97	0.0015	5.474	55.4238
Toll Like Receptor 4 (TLR4) Cascade_R-HSA-166016	10/122	0.00153	4.836	48.50032
Activated TLR4 signalling_R-HSA-166054	9/112	0.0042	4.741	42.66809
Programmed Cell Death_R-HSA-5357801	11/166	0.00428	3.909	35.02182
Ligand-dependent caspase activation_R-HSA-140534	4/17	0.00517	13.88	121.1514
Regulation of TNFR1 signaling_R-HSA-5357905	5/31	0.00523	9.516	83.13201
Innate Immune System_R-HSA-168249	28/807	0.00896	2.047	16.69644
SHC-related events triggered by IGF1R_R-HSA-2428933	3/9	0.0115	19.67	155.0901
Apoptosis_R-HSA-109581	10/163	0.01436	3.619	27.66884
Immune System_R-HSA-168256	44/1547	0.01469	1.678	12.75707
Regulation of gene expression by Hypoxia-inducible Factor_R-HSA-1234158	3/10	0.01531	17.7	133.4916
TNF signaling_R-HSA-75893	5/41	0.01748	7.195	53.17565
Iron uptake and transport_R-HSA-917937	5/43	0.02144	6.86	49.17444
Cellular response to hypoxia_R-HSA-2262749	4/26	0.02381	9.076	63.62731
Cytosolic sensors of pathogen-associated DNA_R-HSA-1834949	6/66	0.02395	5.363	37.75556
Signaling by PTK6_R-HSA-8848021	6/67	0.02421	5.283	36.77103
Regulation of Hypoxia-inducible Factor (HIF) by oxygen_R-HSA-1234174	4/26	0.02423	9.076	63.62731
TP53 Regulates Transcription of Death Receptors and Ligands_R-HSA-6803211	3/12	0.02458	14.75	102.6747
Caspase activation via extrinsic apoptotic signalig pathway_R-HSA-5357769	4/27	0.02623	8.74	59.98581
VEGFA-VEGFR2 Pathway_R-HSA-4420097	14/320	0.02953	2.581	17.36617
p38MAPK events_R-HSA-171007	3/13	0.02955	13.61	91.37597
Signalling to ERKs_R-HSA-187687	12/253	0.03206	2.798	18.50882
TRAF6 Mediated Induction of proinflammatory cytokines_R-HSA-168180	6/72	0.0326	4.916	32.36066
Signaling by VEGF_R-HSA-194138	14/328	0.035	2.518	16.35759
NGF signalling via TRKA from the plasma membrane_R-HSA-187037	15/374	0.04364	2.366	14.81257

**Supplementary Table S8. commonly co-regulated genes by both IRF3 and IRF4 in MM.1S cells;
Integration of intersection of IRF3 and IRF4 binding within 2kb distance to TSS
and both shRNAs-mediated IRF3-depleted transcriptome of MM.1S cells**

Activated genes

HNRNPF	FBXW4	N4BP2	LRRC8B	NANP	NASP	CCM2	KIF11	SNRNP25
AKAP2	MYCL	RAB3B	KCTD9	RGS9	FAM111B	SREBF1	GLDC	ALYREF
LRRC59	PABPC4	DENND5B	GAB2	GPATCH1	CDC25C	FEM1B	DHCR24	RFWD3
RRBP1	GFI1	HM13	FOXRED2	VAR52	ZNF672	ATP8B2	GDE1	PRDM1
CCL3L1	LRRC20	DCAF12	SERINC5	PRR11	AARS	SYNM	NOC3L	EXO1
PGM1	HERPUD1	CCDC85C	WDR76	KANSL3	NCAPH2	LIG1	DST	SRPK2
NUDT3	RBBP5	UHRF1BP1	ARFGF2	NCAM1	HYOU1	CD2AP	SMCHD1	CCSAP
DOLPP1	SKA1	SNX30	GRWD1	MCUR1	CAV1	ARFGF3	BMP8B	RMND5B
IRF4	PLEKHB2	TEX261	GOLT1B	RBBP4	SKAP2	NDRG1	CSE1L	PPHLN1
SSRP1	SNX12	C19orf47	MPC2	ABCB10	POLH	TBL1X	DPYSL2	XRCC6
CASP3	ARHGDI1	DSN1	MIS18A	MACC1	ZDHHC20	SLC31A1	UBR7	HIGD1A
SLC37A4	TRAM2	MCM6	HNRNPUL1	CCHCR1	RAD51AP1	CDV3	LYAR	SLC25A44
RALBP1	STAT2	FOXO3	MPC1	ZNF791	ATP7A	UAP1L1	ZDHHC23	IPO7
DIAPH1	PDIA4	SUZ12	SP3	ARFRP1	BLOC1S5	MCM7	MRPL55	LRRC57
RABL6	C3orf70	CCDC47	EIF4E3	ADD2	ST6GAL1	NGLY1	WDR7	HNRNPH2
IL10RA	FANCG	E2F1	NAB1	LDLR	SULF2	CKAP4	DHFR	DCPS
SCD	KPNA6	IRS2	ARAP1	BLM	SLC36A1	PHAX	PPP6R3	TMPO
MAP3K3	UBE2H	TEC	RNASEH2A	RNGTT	DDIAS	IDH3A	CCL4L2	ATIC
CAP1	CREBL2	MTCH2	PHYH	SEMA5A	SOAT1	H1FX	KCNA3	PSMD11
TPM3	DVL2	AK2	LRRC8A	MRPS18C	ESRRA	MANEA	TLN1	SVIP
DDX21	TWF1	HLA-E	ANKRD16	FANCI	AKR1B1	MDFIC	ATP10D	BTAF1
SRPK1	MRPS16	HIRIP3	MAN1A1	HDAC9	HEMGN	BICD2	TCHP	COA4
RNF168	IMPA2	LSS	TCF4	BBS7	GLTP	PRKCI	JPH1	ZWINT
SEL1L	SLC39A8	TMEM106	L2HGDH	PSMD3	SLC5A3	UQCRC1	JADE1	MBD2
MTHFD2	ACTB	OTUD7B	RUSC1	POM121	TOR3A	GOLIM4	MSI2	AP1S3
ADAR	TMEM214	URB1	COMTD1	NDUFA6	AMOTL1	AMPD1	KNOP1	GSTCD
FNIP2	LONP1	HIPK2	MCM2	SEC24A	MTO1	SYK	CGN	DOT1L
MCM8	APEH	FADS1	NUSAP1	SUB1	CCT8	GUSB	NDUFS1	LRCH3
CERK	DTL	HEXA	PDP2	SHCBP1	ACAA2	SLK	API5	LRRK1
ERC1	SMC1A	TPPP	LSM10	SLFN13	TACC1	SLC25A4	CCP110	TNFRSF13B
GLE1	ZBED4	MRPS24	JAKMIP2	UQCRC1	DHRS13	HS2ST1	RCAN1	ATP6AP1
PM20D2	RTN4	PJA2	HSPA4L	PIK3AP1	HDGF	REXO4	CDYL	KIF20B
NF2	EAF2	SLC4A7	E2F8	RAD1	CALM3	IGF2BP2	SAE1	LANCL1
CCL3	CDCA7L	PIGX	TOP3A	ZBP1	ELK4	SOD2	MIEF1	ARHGAP11A
KIAA0040	DNMT1	MCM3	PFAS	AURKA	COBL1	USP13	PIGU	TNFRSF17
TRIM41	INSR	POU2AF1	LCLAT1	AFF4	WDFY1	SF3B3	SLC44A1	HNRNPUL2
SAMD9L	ENDOD1	LRIG1	THOP1	GHITM	SIGMAR1	TP53INP2	PPM1K	PSMB8-AS1
CS	P2RX5	SLC39A7	POLR3D	KIAA0232	PDXX	NDUFB10	KIF15	TNFRSF21
XPO7	TCF19	UBE3C	SMC2	PRPSAP1	PARG	DNAJC3	PSMC3IP	ACO1
POLR2D	TONSL	SLC25A5	LGALS17A	HSPA8	POLQ	CLN6	GNE	XYLB
MICAL1	ATG3	AFG3L2	TRIM26	PDIK1L	POLA1	MFN2	DERA	NANS
MCC	FOXN3	PAF1	SIPA1	SH3RF1	RAB27A	PDIA6	PSMG1	CSR1

ZNF106	ATP6AP2	ABL2	TEX2	MRPL27	RECQL	CENPJ	TBC1D10B	SUCLG1
SLAMF7	CDK4	MAST2	PUS7L	CDS2	SFXN2	KBTBD8	IDI1	RAB11FIP4
FICD	PIGO	UGGT2	SMC5	LIN54	CERS6	KAT2B	HPS3	DNAJC11
XIAP	TIMELESS	METTTL21A	PLCB3	ZBED8	SPAG5	CDK5RAP2	RABL3	PAIP2B
RAP2C	HEYL	PYCR2	SLC25A45	IL6ST	HJURP	PRRG4	CRY1	EBP
ZNF142	KANK2	CADPS2	EYA3	POLE	NOLC1	SLC25A11	CPOX	TYMS
VARS	POLE3	RAP1B	YWHAQ	SPAG7	MICU1	DNMBP	LMBRD2	LRRRC8C
MAN2A2	FDPS	STK24	ZMPSTE24	DOCK8	CENPL	RAD51D	FKBP4	UHRF1
CEP57	L3MBTL2	RBSN	DCK	RTEL1	FZD1	MMS22L	SEC22C	SFXN4
RAD51	MEF2D	MSX1	DAZAP1	CYP26A1	SMTN	JAKMIP1	XRCC5	NCAPG2
SEPHS1	HEATR5A	EXOC5	LMO7	ZNF770	DEGS1	FNDC3B	CEP55	ANKRD13A
HES6	AP1S2	SLC4A2	PAPSS1	KIF18B	NUS1	GALNT6	CEP57L1	DNMT3B
NPC1	EML6	HAUS2	TPD52	TOMM40	GIN53	NSFL1C	ZNF215	TRIB1
ITGA4	POC1B	UBXN2A	SFXN5	ATP1B3	BZW2	URB2	CDC45	WNK1
RAB4A	ACO2	GNPNAT1	UBQLN1	LAT2	ELL	DENND1B	FZD5	ARHGAP10
ZNF641	ARL6IP6	SLC16A14	RBM47	KLF12	MFAP3	SKIL	NRN1	NDUFS6
LRRCC1	ISG20	KCTD1	DLAT	STK35	ST7	MRPS18B	GAS6	TMEM109
TAPBP	SLBP	CHAF1B	PRKACA	RASGRP3	HMGN2	STIM1	USF2	APPL1
PRKCE	LRRRC45	PGRMC2	STK39	ANKRD33	SLAIN1	PCNT	MCM4	TMEM201
PAXIP1	C2orf88	MRPS36	KATNB1	PRKDC	SOS1	GPRC5D	LIMD1	PAQR4
KIF14	IPO9	HBS1L	TNPO2	ATAD5	DDOST	STK4	KIF13B	PHLPP1
STT3A	MAL2	DMXL1	NEK4	PASK	SLC20A1	CBX3	SDF2L1	FH
HMGN5	EZH2	UBQLN2	ASCC3	AAK1	STAG1	DSCC1	ASNSD1	NABP2
CEP192	MSH2	CBL	HNRNPR	NAGA	PRADC1	STAR4	TLR4	CKAP2L
TIMM21	SMARCA2	SPAG9	ANO8	ERLIN1	ITPKA	MTUS1	BARD1	PRR15
COX6B1	AARS2	COLGALT1	ZWILCH	SLC38A2	MTMR12	UTP23	NCAPD2	DONSON

Repressed genes

CRYBB1	ALDH1B1	B4GALT5	RFFL	PPP1R10	TARBP1	TXLNB	MCAT	NAPA-AS1
SCNN1G	ISCU	P2RX1	RPL36A	NFKB2	NFKBIA	ICK	EHD1	IZUMO4
EI24	SLC2A11	EME2	RPL27	PIP5KL1	OXLD1	BLVRA	R3HDM4	CC2D1A
DAZAP2	LENG8	BAX	RPS9	PHPT1	ARSA	CCDC71L	POLDIP2	ZMAT1
BMF	GALNT18	CCDC24	CLPTM1	SECTM1	CFAP70	LUC7L3	RPL22	ATP6V1C2
RPS28	TP53I11	UNC119	LRWD1	CLTA	RPS7	DLGAP4	RPL35A	TRIP11
GNA12	HMOX1	SSBP4	STAT6	RCSD1	UBFD1	RPS29	RPL38	ASB16-AS1
UNC93B1	FAM171A	GNB1L	RPL6	WDR60	RPS6KA1	HNRNPA0	APOL1	STX16-NPEPL1
BSG	RALGDS	RPS15	RPS10	GALNT2	OGT	RALY-AS1	RPL34	SLC41A3
SNRPA1	IKBKE	APOL2	C1orf52	HRAS	CSNK1G2	RPS27L	C3AR1	PCED1B-AS1
RGS14	CTDNBP1	ARL6IP5	CRK	NINJ1	KDM3A	TGIF2	RPL17	C11orf1
SLC2A1	RPL36	PIGQ	YBX3	SF3B6	RPL7A	RPL15	HIVEP3	SRP14-AS1
CTNNB1	FTL	MAP2K3	RPS19	VAMP3	RNF123	BIRC3	GRB2	RPLP0
MAPT	ECE1	CASP8	CRTC2	GPR137	HOOK2	SGK1	SOAT2	TNFRSF10D
MOB3A	EIF3D	RPS14	STK17A	CAPRIN2	ZSCAN30	CUL7	GABPB2	CDC42SE1
RPS24	PPFIA4	GBP4	WASF1	CXXC5	PARP9	RPL10A	ERCC1	ARID5A
RPL8	COMT	LMAN2L	EIF3G	ELK3	DEF6	NMI	KY	RNF170
SCNN1B	LY86	ZMIZ2	ARPC5	DMWD	MIAT	PTTG1IP	RPS8	TNFRSF10B
MXI1	UBA52	NIPSNAP1	FJX1	IGF1R	SYNGAP1	ZNF580	RPL31	TMEM259

PEA15	ARL1	RPL18A	RPS6	CSNK1G3	PARP8	PAX8-AS1	VPS28	CCDC86
MFSD10	WDR73	DNAJA1	MRPL10	CTSA	VASP	RPS23	RPS3	TMEM255B
JAK3	ZFP36L1	ST14	GTF3C2	GAS5	INAFM2	HSF4	SYF2	APOBEC3F
RGL1	TRMT1	ARPC1A	ABHD17A	RPS3A	RPL23	THUMPD3	ASB13	ARHGEF40
IQCH	ARL2	RPL37A	IRF5	SYTL2	ATP6V1B2	CDK6	SPPL2B	SLC25A23
MKNK2	NEK11	TRADD	NAT9	LARS	WDR48	MAPKAPK	PCDH1	DENND5A
MZF1	LRRC1	ZNF467	GNAI2	IER5	IDNK	EIF4G3	C11orf68	LINC00893
FTSJ3	WNT10A	MR1	NARF	UBXN8	IQSEC1	RHPN1	IL27RA	PLEKHO1
EML4	RPGR	CYB5R1	DTX3L	GALNT10	EIF3F	C1RL-AS1	RPL27A	
MRFAP1	KPTN	BCL3	CSK	C6orf62	IFNGR2	CLSTN1	CABIN1	
ZNF644	AZIN2	CD70	SF1	GRHL3	ATP6V0E1	GOLGA8A	LPIN1	

Supplementary Table S9. Reactome pathways_Enrichr pathway enrichment analysis of genes predicted to be activated by IRF3-IRF4 co-binding

Name of the enriched pathways (Homo sapiens)	Overlap	Adjusted P-value	Odds Ratio	Combined Score
Cell Cycle_R-HSA-1640170	53/566	7.12E-10	3.06	86.8934
Cell Cycle, Mitotic_R-HSA-69278	42/462	1.74E-07	2.971	64.7629
Unwinding of DNA_R-HSA-176974	8/12	2.50E-07	21.79	475.8844
DNA Repair_R-HSA-73894	29/285	6.33E-06	3.325	59.57776
DNA strand elongation_R-HSA-69190	10/32	7.19E-06	10.21	179.3957
DNA Double-Strand Break Repair_R-HSA-5693532	19/145	2.51E-05	4.282	69.0833
Activation of the pre-replicative complex_R-HSA-68962	9/30	3.90E-05	9.804	152.3381
Resolution of D-loop Structures through Synthesis-Dependent Strand Annealing (SDSA)_R-HSA-5693554	8/26	1.35E-04	10.06	142.4407
Mitotic G1-G1/S phases_R-HSA-453279	17/136	1.55E-04	4.085	56.8172
Activation of ATR in response to replication stress_R-HSA-176187	9/37	1.78E-04	7.949	107.8471
S Phase_R-HSA-69242	16/124	1.89E-04	4.217	57.35635
G1/S Transition_R-HSA-69206	15/112	1.94E-04	4.377	58.28267
Pyruvate metabolism and Citric Acid (TCA) cycle_R-HSA-71406	10/48	1.95E-04	6.808	91.1551
G2/M Checkpoints_R-HSA-69481	17/150	3.66E-04	3.704	46.43759
DNA Replication_R-HSA-69306	14/105	3.68E-04	4.357	54.32801
HDR through Homologous Recombination (HRR)_R-HSA-5685942	11/64	3.75E-04	5.617	70.67104
The citric acid (TCA) cycle and respiratory electron transport_R-HSA-1428517	17/153	4.23E-04	3.631	44.54305
Resolution of D-Loop Structures_R-HSA-5693537	8/33	4.40E-04	7.922	96.41805
M/G1 Transition_R-HSA-68874	12/82	5.43E-04	4.782	56.69911
DNA Replication Pre-Initiation_R-HSA-69002	12/82	5.72E-04	4.782	56.69911
Synthesis of DNA_R-HSA-69239	13/97	5.84E-04	4.38	51.39002
Homology Directed Repair_R-HSA-5693538	14/118	0.00106	3.877	43.01631
Homologous DNA Pairing and Strand Exchange_R-HSA-5693579	8/42	0.0023	6.225	63.94539
HDR through Homologous Recombination (HR) or Single Strand Annealing (SSA)_R-HSA-5693567	13/112	0.00245	3.793	38.55949
Resolution of D-loop Structures through Holliday Junction Intermediates_R-HSA-5693568	7/32	0.00257	7.149	72.05244
Cell Cycle Checkpoints_R-HSA-69620	17/182	0.00272	3.053	30.47478
Post-translational protein modification_R-HSA-597592	33/521	0.00406	2.07	19.75569
G1/S-Specific Transcription_R-HSA-69205	5/17	0.00657	9.612	86.75117
Presynaptic phase of homologous DNA pairing and strand exchange_R-HSA-5693616	7/39	0.0084	5.866	51.2962
Assembly of the pre-replicative complex_R-HSA-68867	9/67	0.00993	4.39	37.50475
Citric acid cycle (TCA cycle)_R-HSA-71403	5/19	0.0106	8.6	72.63125
Metabolism of proteins_R-HSA-392499	54/1074	0.01138	1.643	13.7095
Mitotic G2-G2/M phases_R-HSA-453274	15/175	0.01515	2.801	22.48218

AURKA Activation by TPX2_R-HSA-8854518	9/72	0.01524	4.085	32.64071
E2F mediated regulation of DNA replication_R-HSA-113510	6/33	0.01916	5.942	45.9442
Regulation of DNA replication_R-HSA-69304	9/75	0.01959	3.922	30.12717
IRF3-mediated induction of type I IFN_R-HSA-3270619	4/13	0.02059	10.06	76.47073
Cholesterol biosynthesis_R-HSA-191273	5/23	0.02262	7.104	53.17071
Epigenetic regulation of gene expression_R-HSA-212165	11/115	0.03165	3.126	22.2642
HDR through Single Strand Annealing (SSA)_R-HSA-5685938	6/37	0.03173	5.299	37.59699
G2/M Transition_R-HSA-69275	14/173	0.0337	2.645	18.53759
SUMOylation_R-HSA-2990846	10/101	0.03847	3.236	22.1746
Loss of proteins required for interphase microtubule organization?from the centrosome_R-HSA-380284	8/69	0.03952	3.789	25.52021
Loss of Nlp from mitotic centrosomes_R-HSA-380259	8/69	0.04039	3.789	25.52021
STING mediated induction of host immune responses_R-HSA-1834941	4/16	0.04097	8.17	55.09649
Organelle biogenesis and maintenance_R-HSA-1852241	21/326	0.04109	2.105	14.23895
Orc1 removal from chromatin_R-HSA-68949	8/70	0.04163	3.735	24.80183
Regulation of cholesterol biosynthesis by SREBP (SREBF)_R-HSA-1655829	7/55	0.04215	4.159	27.3989
Switching of origins to a post-replicative state_R-HSA-69052	8/70	0.04252	3.735	24.80183
Regulation of PLK1 Activity at G2/M Transition_R-HSA-2565942	9/87	0.04253	3.381	22.30836
Removal of licensing factors from origins_R-HSA-69300	8/72	0.0471	3.631	23.44438
Activation of gene expression by SREBF (SREBP)_R-HSA-2426168	6/42	0.04841	4.669	29.92483